Computational Modelling of an Electromagnetic System for Separation of Solid Inclusions from Molten Aluminum

by

Timothy D. Blaskovich

Department of Mechanical Engineering
McGill University
Montreal, Quebec, Canada

A thesis submitted to the Faculty of Graduate Studies and Research
in partial fulfillment of the requirements for the degree of
Master of Engineering

Abstract

Mathematical models and numerical solution methods for the computer simulation of solid particle trajectories in flows of molten aluminum subjected to steady, uniform, electric and magnetic fields are presented in this thesis. The underlying subject is electromagnetic (EM) filtration of molten metals.

Attention is focused on steady, laminar, fully developed flows of molten aluminum inside a straight separation chamber of uniform rectangular cross-section. The walls of this chamber are assumed to be electrically non-conducting. The investigation is limited to solid inclusions (particles) that are electrically non-conducting and have an effective diameter in the range 5 μm to 100 μm. Steady, uniform, electric and magnetic fields are prescribed, and the induced currents are assumed to be negligible.

Mathematical models of three-dimensional parabolic (developing) and fully developed flows of molten aluminum in the separation chamber are provided, nondimensionalized, and discussed. A rudimentary model of the magnetohydrodynamic (MHD) flow is proposed, in which Maxwell's equations are decoupled from the Navier-Stokes equations. The particle momentum equation is presented, nondimensionalized, and discussed in detail.

The fluid flow problem is solved using a control-volume finite element method (CVFEM). The particle momentum equation is solved using a fourth-order Runge-Kutta (RK) method. An efficient method is proposed for locating the particle in the finite element mesh during the RK integration of the particle momentum equation.

The proposed methods are applied to four test problems, and the results are compared to those obtained using analytical and numerical solutions available in the literature. Finally, the scope of the proposed methods and some of the possibilities they offer are explored by applying them to a simple electromagnetic system for the separation of solid inclusions from molten aluminum.

Résumé

Ce travail de thèse présente la formulation mathématique et les méthodes numériques utilisées dans la simulation des trajectoires de particules dans les écoulements d'Aluminium en fusion soumis à des champs électriques et magnétiques stationnaires et uniformes. Ce sujet entre dans le cadre des études menées dans le domaine de la filtration électromagnétique (EM) des métaux en fusion.

Une attention particulière est accordée aux écoulements stationnaires laminaires pleinement développés d'Aluminium en fusion dans une chambre de séparation droite à section rectangulaire constante. Les parois de la chambre sont électriquement non-conductrices. L'investigation se limite aux inclusions solides non conductrices d'électricité et de diamètre effectif variant entre 5 μm et 100 μm. Des champs électromagnétiques stationnaires et uniformes sont imposés et les courants induits sont supposés négligeables.

Les modèles mathématiques des équations tridimensionnelles adimensionalisées des écoulements paraboliques (non-établis) et pleinement développés d'Aluminium en fusion dans la chambre de séparation sont présentés et commentés. Un modèle rudimentaire d'écoulement magnétohydrodynamique (MHD) est proposé, dans lequel les équations de Maxwell et de Navier-Stokes sont découplées. L'équation de quantité de mouvement des particules est présentée et discutée en détail.

Le problème d'écoulement fluide est résolu en utilisant une méthode au éléments finis/volumes de contrôle (CVFEM). L'équation de quantité de mouvement des particules est résolue au moyen de la méthode de Runge-Kutta (RK) du quatrième ordre.
Une méthode efficace de localisation de la particule dans le maillage aux éléments finis, en cours de l'intégration RK de l'équation de quantité de mouvement de la particule, est de même présentée.

Les méthodes proposées sont appliquées à quatre cas tests et les résultats sont comparés à ceux obtenus par des méthodes analytique et numérique rencontrées en littérature. Finalement, le but des méthodes proposées et les possibilités qu'elles offrent sont explorés à travers leur application à un système électromagnétique de séparation d'inclusions solides dans de l'Aluminium en fusion.

Acknowledgements

First, I want to express my gratitude to Professor B.R. Baliga for his guidance, and assistance in helping me complete this thesis and my degree. He has been a great mentor and friend.

I would also like to acknowledge Pratt & Whitney Canada Inc. for their support through the employee scholar program, and especially my supervisor, Sami Girgis, for providing the flexibility I needed in my schedule to complete this thesis.

A special thanks is given to Toufik Djeridane, who translated the abstract for me.

Finally, I am thankful for my wife, Janita and my two children, Adrianna and Alexander who have been a great source of encouragement to me. It is to them that I dedicate this thesis as I believe that their generation will see the field of magnetohydrodynamics widely implemented in industry.

Table of Contents

Abstract ii
Résumé iii
Acknowledgements iv
Table of Contents v
List of Figures viii
List of Tables x
Nomenclature xi
1 Introduction 1
1.1 Objectives 1
1.2 Background and Motivation 2
1.3 Literature Review 4
1.3.1 Electromagnetic Filtration 5
1.3.2 Control-Volume Finite Element Methods 6
1.3.3 Fully Developed Flows in Straight Ducts Subjected to Uniform, Steady, Electrical and Magnetic Fields 8
1.3.4 Three-dimensional Parabolic Flows in Ducts 9
1.3.5 Motion of a Particle in a Fluid Continuum 12
1.3.6 Particle Tracking Algorithms 14
1.3.7 Computer Simulation of Electromagnetic Separation 15
1.4 Overview of Thesis 16
2 Mathematical Models 17
2.1 Overview of the Physical Problem 17
2.2 Summary of Assumptions 18
2.3 Governing Equations for Three-dimensional Parabolic flow in a Duct 19
2.4 Governing Equations for Fully Developed Flow Subjected to Steady, Uniform, Electric and Magnetic Fields 21
2.5 Particle Momentum Equation 27
2.5.1 Drag Force 29
2.5.2 Buoyancy Force 30
2.5.3 Apparent Mass Force 30

2.5.4 Basset Force....31
2.5.5 Saffman Lift Force....32
2.5.6 Electromagnetic Force on the Particle....33
2.5.7 Simplified Form of the Particle Momentum Equation....34
2.5.8 Non-dimensional Form of the Particle Momentum Equation and Order-of-Magnitude Analysis....35
2.5 Restriction Necessary for One-Way Momentum Coupling Between the Molten Aluminum and the Inclusions....39
3 Numerical Solution Methods....41
3.1 Fully Developed Flow of Molten Aluminum....41
3.1.1 Review of the Problem of Interest....41
3.1.2 Review of the Governing Equations and Generalization....41
3.1.3 Control-Volume Finite Element Method....42
3.2 Particle Tracking Algorithm....51
3.2.1 Fourth-Order Runge-Kutta Scheme....53
3.2.2 Interpolation to Obtain the Local Fluid Velocity and Its Spatial Gradients....54
3.2.3 Method of Locating the Particle in the Triangular Finite Element Mesh....56
3.2.4 Method for Checking When Particle Reaches a Domain Boundary....62
4 Test Problems....65
4.1 Two-dimensional CVFEM for Fluid Flow....65
4.1.1 Problem Statement....65
4.1.2 Results for w_{max}/w_{av} and $f\,\mathrm{Re}$....66
4.1.2 Grid Independence Checks....68
4.2 Particle Settling in a Stationary Fluid Subjected to Gravity and Electromagnetic Forces....70
4.2.1 Problem Statement....70
4.2.2 Particle Terminal Velocity....72
4.2.3 Particle Velocity Distribution and Particle Trajectory....73
4.3 Motion of a Particle in a Couette Flow Layer Adjacent to A Solid, Impermeable, Plane Wall....74
4.3.1 Problem Statement....74

4.3.2 Particle Trajectories..... 76

4.4 Motion of a Particle in a Forced Vortex Flow Field, With and Without the Inclusion of Basset Force.....77

4.4.1 Problem Statement..... 77

4.4.2 Particle Trajectories..... 80

5 Demonstration Problem..... 82

5.1 Overview..... 82

5.2 Forces Experienced by the Particle Along its Trajectory..... 84

5.3 Parametric Study of Particle Trajectories.....88

5.4 Evaluation of the Effectiveness of an Electromagnetic Separation System.....101

5.4.1 Problem Statement..... 101

5.4.2 Pumping Power.....102

5.4.3 Power Required to Generate the Electric Field..... 102

5.4.4 Power Required to Generate the Magnetic Flux Density..... 103

5.4.5 Total Minimum Power Input..... 103

5.4.6 Effectiveness of EM Separation System..... 102

6 Conclusion..... 106

6.1 Review of the Thesis and its Main Contributions.....106

6.2 Recommendations for Extensions of This Work.....108

References.....110

List of Figures

2.1 Schematic illustration of the separation chamber.....18

3.1 Discretization of a calculation domain into three-node triangular elements and polygonal control volumes..... 43

3.2 Details of the domain discretization and related nomenclature: an internal node; (b) a boundary node with three associated elements; and (c) a boundary node with one associated element. 44

3.3 A typical three-node triangular element, related nomenclature, and a local Cartesian coordinate system.....45

3.4 Discretization of the calculation domain..... 51

3.5 Flowchart of computer program for calculating particle trajectories..... 52

3.6 The prismatic element that contains the particle, and related notation 55

3.7 Triangular element occupied by the particle..... 57

3.8 Special cases to illustrate the rules used to locate the particle..... 58

3.9 Particle location possibilities evaluated in subroutine LOCATE2D..... 59

3.10 Possible configurations of the triangular elements in the structured mesh.... 59

3.11 Example used to illustrate updating of the element for IQUAD=0, ITRI=1...61

3.12 Example of particle exiting domain at x=a (I=L1)..... 62

3.13 Back-calculation of final particle position at sidewall boundary..... 63

4.1 Variation of w_{max}/w_{avg} and fRe and with aspect ratio, AR, for fully developed flow in a rectangular duct - comparison of CVFEM results with published data (Lundgren et al., 1964; Shah and London, 1978)..... 68

4.2 Variation of the CVFEM results with grid refinement.....69

4.3 Particle settling in a stationary fluid under the influence of gravity and EM force: Particle velocity distribution and trajectory..... 73

4.4: Particle motion in a Couette flow layer adjacent to a solid, impermeable, plane wall..... 74

4.5 Particle trajectories in a Couette flow layer adjacent to a solid, impermeable, plane wall..... 77

4.6 Particle motion in a forced vortex flow.....78

4.7 Particle trajectory in a forced vortex for $\lambda = 0.5$, St = 0.022, and $\omega = 2$..... 80

5.1 Time-varying forces experienced by the particle for AR = 1, Re = 10, $B_x = 0.01$ T, and $D_p = 90\mu m$: (a) along the y direction; (b) along the z direction..... 86

5.2 Particle trajectory calculations with and without Basset and lift forces for the cases where Re = 10, $B_x = 0.01$ T, $D_p = 90\mu m$: (a) AR = 1; (b) AR = 0.5. 87

5.3 Particle trajectory calculations for AR = 1 and $D_p = 5$ μm..... 89

5.4 Particle trajectory calculations for AR = 1 and $D_p = 15$ μm..... 90

5.5 Particle trajectory calculations for AR = 1 and $D_p = 30$ μm..... 91

5.6 Particle trajectory calculations for AR = 1 and $D_p = 90$ μm..... 92

5.7 Particle trajectory calculations for AR = 0.5 and $D_p = 5$ μm..... 93

5.8 Particle trajectory calculations for AR = 0.5 and $D_p = 15$ μm..... 94

5.9 Particle trajectory calculations for AR = 0.5 and $D_p = 30$ μm..... 95

5.10 Particle trajectory calculations for AR = 0.5 and $D_p = 90$ μm..... 96

5.11 Particle trajectory calculations for AR = 0.2 and $D_p = 5$ μm..... 97

5.12 Particle trajectory calculations for AR = 0.2 and $D_p = 15$ μm..... 98

5.13 Particle trajectory calculations for AR = 0.2 and $D_p = 30$ μm..... 99

5.14 Particle trajectory calculations for AR = 0.2 and $D_p = 90$ μm..... 100

5.15 Schematic illustration of electromagnetic separation system.....101

5.16 Effectiveness of the EM separation vs. interaction parameter and Reynolds Number at AR = 1: (a) $D_p = 5\mu m$, and (b) $D_p = 90$ μm..... 105

List of Tables

1.1 Some inclusions found in molten aluminum (Engh, 1992)..... 2

2.1 Orders of magnitude of the dimensionless groups that multiply the various force terms in the nondimensionalized particle momentum equation..... 38

3.1 Possibilities that must be considered for the determination of the next search element for a returned value of ILOC..... 60

4.1 w_{max}/w_{avg} and $f\,\mathrm{Re}$ values for fully developed flow in a rectangular duct - comparison of CVFEM results with those of Lundgren et al. (1964) and Shah and London (1978)..... 67

4.2 Comparison of numerical and analytical solutions for the terminal velocity of a particle settling in a stationary fluid..... 72

5.1 Values of some of the nondimensional and dimensional parameters that characterize the demonstration problem..... 83

5.2 Orders of magnitude of the dimensionless groups in the non-dimensional particle momentum equation for AR = 1.0; Re = 100, B_o = 0.01T, and D_p = 90μm..... 85

Nomenclature

a	Width of duct cross-section
A	Ratio of particle Reynolds number to the square root of Reynolds number based on velocity gradient
A_{cs}	Duct cross-sectional area
AR	Rectangular duct aspect ratio (2b/2a)
b	Height of duct cross-section
c_D	Drag coefficient
C	Coefficient in Saffman's lift force term
C_m	Mass fraction of dispersed (particulate) phase in particle-fluid flow
D_h	Hydraulic diameter
D_p	Particle diameter
$\vec{B}$	Magnetic field strength
B_o	Magnitude of magnetic field strength
$\vec{E}$	Electric field strength
$\vec{F}_{BASSET}$	Basset force
$\vec{F}_{BUOYANCY}$	Buoyancy force
$\vec{F}_{DRAG}$	Drag force
$\vec{F}_{EM}$	Electromagnetic force
$\vec{F}_{LIFT}$	Lift force
$\vec{F}_{VIRTUAL\ MASS}$	Virtual mass force
$\vec{g}$	Gravitational acceleration
$\vec{i}, \vec{j}, \vec{k}$	Unit vectors in the x, y, and z directions, respectively
$\vec{j}$	Current density
L_{gr}	Length required for particle separation with gravity only
L_{em}	Length required for particle separation when EM-assisted

m_p	Mass of particle
M	Hartman number
N	Magnetic interaction parameter
p	Reduced pressure
$\bar{p}$	Cross-sectional area-averaged reduced pressure
$\tilde{p}$	Local perturbation of cross-sectional area-averaged reduced pressure
P	Static pressure
P_B	Power required to generate magnetic field
P_E	Power required to generate electric field
$P_{pumping}$	Power required to pump molten aluminum through EM separator
R	Electrical resistance per unit length of wire
R	Electrical resistance, and aspect ratio
Re	Conventional Reynolds number of fluid
Re_G	Reynolds number based on velocity gradient
Re_m	Magnetic Reynolds number
Re_p	Particle Reynolds number
RMT	Rate of momentum transport [eq. 3.20]
S_x, S_y, S_z	Components of the source term in the governing equation for fluid flow
St	Stokes number
t	Elapsed time
$\vec{U}$ or $\vec{U}_f$	Local fluid velocity
U_o	Mean cross-sectional fluid velocity
$\vec{U}_p$	Particle velocity
u, v, w or u_f, v_f, w_f	Components of the local fluid velocity
x, y, z	Cartesian coordinates
α_f	Volume fraction of fluid phase for particle-fluid flow

α_p	Volume fraction of particle phase for particle-fluid flow
δ	Ratio of particle diameter to duct width
ε	EM system effectiveness
ϕ	Ratio of particle velocity to fluid velocity
Γ	Constant which is defined by geometry of electromagnet
η	Fluid dynamic viscosity
λ	Ratio of particle density to fluid density
κ	Constant defined using mass concentration of particles in a fluid and the particle and fluid densities
μ	Magnetic permeability of fluid
ρ *or* ρ_f	Fluid density
ς *or* ς_f	Fluid kinematic viscosity
σ *or* σ_f	Electrical conductivity of fluid
σ_p	Electrical conductivity of particle
τ_V	Velocity response time of particle

Chapter 1

Introduction

1.1 Objectives

The main aim of this thesis is the formulation, implementation, and testing of some computational techniques for numerical studies of particle trajectories in molten aluminum subjected to applied electric and magnetic fields. The underlying subject is electromagnetic (EM) filtration of molten metals for the purpose of producing ultra-clean materials. Attention in this work is focused on computer simulations of fully developed flows inside a separation chamber and the modeling of particle trajectories in the molten aluminum.

First, an available control-volume finite element method (CVFEM) for the solution of two-dimensional, steady-state, diffusion problems was modified to enable the calculation of laminar, fully developed flows of Newtonian fluids in straight ducts of constant cross-section. Then, a rudimentary magnetohydrodynamics model was formulated and incorporated into the aforementioned CVFEM, and then used to study the effects of applied electric and magnetic fields on fully developed flows of molten aluminum. In this model, steady, uniform field strengths were prescribed, and it was assumed that the induced fields are negligible. This assumption allowed the formulation of a simplified magnetohydrodynamic model, in which Maxwell's equations are decoupled from the Navier-Stokes equations, and the electromagnetic force is incorporated into the Navier-Stokes equations as a volumetric source term.

Next, a particle momentum equation was formulated and examined to determine which forces have a significant impact on the particle trajectories. In the final simulations, the following forces were included: drag, buoyancy, virtual mass, Basset, lift, and electromagnetic (EM) forces. The trajectories of particles in the flow of molten aluminum were obtained by solving the particle momentum equation, using a fourth-order Runge-Kutta scheme. In the numerical implementation of this scheme, an algorithm suggested by Ren et al. (1995) was modified and adapted to locate the particle in a three-

dimensional finite element mesh, check whether the particle has reached a domain boundary, and determine local fluid velocities during the integration sequence.

1.2 Background and Motivation

The presence of solid impurities such as oxides and other non-metallic inclusions in metals can negatively impact the reliability and performance of processing operations and their products. Such impurities are particularly detrimental on fatigue strength and creep life of materials that are used at high temperatures (El-Kaddah et al., 1995). Inclusions of only a few microns in size can also be detrimental to surface finish and to the strength of materials subjected to high deformation rates and exhibiting small cross-sections (Shivkumar et al., 1991). Thus, progress in modern metals-processing technology is critically influenced by the ability to remove such harmful inclusions from the molten metal.

A key role of refining metallurgy is the removal of impurities and inclusions from molten metals. The impurities may include bits of the raw materials (ores) used in the metal extraction process, and materials picked up during the refining process itself - from the refractory walls, the atmosphere, or the slag. Some of the common particulate impurities (or inclusions) found in unfiltered molten aluminum are listed in **Table 1.1**.

***Table 1.1**: Some inclusions found in molten aluminum (Engh, 1992)*

Particle Type	Source	Typical Size (Microns)	Typical Concentration (p.p.m)
Carbides	Al_4C_3	1-20	5
Borides	TiB2 VB	1-3	10-50 0.5
Oxides	Al_2O_3 Oxides of Mg, Al Other alloy additions Refractories	10-20 1-100 100 100-500	0.01-2 0.01 0.01 0.01
Salts	Mg-Al, Na-K	10-20	0.01

Removal of inclusions has traditionally been carried out using methods such as sedimentation, flotation, and filtration (Eckert et al., 1984; Gauckler et al., 1985; Shivkumar et al., 1991; Frisvold et al., 1992). Gravity sedimentation is effective for cases

where the density differential between the particles and the fluid is sufficient, and it is practically limited to the separation of inclusions with effective diameter greater than 90-100μm (Eckert et al., 1984; Shivkumar et al., 1991). Flotation involves attaching the inclusions to gas bubbles that are passed through the melt, and is generally limited to particle sizes of 30-40μm effective diameter (Eckert et al., 1984; Shivkumar et al., 1991).

Filtration techniques utilize mediums such as packed beds made of refractory materials (for example, in deep-bed filtration), and ceramic foam, among others, and can be useful for particles even smaller than 30μm in effective diameter. The mechanism for inclusion removal when using filters is believed to vary with particle size. Mechanical entrapment appears to be the primary mechanism for particles greater than 30 μm, while surface adsorption appears to be dominant for particles that are smaller than 30 μm (Shivkumar et al., 1991). The large pressure drops associated with this methodology, however, can place a significant burden on the equipment used to pump or move the molten metal (Marty and Alemany, 1982). This methodology also requires the periodic replacement of filters.

Each of the aforementioned methods can find a place in a melt treatment system, depending on its suitability to remove a specific type and size range of inclusions. The commercial attractiveness of any particular method depends on the speed of inclusion removal, capital and energy costs, and the absence of significant technical problems during implementation and operation.

Electromagnetic (EM) filtration is a powerful technique for removing non-metallic particles from molten metal, because the particle migration velocity can be orders of magnitude higher than that of gravitational sedimentation, without exerting a significant additional burden *vis-à-vis* pumping requirements (El-Kaddah, 1996). EM filtration belongs to the category of inclusion removal techniques that exploit the differences in density, electrical conductivity, dielectric constant, and magnetic permeability between the particles and the molten metal. Using these property differences, it is possible to produce a relative velocity between the particle and the molten metal, by exposing the melt to gravitational and electromagnetic force fields. Under such conditions, given enough time, the particles may take on a stratified

arrangement adjacent to a free surface and/or be adsorbed onto solid surfaces at the edges of the separation chamber.

The EM force is generated by crossing electric and magnetic fields, and its impact on electrically non-conducting particles is independent of the particle composition, state (liquid or solid), and density (Patel and El-Kaddah, 1997). The effect of the EM force on the molten metal flow and the particle trajectories can be controlled with simple changes to the strengths and orientations of the electric and magnetic fields.

Several significant analytical and numerical studies have been reported on the topic of EM separation of inclusions from molten metal. They have generally invoked the assumption of fully developed flow (Patel and El-Kaddah, 1997; El-Kaddah, 1988; El-Kaddah, 1996). Furthermore, in the calculation of terminal migration velocity, consideration has been given to drag, buoyancy, and EM forces only. It appears that the effects of lift (associated with large velocity gradients encountered in the vicinity of walls), virtual mass, and Basset forces have been neglected.

In this work, fully developed flows of molten aluminum in the separation chamber are considered. A rudimentary magnetohydrodynamics model is then proposed to enable a study of the effects of applied uniform and steady electric and magnetic fields. Following that, the particle momentum equation is presented and discussed in detail. The lift, virtual mass, and Basset forces are included in the analyses, in addition to the drag, buoyancy, and EM forces.

1.3 Literature Review

There are numerous books that comprehensively cover the basic subjects of thermodynamics, fluid mechanics, and heat transfer. Examples include the works of Bird et al. (1960), Batchelor (1967), Schlichting (1968), Eckert and Drake (1972), Currie (1974), Tritton (1988), Incropera and DeWitt (1990), White (1991), Moran and Shapiro (2000), and Kreith and Bohn (2001). Authoritative overviews of particular topics in these subjects are available in the works of Johnson (1998), Rohsenow and Hartnett (1973), and Harnett et al. (1961-2001).

In the published literature, there are innumerable papers that deal with electromagnetism, electrostatics, electrostatic precipitation, electrohydrodynamics (the

coupling of electric and velocity fields in a dielectric fluid continuum), and magnetohydrodynamics (the phenomena that arise when electromagnetic fields are applied to an electrically conducting fluid). Excellent presentations, overviews, and discussions of these subjects can be found in the works of Panofsky and Phillips (1956), Cowling (1957), Romig (1964, 1973), Kalikhman (1967), Moore (1972), Branover (1978), Davidson et al. (1987), and Hoole and Hoole (1995).

There have also been a tremendous number of contributions to the subjects of numerical analysis and computational fluid dynamics (finite difference, finite volume, and finite element methods for fluid flow and heat transfer). Excellent coverage of these subjects has been provided, for example, by Segerlind (1976), Patankar (1980), Roache (1982), Baker (1983), Reddy (1993), Anderson (1995), Zienkiewicz (1977), Minkowycz and Sparrow (1997), Burden and Faires (1997), and Ferziger and Peric (1999).

The subject of single-phase, laminar, forced convection in ducts has been covered comprehensively in the work of Shah and London (1978). The subjects of gas-particle and liquid-particle flows have been covered in detail in books by Crowe et al. (1998), and Fan and Zhu (1998). Detailed coverage of the subject of filtration of metals is available in the works of Anders (1976), Eckert et al. (1984), Frisvold et al. (1992), and Engh (1992).

The literature review in the remainder of this section is limited to topics that are directly relevant to this thesis. In particular, the following topics are reviewed briefly: electromagnetic filtration; control-volume finite element methods; fully developed flows in ducts; three-dimensional parabolic flows in ducts; motion of a particle in a fluid continuum; particle tracking algorithms; and computer simulation of electromagnetic separation.

1.3.1 Electromagnetic Filtration

EM filtration technology relies on the forces generated in the molten metal by external electric and magnetic fields. For particles modelled as rigid, uncharged, smooth spheres, the magnitude of the applied fields and the difference in electrical conductivity between the particle and the melt are the main variables that influence the effectiveness of

the filtration process, *in addition to those that govern traditional (non-electromagnetic) filtration.*

Initially, the main application for EM filtration (also referred to as magnetohydrodynamic and magnetohydrostatic separation) was the segregation of electrically conducting minerals in an electrolyte. The first patent for such a device appears to be that of Gates (1900), whose invention consisted of deflecting particles of differing electrical conductivity into separate collectors as they descended through an electrolyte. His design was later improved upon by Stroble (1942), who developed the first continuous EM separator. The application of EM filtration to non-metallic particles in molten metals was introduced by Verte (1961) and was based on applied DC electric and magnetic fields. It became evident through subsequent research (summarized by Andres, 1976), that the stirring effect in the melt due to EM forces had to be minimized by careful separator design. This problem was the main reason why promising laboratory experiments could not be successfully implemented in large-scale industrial applications.

Since the late 1980s, proposals for the use of induced EM fields, generated by the application of time-periodic magnetic fields (Hobson et al., 1988; Conti et al., 1989; El-Kaddah, 1990), have prompted a renewed interest in the field of EM filtration of molten metals.

1.3.2 Control-Volume Finite Element Methods

The control-volume finite element method (CVFEM) is a powerful technique in computational fluid dynamics (CFD). It takes advantage of the grid-independent, local and global, conservation properties of the finite volume method (FVM) while providing the capability to address complex geometries, using the flexible meshing aspects of the finite element method (FEM). The steps involved in the formulation of CVFEMs are the following:

1. Discretization of the calculation domain into elements.
2. Construction of non-overlapping control volumes around each node, such that the resultant control-volume occupies a portion of each of the elements that share a common node, and collectively, these control volumes fill the calculation domain completely.

3. Prescription of functions that are used to interpolate the nodal values of the dependent variables and the thermo-physical properties of the fluid over each element.
4. Assembly of algebraic approximations to the governing integral conservation equations applied to individual control-volumes.
5. Solution of the algebraic (or discretized) sets of equations

The seminal works on CVFEMs for fluid flow and heat transfer are those of Baliga (1978) and Baliga and Patankar (1980). They proposed a planar, two-dimensional, CVFEM that incorporated a flow-oriented upwind (FLO) scheme as the interpolation function for deriving an algebraic approximation to convective transport of dependent variables across control-volume boundaries. To preclude unrealistic pressure oscillations in the computed pressure field, they also proposed an unequal-order discretization of the domain into two sets of elements and corresponding control-volumes: one finite element mesh was used to discretize the pressure field; and the other, finer, finite element mesh was used to discretize the velocity components and all other dependent variables. Subsequent extensions of this CVFEM include the following developments:

1. More robust interpolation functions for approximating convective transport of dependent variables, such as the donor-cell method of Prakash (1986) and the mass-weighted (MAW) skew upwind scheme (Hassan et al., 1983; Schneider and Raw, 1986; Saabas, 1991; Baliga and Saabas, 1992; Masson et al., 1994). These techniques are good at preventing negative coefficients in the discretized equations, which can lead to nonphysical solution oscillations and possible divergence of the iterative solution methods (Patankar, 1980), but they are less accurate than the FLO scheme (Masson et al., 1994).
2. Introduction of a co-located equal-order formulation based on a novel momentum interpolation scheme (Prakash and Patankar, 1985). This approach allows the discretization of the calculation domain with just one set of elements and control volumes, while avoiding physically untenable pressure oscillations.
3. Formulations that work with structured and unstructured two-dimensional axisymmetric meshes (Masson et al., 1994), three-dimensional structured

meshes (Saabas, 1991; Saabas and Baliga, 1994), and two-dimensional unstructured, adaptive meshes based on error estimation and minimization (Venditti, 1998; Venditti and Baliga, 1998).

Comprehensive reviews of the development of the CVFEM for the prediction of two- and three-dimensional fluid flow and heat transfer phenomena can be found in the works of Hookey (1989), Saabas (1991), Baliga and Saabas (1992), Baliga (1997), and Venditti (1998).

1.3.3 Fully Developed Flows in Straight Ducts Subjected to Uniform, Steady, Electrical and Magnetic Fields

In this work, attention is limited to steady, laminar, electrically conducting, Newtonian fluid flows in straight ducts of uniform cross-section, subjected to uniform, steady, electrical and magnetic fields. The walls of the ducts of interest are electrical nonconductors. If the flows in such ducts remain isothermal, or if the fluid properties can be assumed constant, then after a sufficient distance downstream from the inlet plane of the duct, the cross-stream velocity components vanish, the axial velocity component ceases to change with axial distance, the pressure distribution in any cross-section adapts to balance the imposed volumetric EM force, and the pressure gradient in the axial direction takes on a constant value. When these conditions are achieved, the flow is termed fully developed (Shah and London, 1978; Patankar, 1980).

The equation that governs the cross-sectional distribution of the axial velocity component in the fully developed regime is akin to that which governs heat conduction or diffusion problems (Patankar, 1980). For such fully developed flows in straight ducts of uniform rectangular and circular cross-sections, the governing equation can be solved analytically (Shah and London, 1978). This equation can also be readily solved numerically, using finite difference, finite volume, or finite element methods, in ducts of rectangular, circular, or arbitrary cross-sections (Shah and London, 1978; Patankar, 1980; Raithby and Schneider, 1988; Reddy, 1993). In this work, a control-volume finite element method (CVFEM) for two-dimensional conduction-type problems (Baliga and Patankar, 1988; Baliga, 1997) was adapted to predict the fully developed flows of interest.

1.3.4 Three-dimensional Parabolic Flows in Ducts

As was stated earlier, attention in this thesis is devoted mainly to the fully developed flow regime. An interesting and useful extension of this work would be an examination of the influence of the three-dimensional parabolic, or developing flow, regime on the performance of the EM filtration process. With this point in mind, as a part of this work, available methods for the prediction of three-dimensional parabolic flows in ducts were reviewed: the findings are reported in this section.

Steady subsonic flows in ducts can be categorized as elliptic, parabolic, or partially-parabolic (Patankar and Spalding, 1972; Pratap and Spalding, 1976; Patankar, 1980). In elliptic flows, the conditions at any point can be influenced by conditions at any other point in the flow. The mechanisms that cause this interaction are convection, diffusion, and pressure transmission (Patankar, 1980). On the other hand, parabolic flows in ducts are characterized by the following features: there exists a predominant flow direction along the duct, and no flow reversal is encountered in that direction; diffusive transport in the direction of the main flow is negligible compared to the corresponding convective transport and the cross-stream diffusive transport; and the downstream pressure field has relatively very little influence on upstream conditions (Patankar and Spalding, 1972; Patankar, 1980). When these conditions are satisfied, the main flow direction can be regarded as a one-way coordinate, in the sense that upstream conditions can influence the downstream conditions, but not vice-versa (Patankar, 1980). The term partially-parabolic is used to describe a class of flows that is intermediate to the parabolic and elliptic categories. They are similar to parabolic flows in that they have a predominant flow direction along which there is no flow reversal, and diffusive transport in that direction is negligible. However, the pressure transmission in partially-parabolic flows is similar to that in elliptic flows, and it is the dominant transmitter of influences in the upstream direction (Pratap and Spalding, 1976). Steady, laminar, developing, Newtonian fluid flows in straight ducts of uniform cross-section can be regarded as parabolic in the main-flow direction (Patankar and Spalding, 1972; Patankar, 1980).

The equations that govern three-dimensional parabolic flows in ducts are intrinsically nonlinear and coupled to each other. In analytical and semi-analytical approaches to the solution of these equations, the inertia terms are linearized and cross-

stream pressure gradients are neglected (Sparrow et al., 1964; Fleming and Sparrow, 1969). Thus, such approaches are limited to problems in which the cross-stream velocity components are negligible, and even then, they cannot handle non-linearities introduced, for example, by non-constant fluid properties. Numerical methods, on the other hand, enjoy a considerably greater degree of versatility, and are better suited for the solution of practical problems (Patankar, 1980).

The pioneering efforts in the development of numerical methods for the prediction of three-dimensional parabolic flows in ducts are the works of Caretto et al. (1972), Curr et al. (1972), and Patankar and Spalding (1972). These methods fully take into account the fluid stresses, diffusive fluxes, and pressure variations in the cross-stream planes. The method proposed by Patankar and Spalding (1972) is one of the most widely referenced of the finite volume methods for the prediction of three-dimensional parabolic flows in ducts. It is based on a pressure-velocity (primitive variables) formulation, and uses a non-iterative marching integration technique to advance the solution in the downstream direction, cross-section by cross-section, starting from the inlet plane where the values of the dependent variables are specified. The non-iterative nature of this method is achieved by using the upstream values of the dependent variables at each axial step to calculate the coefficients in the discretized governing equations. In each cross-sectional plane, Patankar and Spalding (1972) used staggered Cartesian grids for the storage of the velocity components and pressure, in order to avoid pressure-velocity decoupling, and they proposed a scheme called the Semi-Implicit-Method-for-Pressure-Linked-Equations (SIMPLE) for the solution of the coupled, non-linear, discretized equations. SIMPLE and its many variants are now used in most finite volume methods for the prediction of complex two- and three-dimensional fluid flows (Van Doormaal and Raithby, 1984; Raithby and Schneider, 1988). In subsequent papers, Carlson and Hornbeck (1973), and Briley (1974) have proposed methods that are variations of the Patankar-Spalding method. The methods proposed by Caretto et al. (1972), Curr et al. (1972), Patankar and Spalding (1972), Carlson and Hornbeck (1973), and Briley (1974) have been quite successful in the prediction of three-dimensional parabolic fluid flows, but they all suffer from the following short comings: (i) they are limited to ducts in which the boundaries of the cross-section lie along the axes of commonly used orthogonal coordinate systems

(often referred to as regular-shaped cross-sections); (ii) the non-iterative marching integration schemes used in these methods necessitate the use of relatively small axial step sizes; and (iii) in fluid flow problems that involve a large number of dependent variables (for example, flows with heat and mass transfer, and turbulent flows), the overall solution schemes, due to their non-iterative nature, tend to be sensitive to the sequence in which the dependent variables are solved.

Three-dimensional parabolic flow and heat transfer in ducts of irregular-shaped cross-sections can be solved using finite difference or finite volume methods which employ coordinate transformation techniques, or formulations based on curvilinear orthogonal and non-orthogonal coordinates (Roberts and Forester, 1979; Shyy, 1994). Such approaches usually complicate the governing equations, making physical interpretations of the overall numerical formulation quite difficult, and they are not very well suited for handling highly irregular and/or multiply-connected domains. Fluid flows in ducts of irregular-shaped cross-section are best handled by methods that employ finite elements to discretize the calculation domain (Baliga, 1997).

Most currently available finite-element methods for three-dimensional parabolic flows are based on the Galerkin method (Zienkiewicz, 1977; Baker, 1983; Reddy, 1993). One of the earliest attempts to develop such methods is that of Baker (1974). His method is formulated for the solution of three-dimensional compressible and reacting boundary-layer flows (Schlichting, 1968), and all of the discretized governing equations are solved simultaneously. Thus, it cannot be easily adapted to solve duct flow problems, and the computer storage requirements in this method could become disproportionately large, especially in complex problems involving several coupled dependent variables. Del Giudice et al. (1981) have proposed a finite element method that overcomes these limitations. However, their method is based on a non-iterative formulation akin to that used in the finite difference method of Briley (1974), and thus suffers from the limitations mentioned earlier in this subsection.

Pham (1983) has proposed a control-volume finite element method (CVFEM) for three-dimensional parabolic flows in ducts. His method overcomes most of the aforementioned limitations. However, it is an extension of the original two-dimensional elliptic CVFEM of Baliga and Patankar (1983), which is based on an unequal-order

formulation, that uses six-node triangular macroelements, each subdivided into four three-node triangular subelements: pressure is stored at the three vertices of the macroelements; and velocity components are stored at the three vertices of the finer subelements. In the 1970s and the early 1980s, such unequal-order finite-element formulations were used to avoid pressure-velocity decoupling, and the consequent checkerboard pressure distributions, in the solution of incompressible fluid flow problems (Patankar, 1980; Baliga, 1997). However, in unequal-order methods, the topological (grid-related) bookkeeping and associated coding is tedious. Furthermore, the unequal-order formulation becomes quite inaccurate, and hence unnecessarily expensive, in simulations of flows with high Reynolds and/or Peclet numbers, and its extension to three-dimensional elliptic flows is not straightforward (Baliga, 1997). Unequal-order methods have since been replaced by equal-order, co-located, methods that employ the so-called momentum interpolation technique (Rhie and Chow, 1983; Prakash and Patankar, 1985; Rice and Schnipke, 1986) to avoid pressure-velocity decoupling in the solution of incompressible flow problems. Examples of equal-order co-located CVFEMs based on the momentum interpolation technique can be found in the works of Prakash and Patankar (1985), Schneider and Raw (1986), Saabas and Baliga (1994), and Masson et al. (1994). A detailed review of these methods is available in an article by Baliga (1997).

It would be useful to modify and extend the two-dimensional, equal-order, co-located CVFEM of Masson et al. (1994) so that it could be used to predict three-dimensional parabolic flows in ducts. Some of the ideas proposed in the work of Pham (1983) could be incorporated in such a CVFEM: for example, at each axial step, a fully implicit scheme could be used to discretize the governing equations, and the resulting coupled, nonlinear, discretized equations could be solved iteratively. In Chapter 6, the concluding chapter of this thesis, the formulation, implementation, and application of such a three-dimensional parabolic CVFEM is recommended as one of the possible extensions of this work.

1.3.5 Motion of a Particle in a Fluid Continuum

The classical formulation of the motion of a particle in a fluid continuum is based on perturbation theory, whereby the individual terms in the governing momentum

equation are derived using a localized analysis of the disturbance flow field associated with the presence of a sphere. The forces on the spherical particle are then expressed in terms of the local velocity in an undisturbed flow, thus facilitating calculations of momentum transfer between the two phases.

In some of the earliest works in this area, the particle momentum equation was derived for rigid spheres settling out under gravity in a stationary fluid. Examples of such efforts include the combined works of Basset (1888), Boussinesq (1903), and Oseen (1927). In more current versions of the Basset-Boussinesq-Oseen (BBO) equation, the product of the particle mass and its acceleration is equated to the following forces on the particle: (1) steady-state drag force; (2) buoyancy force; (3) virtual mass force; (4) Basset force; and (5) lift force (Rubinow and Keller, 1961; Saffman, 1965; Maxey and Riley, 1983; Crowe et al. 1998).

Saffman (1965) analyzed the translation of a rigid, smooth, sphere in a linear unbounded shear flow, using matched asymptotic expansions. He obtained an expression for the lift force that is valid for low Reynolds numbers based on shear, relative velocity, and angular velocity. The works of Cherukat and McLaughlin (1990), McLaughlin (1991), Asmolov (1993), Cherukat et al. (1994, 1999), and Naumov (1995, 1997) have gone further to develop an expression for the inertial lift that allows for higher Reynolds numbers and accounts for the effects of proximity to walls.

Additional considerations which have been reported in the published literature include the incorporation of Reynolds number effects, turbulence effects, blowing effects due to particle evaporation, particle-particle interactions, and other body forces such as the magnetohydrodynamic (MHD) force employed in this study (Leenov and Kolin, 1954; Vives and Ricou, 1982; Crowe et al. 1998). Leenov and Kolin (1954) used perturbation theory to derive the electromagnetic (EM) separation force on spherical and cylindrical particles due to the local disturbance of the electric field. Their expression is a function of electric and magnetic field strengths and the difference in electrical conductivities of the particle and fluid. The Leenov-Kolin model for the EM separation force is based on the assumption that there are no particle-particle interactions, and the undisturbed electric current density and magnetic fields are uniform. Subsequent experimental works by Marty and Alemany (1982), and Marty et al. (1982) have

confirmed the theoretical results of Leenov and Kolin, which have served as the basis of most subsequent computational studies of EM filtration (Andres 1976, El-Kaddah 1988).

1.3.6 Particle Tracking Algorithms

In numerical simulations of dispersed particles moving in a continuous fluid, it is common to employ a Eulerian-Lagrangian formulation. In such a formulation, the fluid flow is predicted by solving a suitable mathematical model in an Eulerian frame of reference, and the particle trajectories are predicted by solving an appropriate Lagrangian mathematical model. For sufficiently small particles and dilute fluid-particle flows, the momentum coupling is assumed to be one-way, such that the solution to the fluid flow can be obtained independently prior to running a particle-tracking algorithm (Crowe et al. 1998).

Patankar and Karki (1999) have suggested that the two main considerations in the solution of particle trajectories of this sort are (1) the particle locating methodology, and (2) the selection of a suitable time step in order to optimize the trajectory solution in terms of speed and accuracy.

Ren et al. (1995) have proposed a relatively simple and efficient method for locating a particle in a finite element mesh, based on barycentric coordinates (in three dimensions) or area coordinates (in two dimensions). It works in planar two-dimensional meshes consisting of triangular elements by calculating the area coordinates of the latest particle position with respect to the coordinates of the three vertices of the previously occupied element. When all three area coordinates are greater than zero but less than one, then the particle is still within the same element. If not, then there exists a set of rules, which determines the most likely adjacent element to which the particle has moved. Once the occupied element is determined, the area coordinates can be directly used to compute the local continuous phase velocity. The time step selection is based on the particle relaxation time (Crowe et al., 1998).

The work presented in this thesis required particle tracking in fully developed flows, on three-dimensional finite element meshes that were used to discretized the space within straight ducts of uniform cross-section. The particle locating methodology employed in this work consists of identifying the location of the particle in the

longitudinal, or main flow, direction using linear interpolation, and then averaging the cross-sectional coordinates of the particle in the upstream and downstream planes, obtained using a two-dimensional locating algorithm akin to that of Ren et al. (1995).

1.3.7 Computer Simulation of Electromagnetic Separation

Numerical simulations of MHD flows have been used extensively in the metals industry to study flow patterns during EM stirring of the melt prior to casting (El-Kaddah et al., 1984; El-Kaddah et al., 1986; Antille et al., 1992). These studies allowed the development of a capability to analytically design processes that provide a high level of homogeneity in the cast ingots and ensure that molten metal is pushed into all parts of the mold, even during the casting of complex-shaped objects.

The research carried out by El-Kaddah (1988) was one of the first applications of computer simulations for calculating particle trajectories in an EM separation process. Their model was applied to an EM separator, developed by the Oak Ridge National Laboratory (Hobson et al. 1988), that uses an alternating magnetic field and an induced electric field in the melt. Subsequent investigations (El-Kaddah et al., 1995; El-Kaddah, 1996) were aimed at analyzing more efficient separator configurations and validating the numerical model by comparing the predictions to the results of EM filtration experiments.

The goal in the aforementioned simulations was to compute the terminal migration velocity of the inclusions and to determine the length of chamber needed for effective filtration. The models are characterized by simplifications in the EM field equations, in order to make the continuity and Navier-Stokes equations the only governing equations for the fluid flow problem, with a Lorentz force added to the volumetric source terms. Thus, the complex task of solving the complete set of Maxwell's equations is omitted. The problem is further simplified by assuming fully developed flow. As these models are based on the assumption of non-interacting particles, and balance the EM force only against viscous drag on the particle, there are limitations associated with cases where the influence of adjacent particles and the magnitude of other forces on the particle become significant. Furthermore, the impact of the developing flow regime on the overall separator efficiency has not been studied.

1.4 Overview of the Thesis

In the present chapter, the objectives of this thesis and its motivation have been summarized, and an overview of the relevant literature has been presented.

In Chapter 2, the physical problem of interest is introduced, and mathematical models for fluid flow and particle tracking are presented and discussed.

In Chapter 3, the numerical methods formulated and used for the solution of the mathematical models are described.

In Chapter 4, validations of the proposed numerical methods are presented. The proposed methods are used to solve the mathematical models of test problems, and their results are checked against those available in the published literature.

In Chapter 5, the results of a numerical study of several specific EM separation problems are presented and discussed, in order to demonstrate the applicability and scope of the proposed numerical solution methods.

In Chapter 6, the main contributions of this research effort are reviewed, and some recommendations for extensions of this work are presented.

Chapter 2

Mathematical Models

2.1 Overview of the Physical Problem

The problem of interest involves the prediction of inclusion (particle) trajectories in molten aluminum subjected to electromagnetic fields. This problem is schematically illustrated in **Figure 2.1.** The separation chamber is a straight duct of constant rectangular cross-section. The molten aluminum is fed to the duct from a large upstream plenum, and it is assumed to enter with a uniform velocity normal to the inlet plane. At that point, the relative velocity between the inclusions and the molten aluminum is assumed to be zero. Within the separation chamber, the inclusions migrate laterally under the action of surface and body forces that they experience. After a sufficiently large distance downstream of the inlet, the fluid flow becomes fully developed, as was discussed in **Section 1.3.3**.

The longitudinal axis of the separation chamber is oriented along the z-direction of the Cartesian coordinate system. Immersed electrodes, upstream and downstream of the chamber, generate an electric field so that the current flows in the positive z-direction, parallel to the main fluid flow. The applied magnetic field is generated by a suitable electromagnet, such that the field strength is uniform throughout the separation chamber and is oriented in the x-direction, parallel to the wider side of the duct, as illustrated in **Figure 2.1**. These electric and magnetic fields create a resultant electromagnetic (EM) body force on the electrically conducting molten aluminum (similar to the manner in which a current carrying wire experiences a force in the presence of a transverse magnetic field).

In order to predict the inclusion trajectory in the molten aluminum within the separation chamber, it is necessary to solve its momentum equation, which contains surface and body force terms. The most significant of these forces can be interpreted as the drag, buoyancy, virtual (or apparent) mass, Basset (or history), lift, and EM forces. Details are presented later in this chapter, in **Section 2.5**.

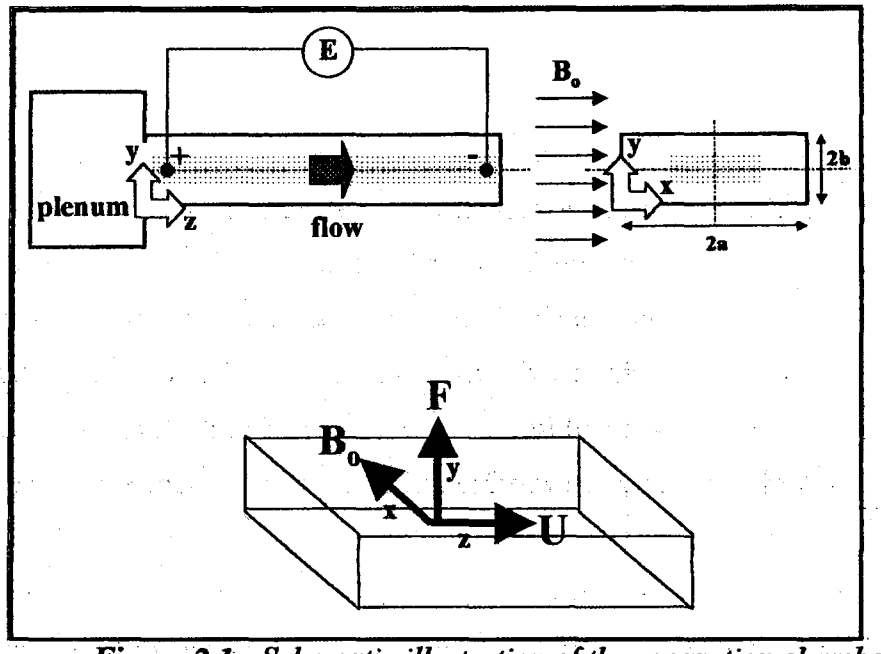

Figure 2.1 - Schematic illustration of the separation chamber

2.2 Summary of Assumptions

This section provides a summary of the assumptions used in the formulation of the electromagnetic filtration model. Further discussions of some of these assumptions are provided in subsequent sections of this chapter.

Fluid Flow

- Steady-state conditions prevail throughout
- Laminar flow
- Newtonian fluid
- Constant fluid mass density, ρ, and dynamic viscosity, η
- The entire fluid domain is isothermal
- There is no flow reversal in the z direction. The fluid flow can be modeled either as a three-dimensional developing parabolic flow, or, after a sufficient distance downstream of the inlet plane, as a two-dimensional fully developed flow.

- The concentration of the inclusions (particles) is low enough that they have no noticeable influence on the fluid flow, though the fluid flow has a significant influence on the inclusion trajectories. In other words, there is only one-way coupling in the transfer of momentum between the molten aluminum and the inclusions (Crowe et al., 1998).

Particle Trajectory

- The particles are all rigid, smooth spheres
- Particle-particle interactions are negligible
- The particle Reynolds number is within the Stokes flow regime (Crowe et al., 1998)

Electromagnetic Effects

- The particles move at non-relativistic speeds
- The particles are neutrally charged
- The applied electric and magnetic fields are uniform and constant
- The applied electric field is along the mainstream, or z coordinate, direction: $\vec{E} = (0, 0, E_z)$
- The applied magnetic field is orthogonal to the electric field: $\vec{B} = (B_x, B_y, 0)$
- The walls of the separation chamber are electrically non-conducting
- The induced electric field in the liquid is negligible

2.3 Governing Equations for Three-Dimensional Parabolic Flow in a Duct

As was stated in Chapter 1, attention in this thesis is focused on fully developed flows in the separation chamber. Nevertheless, it is instructive, useful, and convenient to examine the mathematical model for three-dimensional parabolic flow in a duct, before

presenting the mathematical model for the fully developed flows of interest. The governing equations and discussions in this section are presented in this spirit.

For the horizontal duct depicted in **Figure 2.1**, a reduced pressure, p, is defined as follows:

$$p = P + \rho g y \tag{2.1}$$

where P is the static pressure, ρ is the fluid density, and g is the gravitational acceleration. Following Patankar and Spalding (1972), the reduced pressure field in the duct is now expressed as follows:

$$p(x,y,z) = \bar{p}(z) + \tilde{p}(x,y,z) \tag{2.2}$$

where $\bar{p}(z)$ is the cross-sectional area-averaged reduced pressure at any given stream-wise location, z, and is given by:

$$\bar{p}(z) = \frac{\iint_A p(x,y,z)\,dx\,dy}{\iint_A dx\,dy} \tag{2.3}$$

For three-dimensional parabolic flow in a duct, as discussed by Patankar and Spalding (1972), there is no flow reversal in the z direction, and the diffusion transport in the mainstream direction is negligible compared to the corresponding advection transport and the diffusion transport in the cross-sectional plane. Furthermore, $d\bar{p}/dz >> \partial\tilde{p}/\partial z$, and the spatial derivatives of the reduced pressure can be approximated by:

$$\begin{aligned} \frac{\partial p}{\partial x} &= \frac{\partial \tilde{p}}{\partial x} \\ \frac{\partial p}{\partial y} &= \frac{\partial \tilde{p}}{\partial y} \\ \frac{\partial p}{\partial z} &\cong \frac{d\bar{p}}{dz} \end{aligned} \tag{2.4}$$

With respect to the Cartesian coordinate system shown in **Figure 2.1** and the assumptions listed in **Section 2.2**, the governing equations for three-dimensional parabolic fluid flow in the separation chamber are the following:

x-momentum equation

$$\frac{\partial}{\partial x}(\rho uu)+\frac{\partial}{\partial y}(\rho vu)+\frac{\partial}{\partial z}(\rho wu)=-\frac{\partial \tilde{p}}{\partial x}+\frac{\partial}{\partial x}\left(\eta\frac{\partial u}{\partial x}\right)+\frac{\partial}{\partial y}\left(\eta\frac{\partial u}{\partial y}\right)+F_{EM,UnitVol,x} \tag{2.5}$$

y-momentum equation

$$\frac{\partial}{\partial x}(\rho uv)+\frac{\partial}{\partial y}(\rho vv)+\frac{\partial}{\partial z}(\rho wv)=-\frac{\partial \tilde{p}}{\partial y}+\frac{\partial}{\partial x}\left(\eta\frac{\partial v}{\partial x}\right)+\frac{\partial}{\partial y}\left(\eta\frac{\partial v}{\partial y}\right)+F_{EM,UnitVol,y} \tag{2.6}$$

z-momentum equation

$$\frac{\partial}{\partial x}(\rho uw)+\frac{\partial}{\partial y}(\rho vw)+\frac{\partial}{\partial z}(\rho ww)=-\frac{d\tilde{p}}{dz}+\frac{\partial}{\partial x}\left(\eta\frac{\partial w}{\partial x}\right)+\frac{\partial}{\partial y}\left(\eta\frac{\partial w}{\partial y}\right)+F_{EM,UnitVol,z} \tag{2.7}$$

Continuity equation

$$\frac{\partial}{\partial x}(\rho u)+\frac{\partial}{\partial y}(\rho v)+\frac{\partial}{\partial z}(\rho w)=0 \tag{2.8}$$

The following section describes the derivation of the electromagnetic body force per unit volume, $\vec{F}_{EM,UnitVol}$, the components of which are inserted in Equations (2.5) to (2.7) as volumetric source terms.

2.4 Governing Equations for Fully Developed Flow Subjected to Steady, Uniform, Electric and Magnetic Fields

In this section, the governing magnetohydrodynamic (MHD) equations are presented, starting with the general forms of these equations for steady problems and then incorporating the simplifying assumptions for the particular problem being studied in this thesis.

The formulation of the MHD problem for isothermal, constant-property, liquid metal flows subjected to arbitrary, but steady, electromagnetic fields requires the simultaneous solution of 13 coupled equations (Romig, 1964; Branover, 1978; Davidson et al., 1987):

Navier-Stokes equations

$$\left(\vec{U}\cdot\vec{\nabla}\right)\vec{U} = -\frac{1}{\rho}\vec{\nabla}p + \zeta\nabla^2\vec{U} + \frac{1}{\rho}\left(\vec{j}\times\vec{B}\right) \tag{2.9}$$

Continuity equation

$$\vec{\nabla}\cdot\vec{U} = 0 \tag{2.10}$$

Maxwell's equations

$$\begin{aligned} &\vec{\nabla}\times\vec{E} = 0 \\ &\vec{\nabla}\times\vec{B} = \mu\vec{j} \\ &\vec{\nabla}\cdot\vec{B} = 0 \\ &\vec{\nabla}\cdot(\varepsilon\vec{E}) = \varepsilon\vec{\nabla}\cdot\vec{E} = 0 \end{aligned} \tag{2.11}$$

Ohm's law

$$\vec{j} = \sigma\left(\vec{E} + \vec{U}\times\vec{B}\right) \tag{2.12}$$

where,

$\vec{B}$ = Magnetic Flux Density $[T]$
$\vec{E}$ = Electric Field Strength $[V/m]$
$\vec{j}$ = Current Density $[A/m^2]$
p = Reduced Pressure $[N/m^2]$
$\vec{U}$ = Fluid Velocity $[m/s]$
ε = Dielectric Constant $[C/m-V]$
ζ = Fluid Kinematic Viscosity $[m^2/s]$
μ = Magnetic Permeability of Fluid $[H/m]$
ρ = Fluid Density $[kg/m^3]$
σ = Electrical Conductivity $[mho/m]$

Here, it is implicitly assumed that the dielectric constant, ε, and the magnetic permeability, μ, of the molten metal in the separation chamber are constants, and the walls of this chamber are electrically non-conducting.

The following dimensionless variables and parameters will now be used to express the governing MHD equations in nondimensional form:

$$\nabla^* = a\nabla \;;\; U^* = \frac{U}{U_o} \;;\; p^* = \frac{p - p_{ref}}{\rho U_o^2}$$
$$B^* = \frac{B}{B_o} \;;\; j^* = \frac{j}{B_o / \mu a} \;;\; E^* = \frac{E}{U_o B_o} \tag{2.13}$$
$$\mathrm{Re} = \frac{U_o a}{\varsigma} \;;\; N = \frac{\sigma B_o^2 a}{\rho U_o}$$
$$\mathrm{Re}_m = \mu\sigma U_o a \;;\; M = \sqrt{N \cdot \mathrm{Re}} = B_o a \sqrt{\frac{\sigma}{\eta}}$$

In these equations, a is a characteristic length of the duct; U_o is the mean velocity of the molten aluminum inside the separation chamber; B_o is the applied magnetic flux density; and Re is the conventional Reynolds number based on U_o and a. The magnetic interaction parameter (also known as the Stuart number), N, is the ratio of EM (or ponderomotive) force to inertia force; and the square of the Hartman number, M, is the ratio of EM force to viscous force. The magnetic Reynolds number, $\mathrm{Re_m}$, characterizes the interaction between the applied magnetic field and the induced currents. When $\mathrm{Re_m} \ll 1$, the induced electric field is negligible, and this allows the decoupling of the Maxwell's equations from the Navier-Stokes equations.

Substituting the dimensionless variables and parameters into the governing equations *and dropping the star superscripts* the following nondimensional forms of the governing MHD equations were obtained:

Navier-Stokes equations (nondimensional form)

$$\left(\vec{U}\cdot\vec{\nabla}\right)\vec{U} = -\vec{\nabla}p + \frac{1}{\mathrm{Re}}\nabla^2\vec{U} + N\left(\vec{E}\times\vec{B} + \vec{U}\times\vec{B}\times\vec{B}\right) \tag{2.14}$$

Continuity equation (nondimensional form)

$$\vec{\nabla}\cdot\vec{U} = 0 \tag{2.15}$$

Maxwell's equations (nondimensional form)

$$\vec{\nabla}\times\vec{E} = 0 \tag{2.16}$$

$$\vec{\nabla}\times\vec{B} = \mathrm{Re}_m\left(\vec{E} + \vec{U}\times\vec{B}\right) \tag{2.17}$$

$$\vec{\nabla}\cdot\vec{B}=0 \tag{2.18}$$

$$\vec{\nabla}\cdot\vec{E}=0 \tag{2.19}$$

Equation (2.17) shows that induced fields can be neglected for $Re_m \ll 1$. For liquid metal filtration, it is reasonable to assume the following orders of magnitude for reference quantities (Cramer and Pai, 1973; Branover, 1978; El-Kaddah, 1988):

$$\begin{aligned} &a \approx O[10^{-2}]\cdots[m]\ ;\ B_o \approx O[10^{-1}]\cdots[T]\ ;\ E_o \approx O[1]\cdots[V/m] \\ &U_o \approx O[10^{-1}]\cdots[m/s]\ ;\ \varsigma \approx O[10^{-6}]\cdots[m^2/s]\ ;\ \mu \approx O[10^{-6}]\cdots[H/m] \\ &\rho \approx O[10^{3}]\cdots[kg/m^3]\ ;\ \sigma \approx O[10^{6}]\cdots[mho/m] \end{aligned} \tag{2.20}$$

Hence, the nondimensional parameters for the EM filtration problem have the following orders of magnitude:

$$\begin{aligned} M &\approx O[10^2] \\ N &\approx O[1] \\ \mathrm{Re} &\approx O[10^3] \\ \mathrm{Re}_m &\approx O[10^{-3}] \end{aligned} \tag{2.21}$$

It is observed that the value of magnetic Reynolds number is of the order of $O[10^{-3}]$, which implies that the assumption of negligible induced fields is reasonable. This allows the EM field equations to be decoupled from the fluid flow equations, except for the EM force, which is treated as a source term in the Navier-Stokes equations.

When expanded for a Cartesian coordinate system, the components of the EM force per unit volume become:

$$\begin{aligned} F_{EM,UnitVol,x} &= \sigma\left[-E_z B_y + E_y B_z - u\left(B_z^2 + B_y^2\right) + B_x\left(wB_z + vB_y\right)\right] \\ F_{EM,UnitVol,y} &= \sigma\left[-E_x B_z + E_z B_x - v\left(B_x^2 + B_z^2\right) + B_y\left(uB_x + wB_z\right)\right] \\ F_{EM,UnitVol,z} &= \sigma\left[-E_y B_x + E_x B_y - w\left(B_y^2 + B_x^2\right) + B_z\left(vB_y + uB_x\right)\right] \end{aligned} \tag{2.22}$$

The EM fields used in this study were defined in **Section 2.2** as,

$$\begin{aligned} \vec{E} &= (0, 0, E_z) \\ \vec{B} &= (B_x, B_y, 0) \end{aligned} \tag{2.23}$$

Therefore, Equations (2.22) can be simplified as follows:

$$
\begin{aligned}
F_{EM,UnitVol,x} &= \sigma\left(vB_xB_y - E_zB_y\right) - \left(\sigma B_y^2\right)u \\
F_{EM,UnitVol,y} &= \sigma\left(uB_xB_y + E_zB_x\right) - \left(\sigma B_x^2\right)v \\
F_{EM,UnitVol,z} &= -\sigma\left(B_x^2 + B_y^2\right)w
\end{aligned}
\tag{2.24}
$$

Having made the necessary simplifications, it is now possible to summarize the complete set of governing equations valid for steady, laminar, **three-dimensional parabolic** (developing) flows of molten metals in ducts of constant cross-section and electrically non-conducting walls, subjected to steady, uniform, electric and magnetic fields oriented as shown in **Figure 2.1**. They can be expressed, in dimensional forms, as follows:

x-momentum

$$
\begin{aligned}
&\frac{\partial}{\partial x}(\rho uu) + \frac{\partial}{\partial y}(\rho vu) + \frac{\partial}{\partial z}(\rho wu) = \\
&\qquad -\frac{\partial \tilde{p}}{\partial x} + \frac{\partial}{\partial x}\left(\eta\frac{\partial u}{\partial x}\right) + \frac{\partial}{\partial y}\left(\eta\frac{\partial u}{\partial y}\right) + \sigma\left(vB_xB_y - E_zB_y\right) - \left(\sigma B_y^2\right)u
\end{aligned}
\tag{2.25}
$$

y-momentum

$$
\begin{aligned}
&\frac{\partial}{\partial x}(\rho uv) + \frac{\partial}{\partial y}(\rho vv) + \frac{\partial}{\partial z}(\rho wv) = \\
&\qquad -\frac{\partial \tilde{p}}{\partial y} + \frac{\partial}{\partial x}\left(\eta\frac{\partial v}{\partial x}\right) + \frac{\partial}{\partial y}\left(\eta\frac{\partial v}{\partial y}\right) + \sigma\left(uB_xB_y + E_zB_x\right) - \left(\sigma B_x^2\right)v
\end{aligned}
\tag{2.26}
$$

z-momentum

$$
\begin{aligned}
&\frac{\partial}{\partial x}(\rho uw) + \frac{\partial}{\partial y}(\rho vw) + \frac{\partial}{\partial z}(\rho ww) = \\
&\qquad -\frac{d\bar{p}}{dz} + \frac{\partial}{\partial x}\left(\eta\frac{\partial w}{\partial x}\right) + \frac{\partial}{\partial y}\left(\eta\frac{\partial w}{\partial y}\right) - \sigma\left(B_x^2 + B_y^2\right)w
\end{aligned}
\tag{2.27}
$$

Continuity

$$
\frac{\partial}{\partial x}(\rho u) + \frac{\partial}{\partial y}(\rho v) + \frac{\partial}{\partial z}(\rho w) = 0 \tag{2.28}
$$

In the **fully developed flow regime**, the following conditions prevail: the mainstream (z or axial direction) gradients of all dependent variables, except pressure, are

essentially zero; the axial gradient of pressure is a constant; the velocity components in the x and y directions vanish ($u = v = 0$); and the cross-sectional distribution of pressure adjusts to balance the electromagnetic force on the molten aluminum. With these conditions, the continuity equation, Equation (2.28), is automatically satisfied (or may be considered irrelevant), and the x- and y-momentum equations reduce to the following forms, respectively:

$$0 = -\frac{\partial \tilde{p}}{\partial x} - \sigma E_z B_y \tag{2.29}$$

$$0 = -\frac{\partial \tilde{p}}{\partial y} + \sigma E_z B_x \tag{2.30}$$

In the problems of interest, σ, B_x, and B_y are specified constants. Thus, Equations (2.29) and (2.30) can be readily integrated to obtain the following cross-sectional distribution of the reduced pressure:

$$\tilde{p} = \sigma(E_z B_x y - E_z B_y x) + \tilde{p}_{ref} \tag{2.31}$$

where $\tilde{p}_{ref}$ is a reference value $\tilde{p}$ at $x = y = 0$. Here, as the fluid is assumed to be incompressible, the absolute value of $\tilde{p}$ is irrelevant; rather, only the gradients of this variable matter (Patankar, 1980). Thus, the value of $\tilde{p}_{ref}$ was arbitrarily set to the convenient value of zero. With these conditions, the axial (z direction) gradient of the reduced pressure, dp/dz, becomes a constant, and the z-momentum equation reduces to the following form:

$$0 = -\frac{dp}{dz} + \frac{\partial}{\partial x}\left(\eta \frac{\partial w}{\partial x}\right) + \frac{\partial}{\partial y}\left(\eta \frac{\partial w}{\partial y}\right) - \sigma\left(B_x^2 + B_y^2\right) w \tag{2.32}$$

In this equation, the reduced pressure gradient, dp/dz, can be specified (and the resulting mass flow rate can be calculated) or it can be adjusted to achieve a desired mass flow rate. The latter approach was adopted in this work. Details of the numerical implementation of this approach are given in Chapter 3.

2.5 Particle Momentum Equation

The equation that governs the momentum of a particle moving in a fluid can be cast in the following general form (Crowe et al, 1998):

$$m_p \frac{d\vec{U}_p}{dt} = \sum \vec{F} = \sum \vec{F}_{body} + \sum \vec{F}_{surface} \tag{2.33}$$

In the problems of interest, the particle (inclusion) moves in molten aluminum subjected to electric, magnetic, and gravitational fields. The body forces are the gravitational force and the electromagnetic (EM) force:

$$\sum \vec{F}_{body} = \left(\frac{\pi D_p^3}{6}\right)\rho_p \vec{g} + \int_{Volume\ of\ particle} (\vec{j}_{in\ particle} \times \vec{B}) dV \tag{2.34}$$

where $\vec{j}_{in\ particle}$ is the current density *within* the particle and $\vec{B}$ is the applied uniform magnetic field (see **Figure 2.1**). As was mentioned earlier, in the problems of interest, the particles (inclusions) are assumed to be electrically non-conducting. Thus, strictly, the current density within the particle is zero. At this stage of the presentation, however, for the sake of generality, the electromagnetic body force on the particle is retained, though it will be discarded later on in this section.

In the absence of the particle, the velocity of the molten aluminum is given by $\vec{U}_f$ and the current density is given by $\vec{j}$. *The presence of the particle and its motion through the fluid* modifies the velocity and the current density in the fluid *locally*: these modified fields are denoted here by $\vec{V}$ and $\vec{j}_{in\ fluid}$, respectively. The modified flow satisfies the following forms of the Navier-Stokes and continuity equations in the vicinity of the particle:

$$\rho_f \left(\frac{\partial \vec{V}}{\partial t} + \vec{V}.\vec{\nabla}\vec{V}\right) = -\vec{\nabla}P + \rho_f \vec{g} + \vec{j}_{in\ fluid} \times \vec{B} + \eta \nabla^2 \vec{V} \tag{2.35}$$

$$\vec{\nabla}.\vec{V} = 0 \tag{2.36}$$

where P is the static pressure in the fluid. The boundary conditions on $\vec{V}$ are the no-slip condition on the surface of the sphere (fluid velocity matches the translational and

angular velocities of the particle at its the surface) and asymptotic approach to $\vec{U}_f$ far from the sphere. Let σ_{ij} denote the fluid stress tensor:

$$\sigma_{ij} = -P\delta_{ij} + \eta\left(\frac{\partial V_i}{\partial x_j} + \frac{\partial V_j}{\partial x_i}\right) \tag{2.37}$$

where δ_{ij} is the Kronecker delta function. Then, the surface forces on the particle are given by the following equation:

$$\sum F_{surface,i} = \oint_{surface} \sigma_{ij} n_j ds \tag{2.38}$$

where the surface integral is performed over the entire surface of the spherical particle, and $\vec{n}$ is the unit outward normal to the surface of the particle.

The problem now is to evaluate the current densities inside the spherical particle and in the fluid, $\vec{j}_{in\ particle}$ and $\vec{j}_{in\ fluid}$, respectively, and then evaluate the fluid stress tensor on the surface of the particle. The solution to this problem can be obtained by combining the analyses and solutions proposed by Leenov and Kolin (1954), Saffman (1965), Maxey and Riley (1983), and Crowe et al. (1998). Their analyses and solutions could be used here because the problems of interest satisfy the following restrictions:

$$\mathrm{Re}_p \equiv \frac{|U_f - U_p| D_p}{\varsigma_f} \leq 1 \; ; \; (D_p U_o / \varsigma_f)(D_p / a) \ll 1 \; ; \; (D_p / a) \ll 1 \; ; \; (U_o B_o / E_o) \ll 1 \tag{2.39}$$

The final result can be expressed as follows:

$$m_p \frac{d\vec{U}_p}{dt} = m_f \frac{D\vec{U}_f}{Dt} + \vec{F}_{DRAG} + \vec{F}_{BUOYANCY} + \vec{F}_{VIRTUAL\ MASS} + \vec{F}_{BASSET} + \vec{F}_{LIFT} + \vec{F}_{EM,p} \tag{2.40}$$

In this equation, $m_p = (\pi D_p^3 / 6)\rho_p$, $m_f = (\pi D_p^3 / 6)\rho_f$, and $D\vec{U}_f / Dt$ is the total derivative of the undisturbed fluid velocity field, evaluated at the position where the particle is located. For steady fully developed flows, akin to those considered in this work, $D\vec{U}_f / Dt = 0$. In the remainder of this section, each of the forces mentioned on the right-hand side of Equation (2.40) will be discussed briefly, and then an appropriately simplified particle momentum equation will be cast in a convenient (rearranged) form. Then, the simplified particle momentum equation will be non-dimensionalized in order to

assess the relative magnitudes of the aforementioned forces in the EM filtration problem. Finally, the restriction required for the validity of the one-way coupling in the momentum transfer between the fluid and the particles will be discussed. For clarity in the presentation, the subscripts *f* and *p* will be used, when deemed necessary, to distinguish quantities associated with the fluid and the particles, respectively.

2.5.1. Drag Force

This is the so-called "steady-state" drag force which acts on the particle or inclusion in a uniform pressure field when there is no time rate of change of the relative velocity between the particle and the conveying fluid (Crowe et al., 1998). This drag force can be conveniently expressed as follows:

$$\vec{F}_{DRAG} = \frac{1}{2}\rho_f \frac{\pi D_p^{\,2}}{4} C_D \left(\vec{U}_f - \vec{U}_p\right)\left|\vec{U}_f - \vec{U}_p\right| \tag{2.41}$$

In Equation (2.41), C_D is the drag coefficient. The particle Reynolds number, Re_p, is defined as follows:

$$\mathrm{Re}_p \equiv \frac{\left|U_f - U_p\right| D_p}{\varsigma_f} \tag{2.42}$$

When this particle Reynolds number is of order O[1], the flow around the sphere is said to be in the Stokes regime. For uniform free stream velocity, and Stokes flow around the particle, the drag coefficient is given by:

$$C_D = \frac{24}{\mathrm{Re}_p} \qquad \mathrm{Re}_p \equiv \frac{\left|U_f - U_p\right| D_p}{\varsigma_f} < 1 \tag{2.43}$$

Substituting these expressions for C_D and Re_p in Equation (2.41), and rearranging, the following expression is obtained for the drag force:

$$\vec{F}_{DRAG} = 3\pi D_p \eta \left(\vec{U}_f - \vec{U}_p\right) \tag{2.44}$$

The Stokes drag force given by Equation (2.44) is based on a uniform free stream velocity. To account for the effect of a non-uniform flow field, the so-called Faxen force must be added to the Stokes drag force (Maxey and Riley, 1983; Crowe et al., 1998):

$$\vec{F}_{DRAG} = 3\pi D_p \eta\left(\vec{U}_f - \vec{U}_p\right) + (\eta\pi D_p^3 \nabla^2 \vec{U}_f)/8 \tag{2.45}$$

where $\nabla^2 \vec{U}_f$ is evaluated at the position of the particle. For a uniform flow field, the Faxen force reduces to zero. Crowe et al. (1998) have shown that the ratio of the Faxen force to the Stokes drag varies as follows:

$$(F_{Faxen} / F_{Stokes}) \sim (D_p / a)^2 \tag{2.46}$$

In this work, $D_p \leq 100\ \mu m$ and $a \sim 0.01 m$. Thus, Equation (2.46) shows that $(F_{Faxen} / F_{Stokes}) \sim (D_p / a)^2 \leq 10^{-4}$. Therefore, Equation (2.44) gives the drag force quite adequately, and it was adopted in all the test and demonstration problems. Furthermore, in the problems considered here, $Re_p < 1$, so the C_D expression given in Equation (2.43) was used. For the interested readers, expressions for C_D at $Re_p > 1$ are available in the work of Crowe et al. (1998).

2.5.2 Buoyancy Force

The buoyancy force acting on the particle is given by,

$$\vec{F}_{BUOYANCY} = \left(\frac{\pi D_p^3}{6}\right)(\rho_p - \rho_f)\vec{g} \tag{2.47}$$

2.5.3 Apparent Mass Force

The apparent (or virtual) mass force is associated with relative acceleration between the particle and the fluid. When the particle accelerates, it also induces acceleration in the surrounding fluid, and the surrounding fluid resists this acceleration. Using the analysis of Maxey and Riley (1983), for a small, rigid, smooth, sphere, moving in a nonuniform fluid flow, the virtual mass force is given by:

$$\vec{F}_{VIRTUAL\,MASS} = \frac{1}{2}\rho_f \left(\frac{\pi D_p^3}{6}\right)\left(\frac{d\vec{U}_f}{dt} - \frac{d\vec{U}_p}{dt} + \frac{d(D_p^2 \nabla^2 \vec{U}/40)}{dt}\right) \tag{2.48}$$

Here again, using reasoning akin to that of Crowe et al. (1998), and noting the $(D_p / a)^2 \ll 1$, the term involving $\nabla^2(\vec{U}_f)$ was neglected, and the expression for the virtual mass force was reduced to the following:

$$\vec{F}_{VIRTUAL\,MASS} = \frac{1}{2}\rho_f\left(\frac{\pi D_p^3}{6}\right)\left(\frac{d\vec{U}_f}{dt} - \frac{d\vec{U}_p}{dt}\right) \tag{2.49}$$

It should be noted that in Equation (2.49), the term $d\vec{U}_f / dt$ denotes the time derivative of the fluid velocity *following the moving particle*, so that:

$$\frac{d\vec{U}_f}{dt} = \frac{\partial \vec{U}_f}{\partial t} + \vec{U}_p.\vec{\nabla}\vec{U}_f \tag{2.50}$$

2.5.4 Basset Force

The Basset force, or the "history" term, as it is often called, accounts for the temporal boundary layer development on the particle, as the relative velocity changes with time (Odar and Hamilton, 1964; Odar, 1966; Crowe et al., 1998). For the general case where there is a non-zero initial relative velocity between the particle and fluid, and nonuniform undisturbed flow, following the analyses of Maxey and Riley (1983), Reeks and McKee (1984), and Crowe et al. (1998), the Basset force is given by:

$$\vec{F}_{BASSET} = \frac{3}{2}D_p^{\,2}\sqrt{\pi\rho\eta}\left[\int_0^t \frac{\left(\frac{d\vec{U}_f}{dt} - \frac{d\vec{U}_p}{dt} + \frac{d(D_p^2\nabla^2\vec{U}_f/24)}{dt}\right)}{\sqrt{t-t'}}\,dt' + \frac{\left(\vec{U}_f - \vec{U}_p\right)_{initial}}{\sqrt{t}}\right] \tag{2.51}$$

Again, using reasoning akin to that of Crowe et al. (1998) and noting the $(D_p/a)^2 \sim 1$, the term involving $\nabla^2(\vec{U}_f)$ was neglected. Furthermore, in the problems of interest, $(\vec{U}_f - \vec{U}_p)_{initial} = 0$. Thus, the expression for the Basset force could be reduced to the following:

$$\vec{F}_{BASSET} = \frac{3}{2}D_p^{\,2}\sqrt{\pi\rho\eta}\left[\int_0^t \frac{\left(\frac{d\vec{U}_f}{dt} - \frac{d\vec{U}_p}{dt}\right)}{\sqrt{t-t'}}\,dt'\right] \tag{2.52}$$

As is clear from this equation, the importance of the Basset force terms depends on the time rate of change in relative velocity and the time period over which this relative acceleration takes place.

2.5.5 Lift Force

A spherical particle experiences a lift force when there is fluid circulation around it. One situation under which such a lift force arises is that of flow past a spinning particle (Magnus lift force). A lift force may also be felt by particles moving in regions of shear flow. In this work, the Magnus lift force was assumed to be negligible, which is a reasonable assumption for small particle Reynolds numbers (Naumov, 1995). However, the lift force due to shear flow was included in the analyses.

Using matched asymptotic series for the inner and outer flow regions around a sphere in unbounded shear flow, Saffman (1965) derived an expression for the lift force based on the following assumptions:

$$\begin{aligned} \mathrm{Re}_G &\equiv \left(\frac{dU_f}{dn}\right)\frac{D_p^{\,2}}{4\varsigma_f} << 1 \\ \mathrm{Re}_p &\equiv \frac{\left|U_f - U_p\right| D_p}{\varsigma_f} << 1 \\ A &\equiv \frac{\mathrm{Re}_p}{\sqrt{\mathrm{Re}_G}} << 1 \end{aligned} \tag{2.53}$$

Where n is a coordinate in the direction of the velocity gradient, Re_G is a "shear" Reynolds number based on the velocity gradient, and Re_p is the particle Reynolds number.

The general form of the Saffman lift force term is given by (Saffman, 1965; Crowe et al., 1998):

$$\vec{F}_{LIFT} = \frac{CD_p^{\,2}}{4}\left(\eta\rho_f\right)^{1/2}\left|\vec{\nabla}\times\vec{U}_f\right|^{-1/2}\left[\left(\vec{U}_f - \vec{U}_p\right)\times\left(\vec{\nabla}\times\vec{U}_f\right)\right] \tag{2.54}$$

By carrying out the matched asymptotic series solutions to the first order in the particle Reynolds number, it can be shown the appropriate value of C is 6.46. In the EM filtration problems considered here, with fully developed flow of molten aluminum in the separation chamber, the lift force can be broken down into its three components in the Cartesian coordinate system as follows:

$$F_{LIFTx} = 1.615 D_p^{\,2} \left(\eta \rho_f\right)^{1/2} \left|\vec{\nabla} \times \vec{U}_f\right|^{-1/2} \left[\left(w_f - w_p\right)\left(\frac{\partial w_f}{\partial x}\right)\right]$$

$$F_{LIFTy} = 1.615 D_p^{\,2} \left(\eta \rho_f\right)^{1/2} \left|\vec{\nabla} \times \vec{U}_f\right|^{-1/2} \left[\left(w_f - w_p\right)\left(\frac{\partial w_f}{\partial y}\right)\right] \qquad (2.55)$$

$$F_{LIFTz} = 1.615 D_p^{\,2} \left(\eta \rho_f\right)^{1/2} \left|\vec{\nabla} \times \vec{U}_f\right|^{-1/2} \left[u_p\left(\frac{\partial w_f}{\partial x}\right) + v_p\left(\frac{\partial w_f}{\partial y}\right)\right]$$

where,

$$\left|\vec{\nabla} \times \vec{U}_f\right|^{-1/2} = \left[\left(\frac{\partial w_f}{\partial y}\right)^2 + \left(\frac{\partial w_f}{\partial x}\right)^2\right]^{-1/4} \qquad (2.56)$$

2.5.6 Electromagnetic Force on the Particle

The expression for the electromagnetic force on the particle was obtained from the analysis of Leenov and Kolin (1954). It can be cast in the following form:

$$\vec{F}_{EM,p} = -\frac{3}{2}\left(\frac{\pi D_p^3}{6}\right)\left(\frac{\sigma_f - \sigma_p}{2\sigma_f + \sigma_p}\right)\vec{F}_{EM,UnitVol} \qquad (2.57)$$

where $\vec{F}_{EM,UnitVol}$ is the undisturbed EM force per unit volume in the molten aluminum. It is given by:

$$\vec{F}_{EM,UnitVol} = \vec{j} \times \vec{B} = \{\sigma_f(\vec{E} + \vec{U}_f \times \vec{B})\} \times \vec{B} \qquad (2.58)$$

It is to be noted here that in the analysis of Leenov and Kolin (1954), the $\vec{U}_f \times \vec{B}$ term is assumed to be negligible compared to $\vec{E}$. This assumption is valid in the problems considered here. However, in the analyses presented in this thesis, the full form of $\vec{F}_{EM,UnitVol}$, as given in Equation (2.58), was retained, for completeness and for consistency with the mathematical model of the flow of molten aluminum, given in **Section 2.4.**

Only electrically non-conducting inclusions were considered in this work. Thus, $\sigma_p = 0$, and Equation (2.58) simplifies to the following:

$$\vec{F}_{EM,p} = -\frac{3}{4}\left(\frac{\pi D_p^3}{6}\right)\vec{F}_{EM,UnitVol} \tag{2.59}$$

Furthermore, for fully developed flow of molten aluminum in the separation chamber shown in **Figure 2.1**, using the equations in **Section 2.4**, the expression for $\vec{F}_{EM,UnitVol}$ is the following:

$$\begin{aligned}
\vec{F}_{EM,UnitVol} &= F_{EM,UnitVol,x}\vec{i} + F_{EM,UnitVol,y}\vec{j} + F_{EM,UnitVol,z}\vec{k} \\
F_{EM,UnitVol,x} &= -\sigma E_z B_y \\
F_{EM,UnitVol,y} &= \sigma E_z B_x \\
F_{EM,UnitVol,z} &= -\sigma(B_x^2 + B_y^2)
\end{aligned} \tag{2.60}$$

where $\vec{i}, \vec{j}, \vec{k}$ are unit vectors in the x, y, and z directions, respectively.

2.5.7 Simplified Form of the Particle Momentum Equation

Using the discussions and the expressions for the various force terms given in the previous subsections, the particle momentum equation can be simplified and rewritten as follows:

$$\begin{aligned}
m_p\frac{d\vec{U}_p}{dt} &= 3\pi D_p\eta\left(\vec{U}_f - \vec{U}_p\right) + \left(\frac{\pi D_p^3}{6}\right)(\rho_p - \rho_f)\vec{g} \\
&+ \frac{1}{2}\rho_f\left(\frac{\pi D^3}{6}\right)\left(\frac{d\vec{U}_f}{dt} - \frac{d\vec{U}_p}{dt}\right) + \frac{3}{2}D_p^{\,2}\sqrt{\pi\rho\eta}\left[\int_0^t \frac{\left(\frac{d\vec{U}_f}{dt} - \frac{d\vec{U}_p}{dt}\right)}{\sqrt{t-t'}}\,dt'\right] \\
&+ \frac{CD_p^{\,2}}{4}\left(\eta\rho_f\right)^{1/2}\left|\vec{\nabla}\times\vec{U}_f\right|^{-1/2}\left[\left(\vec{U}_f - \vec{U}_p\right)\times\left(\vec{\nabla}\times\vec{U}_f\right)\right] \\
&- \frac{3}{4}\left(\frac{\pi D_p^3}{6}\right)\vec{F}_{EM,UnitVol}
\end{aligned} \tag{2.61}$$

In this equation, the general expression for the EM force per unit volume is given by:

$$\vec{F}_{EM,UnitVol} = \sigma_f\left(\vec{E}\times\vec{B} + \vec{U}_f\times\vec{B}\times\vec{B}\right) \tag{2.62}$$

Noting that $m_p = \rho_p(\pi D_p^3/6)$, Equation (2.61) can be rewritten in the following form, which is convenient in the implementation of the numerical solution methods presented in Chapter 3:

$$
\begin{aligned}
m_p\left(1+\frac{1}{2}\frac{\rho_f}{\rho_p}\right)\frac{d\vec{U}_p}{dt} &= 3\pi D_p\eta\left(\vec{U}_f-\vec{U}_p\right)+\left(\frac{\pi D_p^3}{6}\right)(\rho_p-\rho_f)\vec{g} \\
&+\frac{1}{2}\rho_f\left(\frac{\pi D^3}{6}\right)\left(\frac{d\vec{U}_f}{dt}\right)+\frac{3}{2}D_p{}^2\sqrt{\pi\rho\eta}\left[\int_0^t\frac{\left(\frac{d\vec{U}_f}{dt}-\frac{d\vec{U}_p}{dt}\right)}{\sqrt{t-t'}}dt'\right] \\
&+\frac{CD_p{}^2}{4}\left(\eta\rho_f\right)^{1/2}\left|\vec{\nabla}\times\vec{U}_f\right|^{-1/2}\left[\left(\vec{U}_f-\vec{U}_p\right)\times\left(\vec{\nabla}\times\vec{U}_f\right)\right] \\
&-\frac{3}{4}\left(\frac{\pi D_p^3}{6}\right)\vec{F}_{EM,UnitVol}
\end{aligned}
\tag{2.63}
$$

2.5.8 Nondimensional Form of the Particle Momentum Equation and Order-of-Magnitude Analysis

In this section, the particle momentum equation is non-dimensionalized, and then an order-of-magnitude analysis is presented.

The non-dimensional variables and parameters used in this discussion are summarized in the equation given below.

$$
\begin{aligned}
\nabla^* &= a\nabla & \mathrm{Re} &= \frac{\rho_f U_o a}{\eta} \\
U^* &= \frac{U}{U_o} & \mathrm{Re}_p &= \frac{\rho_f\left|U_f-U_p\right|D_p}{\eta} \\
B^* &= \frac{B}{B_o} & \tau_V &= \frac{\rho_p D_p^2}{18\eta} \\
E^* &= \frac{E}{U_o B_o} & St &= \frac{\tau_V U_o}{a} \\
p^* &= \frac{p-p_{ref}}{\rho_f U_o^2} & t^* &= \frac{t}{(a/U_o)} \\
g^* &= \frac{g}{U_o^2/a} & N &= \frac{\sigma B_o^2 a}{\rho_f U_o} \\
\delta &= \frac{D_p}{a} & \phi &= \frac{U_p}{U_f} \\
\lambda &= \frac{\rho_p}{\rho_f} & U_f^*(1-\phi) &= \frac{\left(U_f-U_p\right)}{U_o}
\end{aligned}
\tag{2.64}
$$

In the above equations, a is the duct width, D_p is the particle diameter, U_o is the average velocity of the molten aluminum (fluid) in the z direction, B_o is the magnitude of the applied magnetic flux density, ρ_f is the fluid density, η is the fluid dynamic viscosity, ρ_p is the particle density, and t is the elapsed time. The responsiveness of the particle to changes in fluid velocity is indicated by its *velocity response time*, τ_V, as discussed by Crowe et al. (1998). The ratio of the particle velocity response time to the characteristic time associated with the carrier fluid flow $(\tau_F = a/U_o)$ is defined as the Stokes number, *St*. Other quantities which relate the particle and the fluid flow dynamics are the ratio of particle diameter to duct width, δ, the particle-fluid density ratio, λ, and the particle-fluid velocity ratio, ϕ. Crowe et al. (1998) provide the following approximate relationship between ϕ and St:

$$\phi \sim \frac{1}{1+St} \tag{2.65}$$

Equation (2.65) is useful in assessing the relative magnitudes of the terms in the nondimensionalized particle momentum equation. The remaining parameters, which include the duct Reynolds number, Re, particle Reynolds number, Re_p, and the interaction parameter, N, have been defined and discussed earlier in this chapter.

The nondimensional variables and parameters in Equation (2.64) were inserted into Equations (2.61) and (2.62). The resulting equation was rearranged, and the *star superscripts used earlier to indicate dimensionless variables were dropped*, to obtain the following nondimensional form of the particle momentum equation:

$$\begin{aligned}\frac{d\vec{U}_p}{dt} &= \left(\frac{1}{St}\right)\left(\vec{U}_f - \vec{U}_p\right) + \left(1-\frac{1}{\lambda}\right)\vec{g} + \left(\frac{1}{2\lambda}\right)\left(\frac{d\vec{U}_f}{dt} - \frac{d\vec{U}_p}{dt}\right) \\ &+ \left(\frac{9}{\pi^{1/2}\lambda\delta\,\mathrm{Re}^{1/2}}\right)\left[\int_0^t \frac{\left(\frac{d\vec{U}_f}{dt} - \frac{d\vec{U}_p}{dt}\right)}{\sqrt{t-t'}}\,dt'\right] \\ &+ \left(\frac{3C}{2\pi\,\mathrm{Re}^{1/2}\,\lambda\delta}\right)\left|\vec{\nabla}\times\vec{U}_f\right|^{-1/2}\left[\left(\vec{U}_f - \vec{U}_p\right)\times\left(\vec{\nabla}\times\vec{U}_f\right)\right] \\ &- \left(\frac{3N}{4\lambda}\right)\left(\vec{E}\times\vec{B} + \vec{U}_f\times\vec{B}\times\vec{B}\right)\end{aligned} \tag{2.66}$$

The following orders of magnitude are relevant to the problem of electromagnetic filtration of molten aluminum (Patel and El-Kaddah, 1997):

$$
\begin{aligned}
a &\approx O[10^{-2}]\cdots[m] \\
D_p &\approx O[10^{-4}]\cdots[m] \\
U_o &\approx O[10^{-1}]...[m/s] \\
\eta &\approx O[10^{-3}]\cdots[kg/m-s] \\
\rho_f &\approx O[10^{3}]\cdots[kg/m^3] \\
\rho_p &\approx O[10^{3}]\cdots[kg/m^3] \\
\varsigma_f &\approx O[10^{-6}]\cdots[m^2/s]
\end{aligned}
\tag{2.67}
$$

When these values, which are appropriate in the physical problem of interest, are incorporated into Equation (2.64), the following magnitudes of the corresponding nondimensional parameters are obtained:

$$
\begin{aligned}
\mathrm{Re} &\approx O[10^{3}] \\
\mathrm{Re}_p &\approx O[10^{-1}] \\
St &\approx O[10^{-2}] \\
U_f^*(1-\phi) &\approx O[10^{-2}] \\
\delta &\approx O[10^{-2}] \\
\lambda &\approx O[1] \\
\tau_V &\approx O[10^{-3}]
\end{aligned}
\tag{2.68}
$$

The values of each of the nondimensional groups, $\left(\frac{\cdot\cdot}{\cdot\cdot}\right)$, that appear in the expressions for the dimensionless forces in Equation (2.66) were calculated using exact values of the properties and dimensions used in the electromagnetic filtration problems: the corresponding orders of magnitude are summarized in **Table 2.1**.

Table 2.1: Orders of magnitude of the dimensionless groups that multiply the various force terms in the nondimensionalized particle momentum equation

Dimensionless Group	Order of Magnitude
$\left(\frac{1}{St}\right)$	10^2
$\left(1-\frac{1}{\lambda}\right)$	1
$\left(\frac{1}{2\lambda}\right)$	1
$\left(\frac{9}{\pi^{1/2}\lambda\delta\,\mathrm{Re}^{1/2}}\right)$	1
$\left(\frac{3C}{2\pi\,\mathrm{Re}^{1/2}\,\lambda\delta}\right)$	1
$\left(\frac{3N}{4\lambda}\right)$	1

For the problems under consideration, the following deductions can be made based on the orders of magnitude given in Equation (2.68) and in **Table 2.1**:

1. The particle velocity response time is two orders of magnitude lower than the characteristic time associated with the flow of molten aluminum.
2. The particle Reynolds number is quite small, so the assumption that the Stokes flow condition prevails is valid.
3. The dimensionless group that appears in the nondimensional drag force is of order $O[10^2]$, whereas the dimensionless groups associated with the other nondimensional force terms are of order $O[1]$. Thus, the magnitude of the relative velocity between the molten aluminum and the inclusions (particles) can be expected to be small compared to $|\vec{U}_f|$.
4. The dimensionless groups associated with the nondimensional buoyancy, virtual mass, Basset, lift, and EM forces are all of the same order of magnitude, $O[1]$. Thus, it would be wise to retain all of these terms in the particle momentum equation.

2.6 Restriction Necessary for One-Way Momentum Coupling Between the Molten Aluminum and the Inclusions

In order to justify the assumption of one-way momentum coupling between the molten aluminum and the inclusions (particles), the average distance between particles should be at least ten times the average particle diameter (Crowe et al., 1998).

Consider the molten aluminum to be divided into cubic control volumes of size $£^3$, with each of these control volumes containing a single spherical particle of diameter D_p. Then the volume fraction of the particulate phase, α_p, is the following:

$$\alpha_p = \frac{\left(\pi D_p^3 / 6\right)}{£^3} \tag{2.69}$$

The ratio of the average spacing between adjacent particles to the diameter of a single particle can be estimated by the following equation:

$$\frac{£}{D_p} = \left(\frac{\pi}{6\alpha_p}\right)^{1/3} \tag{2.70}$$

In practice, it is customary to express this ratio in terms of bulk material properties such as mass concentration of the particulate phase, C_m, particle density, ρ_p, and continuous phase (or fluid) density, ρ_f, which are all easily measured. First, a constant, κ, is defined by:

$$\kappa = C_m \frac{\rho_f}{\rho_p} \tag{2.71}$$

For $C_m \ll 1$,

$$\alpha_p = \alpha_f C_m \frac{\rho_f}{\rho_p} \tag{2.72}$$

Then, noting that $\alpha_p = 1 - \alpha_f$, it can be shown that

$$\alpha_p = \frac{\kappa}{1+\kappa} \tag{2.73}$$

Using this equation, Equation (2.70) can then be recast as follows:

$$\frac{£}{D_p} = \left((\frac{\pi}{6})(\frac{1+\kappa}{\kappa}) \right)^{1/3} \tag{2.74}$$

For typical concentrations and densities of aluminum oxides, as reported in **Table 1.1**, and conditions representative of molten aluminum filtration (Patel and El-Kaddah, 1997), it can be shown that the requirement for one-way momentum coupling between the fluid and the inclusions (namely, $(£/D_p) \geq 10$) is met when the mass concentration of the particulate phase satisfies the following restriction:

$$C \leq O[10^{-3}] \tag{2.75}$$

Chapter 3

Numerical Solution Methods

The numerical methods that were formulated, implemented, and used to solve the mathematical models described in Chapter 2 are presented in this chapter. First, the method that was used to predict fully developed flows of molten aluminum in the separation chamber is described. Following that, an algorithm that was used to predict the trajectories of the inclusions in the molten aluminum is presented.

3.1 Fully Developed Flow of Molten Aluminum

3.1.1 Review of the Problem of Interest

The problem of interest is the flow of molten aluminum in the separation chamber depicted schematically in **Figure 2.1**. The separation chamber is a straight duct of rectangular cross-section, and its walls are assumed to be electrically non-conducting. The molten aluminum is assumed to remain essentially isothermal as it flows through this separation chamber. The duct and the molten aluminum flowing through it are subjected to uniform electric and magnetic fields, as shown in **Figure 2.1**. All other assumptions invoked in this analysis have already been presented and discussed in Chapter 2, so they will not be repeated here. Attention in this work is focused on the fully developed regime, where, as was discussed in Chapter 2, the following conditions prevail: the mainstream (z or axial direction) gradients of all dependent variables, except the reduced pressure, are essentially zero; the axial gradient of the reduced pressure (dp/dz) is a constant; the velocity components in the x and y directions vanish (u = v = 0); and the cross-sectional distribution of the reduced pressure, $\tilde{p}$, adjusts to balance the electromagnetic force on the molten aluminum.

3.1.2 Review of the Governing Equations and Generalization

The assumptions and differential equations that govern the problem of interest were presented in Chapter 2. In the fully developed regime, the distribution of the w

velocity component in any cross-section of the separation chamber is obtained by solving the z-momentum equation, which reduces to the following form:

$$-\frac{dp}{dz}+\frac{\partial}{\partial x}\left(\eta\frac{\partial w}{\partial x}\right)+\frac{\partial}{\partial y}\left(\eta\frac{\partial w}{\partial y}\right)-\sigma\left(B_x^2+B_y^2\right)w=0 \tag{3.1}$$

The no-slip boundary condition (w = 0) applies on the walls of the separation chamber. In the problems of interest, σ, η, B_x, and B_y are specified. The reduced pressure gradient, *dp/dz*, can either be prescribed *a priori* (and the corresponding mass flow rate can be calculated after the distribution of w in the cross-section is computed) or it can be adjusted iteratively to achieve a desired mass flow rate (or Reynolds number). The latter approach was used in this work. Its implementation details are presented in **Section 3.1.6**.

Equation (3.1) is akin to the following general steady-state diffusion equation (Patankar, 1980):

$$\frac{\partial}{\partial x}\left(\Gamma_\phi\frac{\partial\phi}{\partial x}\right)+\frac{\partial}{\partial y}\left(\Gamma_\phi\frac{\partial\phi}{\partial y}\right)+S_\phi=0 \tag{3.2}$$

where ϕ is a general specific scalar dependent variable, Γ_ϕ is the corresponding diffusion coefficient, and S_ϕ is the corresponding volumetric source term (Patankar, 1980). In the formulation of the numerical solution method, the volumetric source term was linearized, when required, and cast in the following form (Patankar, 1980):

$$S_\phi=S_C^\phi+S_P^\phi\phi \tag{3.3}$$

Equation (3.1) can be obtained from Equation (3.2) by the following settings:

$$\phi=w\ ;\ \Gamma_\phi=\eta\ ;\ S_C^\phi=-\frac{dp}{dz}\ ;\ S_P^\phi=-\sigma\left(B_x^2+B_y^2\right) \tag{3.4}$$

3.1.3 Control-Volume Finite Element Method

A control-volume finite element method (CVFEM) for two-dimensional planar diffusion problems was used to solve the equation that governs the fully developed flow of molten aluminum in the separation chamber. This CVFEM is well established, and it

is described in detail in the works of Baliga and Patankar (1978) and Baliga (1997). A concise description of this method is provided in this section.

Domain Discretization

The calculation domain is first divided into three-node triangular elements. Then the centroids of the elements are joined to the midpoints of the corresponding sides, to create polygonal control volumes around each node (vertices of the triangular elements) in the finite element mesh. A sample unstructured grid is shown in **Figure 3.1**: the solid lines denote the domain and element boundaries; the dashed lines represent the control-volume faces; and the shaded areas show the control volumes associated with one internal node and two boundary nodes. In this discretization scheme, curved boundaries are approximated by piecewise-linear curves.

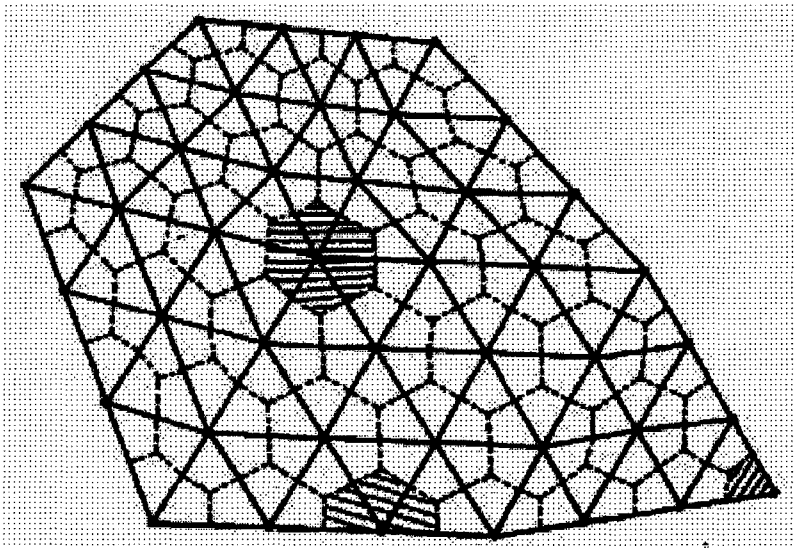

Figure 3.1: Discretization of a calculation domain into three-node triangular elements and polygonal control volumes.

The rationale behind the choice of triangular elements over quadrilateral elements and the aforementioned procedure for generating polygonal control volumes is discussed in Baliga (1997).

Integral Conservation Equation for a Control Volume

Consider a typical node *i* in the calculation domain: it could be an internal node, like the one shown in **Figure 3.2a**, or a boundary node, similar to the ones shown in **Figures 3.2b** and **3.2c**.

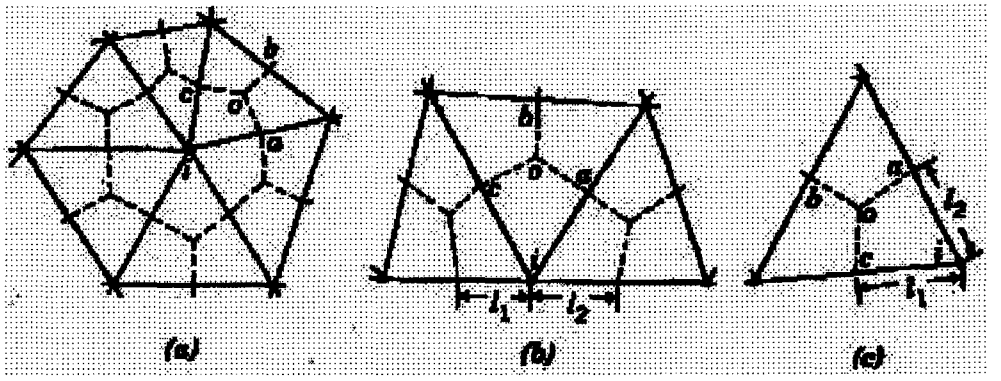

Figure 3.2: Details of the domain discretization and related nomenclature: (a) an internal node; (b) a boundary node with three associated elements; and (c) a boundary node with one associated element.

An integral formulation corresponding to Equation (3.2) can be obtained by applying the conservation principle for ϕ to a control volume, $\mathcal{V}$, that is fixed in space. The resulting integral conservation equation, when applied to the polygonal control volume that surrounds node *i* in **Figure 3.2**, can be cast in the following form:

$$\begin{aligned}&[\int_a^o \vec{J}.\vec{n}ds + \int_o^c \vec{J}.\vec{n}ds - \int_{iaoc} S_\phi dV] + \\ &[\textit{similar contributions from other elements associated with node } i] + \\ &[\textit{boundary contributions, if applicable}] = 0\end{aligned} \tag{3.5}$$

where $\vec{n}$ is a unit normal to the differential area element *ds*, pointing outwards with respect to the control volume associated with node *i*, and $\vec{J}$ is the diffusion flux of ϕ:

$$\vec{J} = -\Gamma_\phi \vec{\nabla}\phi \tag{3.6}$$

The form of Equation (3.5) emphasizes that it can be assembled using an element-by-element procedure. The two-dimensional domains being considered in this description are assumed to have unit depth normal to the plane (or cross-section) of interest; thus, volume and area integrals reduce to surface and line integrals, respectively.

Interpolation Functions

The derivation of algebraic approximations to the integrals and derivatives in Equation (3.5) requires the specification of functions for the interpolation of the

dependent variable, ϕ, the diffusion coefficient, Γ_ϕ, and the source term, S_ϕ, in each of the three-node triangular elements.

Interpolation functions for Γ_ϕ and S_ϕ: In each three-node triangular element, the centroidal value of Γ_ϕ is stored and assumed to prevail over the corresponding element. The source term is linearized, as in Equation (3.3). In *each element*, the three nodal values of S_C^ϕ and S_P^ϕ [$\{S_C^\phi\}_{i=1,2,3}$ and $\{S_P^\phi\}_{i=1,2,3}$] are stored and assumed to prevail over the corresponding portions of the three associated polygonal control volumes contained within the element.

Interpolation function for ϕ: The specific scalar function, ϕ, is interpolated linearly in each three-node triangular element. Thus, with respect to a local Cartesian coordinate system with its origin at the centroid of the element, as shown in Fig. 3.3, ϕ is expressed as follows:

$$\phi = Ax + By + C \tag{3.7}$$

The constants, A, B, and C, in this interpolation can be uniquely determined in terms of the x and y coordinates of the three nodes, and the corresponding values of ϕ.

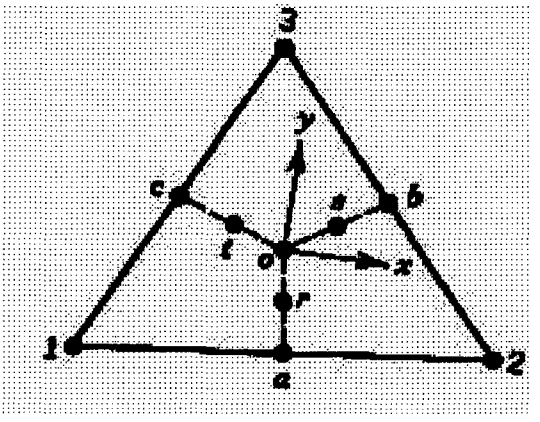

Figure 3.3: A typical three-node triangular element, related nomenclature, and a local Cartesian coordinate system.

With reference to the element 123 and the local Cartesian coordinate system shown in **Figure 3.3**, the expressions for the constants A, B, and C are the following:

$$A = [(y_2 - y_3)\phi_1 + (y_3 - y_1)\phi_2 + (y_1 - y_2)\phi_3]/DET$$
$$B = [(x_3 - x_2)\phi_1 + (x_1 - x_3)\phi_2 + (x_2 - x_1)\phi_3]/DET \quad (3.8)$$
$$C = [(x_2 y_3 - x_3 y_2)\phi_1 + (x_3 y_1 - x_1 y_3)\phi_2 + (x_1 y_2 - x_2 y_1)\phi_3]/DET$$

where the term DET is given by:

$$DET = (x_1 y_2 + x_2 y_3 + x_3 y_1 - y_1 x_2 - y_2 x_3 - y_3 x_1) \quad (3.9)$$

Discretized Equations

The discretized equations are algebraic approximations to the integral conservation equations applied to each polygonal control volume in the calculation domain. First, algebraic approximations to the element contributions to the integral conservation equations are derived. Then, the algebraic approximations to the element contributions are assembled appropriately to obtain the discretized equations (Baliga, 1997). Algebraic approximations to the boundary contributions, if applicable, are also derived and added to the assembled element contributions. The following derivations pertain to node 1 of the element 123 shown in **Figure 3.3**.

In each element, the diffusion flux, $\vec{J}$, can be expressed in terms of its components in the x and y directions as follows:

$$\vec{J} = J_x \vec{i} + J_y \vec{j} = (-\Gamma_\phi \frac{\partial \phi}{\partial x})\vec{i} + (-\Gamma_\phi \frac{\partial \phi}{\partial y})\vec{j} \quad (3.10)$$

where $\vec{i}$ and $\vec{j}$ are unit vectors in the x and y directions, respectively. The interpolation function given in Equation (3.7) is used to approximate J_x and J_y:

$$J_x = -A\Gamma_\phi \; ; \; J_y = -B\Gamma_\phi \quad (3.11)$$

where A and B are given by the expressions in Eq. (3.8).

Using Equation (3.11), with reference to node 1 of element 123 and the local Cartesian coordinate system in **Figure 3.3**, the integrals in Equation (3.5) that represent the diffusion transport of ϕ cam now be approximated as follows:

$$\int_a^o \vec{J}.\vec{n}ds = (A\Gamma_\phi)y_a - (B\Gamma_\phi)x_a$$
$$\int_o^c \vec{J}.\vec{n}ds = -(A\Gamma_\phi)y_c + (B\Gamma_\phi)x_c \quad (3.12)$$

The integral involving the source term is approximated as follows:

$$\int_{1aoc} S_\phi dV = \frac{A_e}{3}\{S_C^\phi\}_1 + \frac{A_e}{3}\{S_P^\phi\}_1\phi_1 \tag{3.13}$$

where A_e is the area of the triangular element 123:

$$A_e = |DET|/2 \tag{3.14}$$

with DET given by Eq. (3.9).

Substituting the expressions in Equation (3.8) into those in Equation (3.12), and then adding up Equations (3.12) and (3.13), the total contribution of element 123 to the integral conservation equation for the control volume associated with node 1 is obtained. This total element contribution can be expressed compactly in the following form (Baliga, 1997):

$$[\int_a^o \vec{J}.\vec{n}ds + \int_o^c \vec{J}.\vec{n}ds - \int_{1aoc} S_\phi dV] = C_1^1\phi_1 + C_2^1\phi_2 + C_3^1\phi_3 + B^1 \tag{3.15}$$

where

$$\begin{aligned}
C_1^1 &= \frac{\Gamma_\phi}{DET}[(y_a - y_c)(y_2 - y_3) + (x_a - x_c)(x_2 - x_3)] - \frac{A_e}{3}\{S_P^\phi\}_1 \\
C_2^1 &= \frac{\Gamma_\phi}{DET}[(y_a - y_c)(y_3 - y_1) + (x_a - x_c)(x_3 - x_1)] \\
C_3^1 &= \frac{\Gamma_\phi}{DET}[(y_a - y_c)(y_1 - y_2) + (x_1 - x_2)(x_2 - x_3)] \\
B^1 &= -\frac{A_e}{3}\{S_C^\phi\}_1
\end{aligned} \tag{3.16}$$

Discretized equations for internal nodes: Expressions similar to Equation (3.15) can be derived for the contributions of all elements associated with the internal node i shown in **Figure 3.2a**. Such expressions, when substituted into Equation (3.5), yield the complete (assembled) discretized equation for node i. This discretized equation can be cast in the following general form (Baliga, 1997):

$$a_i^i\phi_i = \sum_{nb} a_{nb}^i\phi_{nb} + b^i \tag{3.17}$$

where the summation is taken over all the immediate neighbors of node i. Equations similar to Equation (3.17) can be derived for all internal nodes in the calculation domain.

Element-by-element procedures for the compilation, storage, and assembly of the element contributions, such as those in Equation (3.15), to obtain the complete discretized

equations, such as Equation (3.17), are described in Baliga (1978) for structured Cartesian grids and in Venditti (1999) for unstructured grids.

Discretized equations for boundary nodes: For the nodes that lie on the boundaries of the calculation domain, the assembly of element contributions, such as that in Equation (3.15), is insufficient to complete Equation (3.5). The surfaces of control volumes associated with boundary nodes have segments that lie along the domain boundaries. In order to obtain the complete integral conservation equations for such control volumes, the rates of transport of ϕ crossing the boundary segments must be added appropriately to the assembled element contributions. Information regarding such boundary transport rates can be obtained from the prescribed boundary conditions pertaining to the problem of interest.

When the value of ϕ at a boundary node i is specified, the corresponding discretized equation is replaced by the following equation (Baliga, 1997):

$$\phi_i = \phi_{specified} \tag{3.18}$$

After all the unknown values of ϕ have been computed, the discretized equation associated with any specified-value boundary node i can be used to compute the corresponding boundary flux of ϕ (Baliga, 1978; Baliga, 1997).

Solution of the Discretized Equations

The discretized equations derived in the previous subsection form a set of simultaneous algebraic equations that, in general, could be nonlinear. The following iterative process was used to solve these equations:

1. Guess all unknown values of ϕ in the calculation domain.
2. Calculate the coefficients in the linearized forms of the discretized equations, using the latest available values of the dependent variables.
3. Solve the resulting set of linear, or linearized, simultaneous algebraic equations.
4. Repeat steps 2 and 3 until convergence.

Step 3 of this iterative procedure involves the solution of a set of linear algebraic equations. Any suitable method may be used to solve these equations. Information on

such methods, including their advantages and disadvantages, is available in Patankar (1980) and Ferziger and Peric (1996). If the domain discretization scheme is such that the nodes in the finite element mesh lie along definite and easily identifiable line patterns, then a simple line-by-line tridiagonal matrix algorithm (Patankar, 1980) may be used to solve the set of linear, or linearized, discretized equations, and was done to obtain the solutions to the test and demonstration problems presented later in **Chapters 4 and 5**.

Convergence Criterion

For any given finite element mesh (grid), the aforementioned iterative algorithm for the solution of the discretized equations was considered to have converged when the maximum value of the absolute normalized residues was less than 10^{-12}.

At any node, j, in the finite element mesh, the residue of the discretized equation is defined as follows:

$$(Residue)_j = \{a_i^i \phi_i - \sum_{nb} a_{nb}^i \phi_{nb} + b^i\}_j \tag{3.19}$$

With respect to the physical problem of fully developed flow of molten aluminum in the separation chamber, this residue represents an imbalance in the rate of transport of momentum in the axial direction, due to lack of convergence of the iterative solution procedure. In this work, this residue was normalized with reference to an average rate of transport of axial momentum across each control volume, calculated as follows at the end of each of the iterations:

$$\{RMT\}_{av} = [\rho_f w_{av} \{4ab/(L1 \times M1)\}] w_{av} \tag{3.20}$$

where (L1 x M1) is the total number of nodes in the finite element mesh, $4ab$ is the total cross-sectional area of the separation chamber (see **Figure 2.1**), and ρ_f and w_{av} are the density of the molten aluminum and its average velocity, respectively. The value of w_{av} was computed as follows:

$$w_{av} = \{\sum_j w_j A_{cs,cv,j}\}/(4ab) \tag{3.21}$$

Thus, the convergence criterion used in the work can be expressed as follows:

$$\{|Residue|_{\max}/(RMT)_{av}\} \leq 10^{-12} \tag{3.22}$$

Calculation of *dp/dz*

In each run of the CVFEM code, the value of *dp/dz* was adjusted iteratively to obtain a desired Reynolds number, $(\mathrm{Re}_{D_h})_{desired}$:

$$(\mathrm{Re}_{D_h})_{desired} = (\rho_f w_{av} D_h / \eta)_{desired} \tag{3.23}$$

Thus,

$$(w_{av})_{desired} = (\mathrm{Re}_{D_h})_{desired} \eta / (\rho_f D_h) \tag{3.24}$$

For steady, laminar, fully developed flows of molten aluminum in the separation chamber, and fixed values of the electric field strength, E_o, and magnetic flux density, B_o, the product of Re_{D_h} and a friction factor based on *dp/dz* would be a constant (White, 1991):

$$\left(\frac{-(\frac{dp}{dz})D_h}{0.5\rho_f w_{av}^2} \right) \left(\frac{\rho_f w_{av} D_h}{\eta} \right) = Constant \tag{3.25}$$

The information contained in this equation was used to design an efficient iterative scheme to obtain a *dp/dz* value that produces the desired value of Reynolds number, $(\mathrm{Re}_{D_h})_{desired}$, or the corresponding value of $(w_{av})_{desired}$ calculated using Equation (3.24). At the start of each run, a guess value of *dp/dz* was provided as an input, and the iterations were initiated. Following that, at the end of any iteration, *n*, the value of *dp/dz* for the next iteration was calculated as follows:

$$\left(\frac{dp}{dz} \right)^{n+1} = \left(\frac{dp}{dz} \right)^{n} \left(\frac{(w_{av})_{desired}}{(w_{av})^n} \right) \tag{3.26}$$

The value of w_{av} at the end of each of the iterations was calculated using Equation (3.21). This iterative scheme was considered to have converged when the following criterion was met:

$$| (w_{av}^{n+1} - w_{av}^{n}) / w_{av}^{n+1} | \leq 10^{-12} \tag{3.27}$$

3.2 Particle Tracking Algorithm

The algorithm that was used to calculate the trajectories of the inclusions (particles) in the molten aluminum flowing inside the separation chamber is described in this section. This algorithm requires as inputs the velocity distribution of the molten aluminum, which was calculated using the CVFEM described in the previous section. The algorithm is executed independently from the fluid flow calculation described in **Section 3.1**.

The calculation domain is the three-dimensional space within the separation chamber. This calculation domain was discretized using a structured three-dimensional finite element mesh. In the mainstream, or *z*, direction, this mesh had a plane-by-plane structure; each of these cross-sectional planes was discretized into rectangles using a line-by-line structured grid; and each of the rectangles was further divided into two triangular elements. The resulting three-dimensional finite element mesh consisted of elements that resembled extruded triangular prisms in the *z*-direction. An example of such a three-dimensional finite element mesh is shown in **Figure 3.4**.

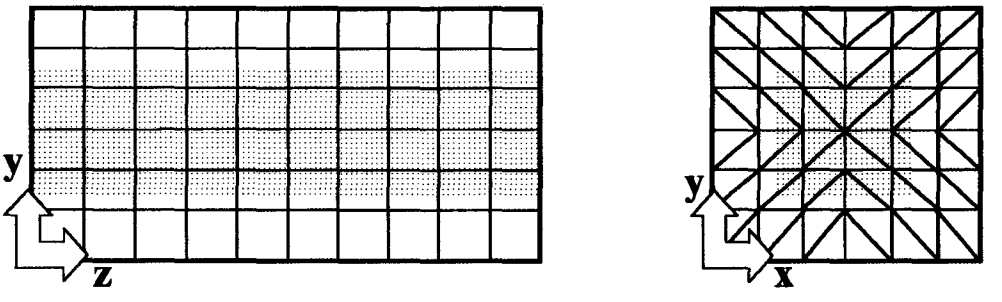

***Figure 3.4**: Discretization of the calculation domain*

Only fully developed flows and one-way momentum coupling were considered in this work. However, it should be noted that the proposed particle-tracking algorithm could be readily extended to elliptic or partially-parabolic flows with two-way momentum coupling between the fluid flow and the particles. In this algorithm, particle-particle interactions are assumed to be nonexistent (or negligible) and particle-wall collisions are assumed to be inelastic.

The computer program that was prepared for the prediction of the particle trajectories was called MAIN_PARTICLE. Its structure and operation is succinctly illustrated by the flowchart given in **Figure 3.5**. For a given set of problem parameters, this program first reads in information about the discretization of the calculation domain and the corresponding flow field data at the nodes of the finite element mesh, using a subroutine called READ_FLOW. The mesh and flow field data are obtained by running the CVFEM code. Then, the particle-tracking program invokes a subroutine called RUNGE_KUTTA, which incorporates a fourth-order Runge-Kutta solution scheme. Details of this scheme are given later in this section.

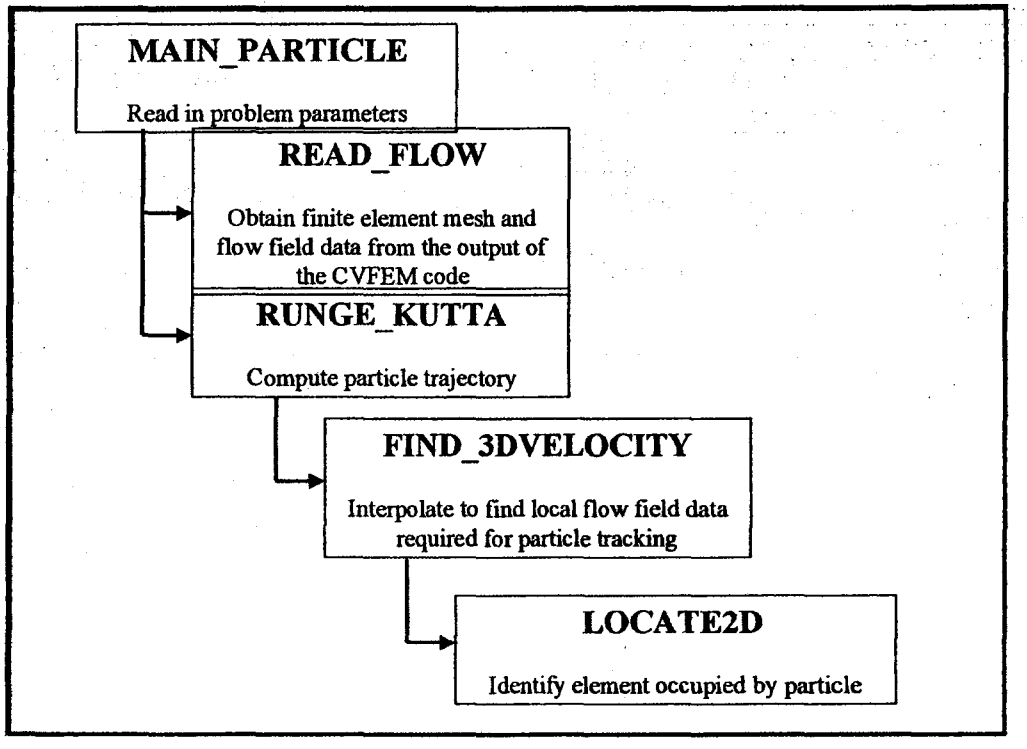

***Figure 3.5**: Flowchart of computer program for calculating particle trajectories*

Once the program MAIN_PARTICLE is initialized, and the starting particle position and velocity, and a suitable time step, are specified, the subroutine RUNGE_KUTTA carries out the particle trajectory calculations by repeating the fourth-order Runge-Kutta scheme for each time step, until the specified maximum number of time steps is reached, or the particle reaches a domain boundary. During the computations needed to advance the solution by one time step, the RUNGE_KUTTA

subroutine calls the subroutine FIND_3DVELOCITY, which is a subroutine that interpolates for the local fluid velocity, and calculates all required velocity gradients, based on the particle position at the last time step. In order to compute these quantities, the subroutine LOCATE2D is called from within FIND_3DVELOCITY, to identify the three vertices of the triangular cross-section of the element within which the particle is currently located. The required velocity components and their gradients are first obtained using interpolation over the two triangular cross-sections corresponding to the upstream and downstream K-planes of the prismatic element, and then linear interpolation is used to determine the required values at the precise current particle position (x_p, y_p, z_p).

During each call to FIND_3DVELOCITY, the code checks whether the particle has been pushed into a non-existent element outside the calculation domain. If this is the case, then the marching Runge-Kutta integration sequence is stopped, the particle is brought back to its previous time step, and then traversed using its latest velocity and a customized time step chosen to ensure that the particle stops exactly at a wall or an outflow boundary.

In the remaining parts of this section, some of the ingredients of the aforementioned particle-tracking algorithm are discussed in more detail.

3.2.1 Fourth-Order Runge-Kutta Scheme

The particle trajectory calculations in this work were done using a fourth-order Runge-Kutta (RK) scheme (Dahlquist and Bjorck, 1974). To facilitate the implementation of the RK scheme, the particle momentum equation is first cast into the following form:

$$\begin{aligned} &\frac{\partial \vec{U}_p}{\partial t} = c_1 \vec{U}_p + c_2 \\ &\frac{\partial \vec{x}_p}{\partial t} = \vec{U}_p \\ &\vec{U}_p(t=0) = \vec{U}_{po} \\ &\vec{x}_p(t=0) = \vec{x}_{po} \end{aligned} \tag{3.28}$$

The particle trajectory was computed independently along each coordinate direction, by calculating the corresponding components of the relevant forces and including them in the expressions for c_1 and c_2.

The RK scheme for advancing the x coordinate of the particle trajectory one time step, from t to $t+\Delta t$, is summarized below.

$$\begin{aligned} k_1 &= \Delta t U_p^t & l_1 &= \Delta t\left(c_1 U_p^t + c_2\right) \\ k_2 &= \Delta t\left(U_p^t + \tfrac{l_1}{2}\right) & l_2 &= \Delta t\left(c_1\left[U_p^t + \tfrac{l_1}{2}\right] + c_2\right) \\ k_3 &= \Delta t\left(U_p^t + \tfrac{l_2}{2}\right) & l_3 &= \Delta t\left(c_1\left[U_p^t + \tfrac{l_2}{2}\right] + c_2\right) \\ k_4 &= \Delta t\left(U_p^t + l_3\right) & l_4 &= \Delta t\left(c_1\left[U_p^t + l_3\right] + c_2\right) \end{aligned} \tag{3.29}$$

$$\begin{aligned} x_p^{t+\Delta t} &= x_p^t + \left(\frac{k_1 + 2k_2 + 2k_3 + k_4}{6}\right) \\ U_p^{t+\Delta t} &= U_p^{t+\Delta t} + \left(\frac{l_1 + 2l_2 + 2l_3 + l_4}{6}\right) \end{aligned} \tag{3.30}$$

The full particle trajectory is obtained by repeating the RK integration time-step-by-time-step until the particle exits the separation chamber at its outlet plane, or hits one of its walls along one of the transverse (x-coordinate or y-coordinate) directions. The RK integration is simultaneously carried out in all three directions using the same time step.

3.2.2 Interpolation to Obtain the Local Fluid Velocity and Its Spatial Gradients

During the RK integration for each time step, it is necessary to update the coefficients c_1 and c_2, which are functions of the forces experienced by the particle along each coordinate direction. Thus, the calculation of these coefficients requires values of the velocity components and their spatial gradients, the electric field strength, and the magnetic flux density at the current location of the particle. It is, therefore, necessary to determine the particular prismatic element that contains the particle, and use suitable interpolation functions to compute the required quantities at the precise position of the particle. For the problems addressed in this thesis, it was necessary to obtain the three

components of the local fluid velocity, u_f, v_f, w_f, and the gradients of w_f along the x and y directions $(\frac{\partial w_f}{\partial x}, \frac{\partial w_f}{\partial y})$.

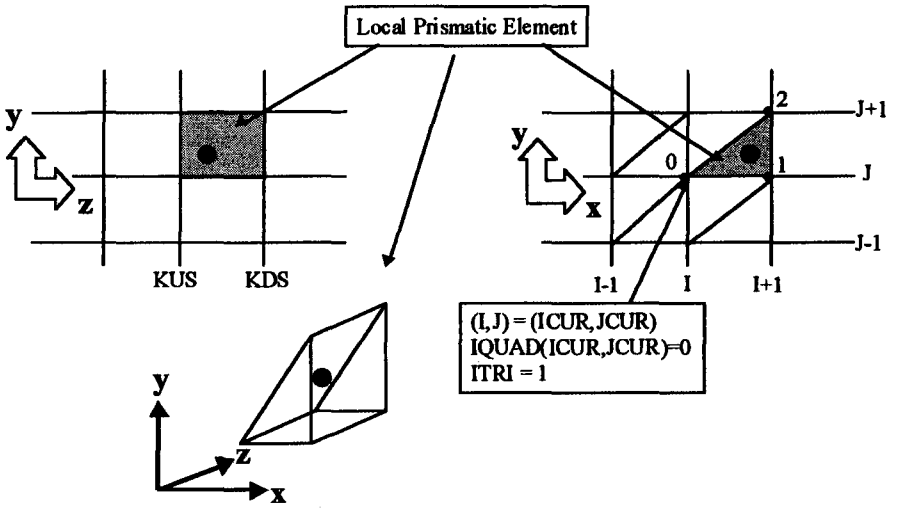

***Figure 3.6:** The prismatic element that contains the particle, and related notation*

Figure 3.6 shows a particle at a specific time, t. The procedure for obtaining the local fluid velocity components and their gradients is summarized below, using the w_f velocity component as an example.

1. Using the LOCATE2D subroutine, described in **Section 3.2.3**, and the current particle coordinates, obtain the (I,J) indices of the three vertices, 0-1-2, of the triangular cross-section of the element that contains the particle.
2. Using the z coordinate of the particle, determine the K indices, KUS and KDS, of the upstream and downstream planes of the element that contains the particle.
3. Compute the local w_f velocity at the correct x_p and y_p coordinates in the upstream K-plane, using the following interpolation function:

$$w_{f,US} = Ax + By + C \tag{3.31}$$

The coefficients, A, B, and C in this equation are obtained by solving:

$$\begin{Bmatrix} w_0 \\ w_1 \\ w_2 \end{Bmatrix}_{US} = \begin{bmatrix} x_0 & y_0 & 1 \\ x_1 & y_1 & 1 \\ x_2 & y_2 & 1 \end{bmatrix} \begin{Bmatrix} A \\ B \\ C \end{Bmatrix}_{US}$$

$$\{W\}_{US} = [X]\{A\}_{US} \tag{3.32}$$

$$\{A\}_{US} = [X]^{-1}\{W\}_{US}$$

4. Compute the local w_f velocity at the downstream K-plane in the same manner.
5. Compute the local w_f velocity at the correct z_p value, by using one-dimensional linear interpolation between the upstream and downstream K-planes:

$$w_f(x_p, y_p, z_p) = w_f(x_p, y_p)_{US} + \left(\frac{z_p - z_{US}}{z_{DS} - z_{US}}\right)\left(w_f(x_p, y_p)_{DS} - w(x, y)_{US}\right) \tag{3.33}$$

6. Obtain the local velocity gradients, $\frac{\partial w_f}{\partial x} = A$, and $\frac{\partial w_f}{\partial y} = B$ in the same manner:

$$\begin{aligned} \frac{\partial w_f}{\partial x}(x_p, y_p, z_p) &= A(x_p, y_p)_{US} + \left(\frac{z_p - z_{US}}{z_{DS} - z_{US}}\right)\left(A(x_p, y_p)_{DS} - A(x_p, y_p)_{US}\right) \\ \frac{\partial w_f}{\partial y}(x_p, y_p, z_p) &= B(x_p, y_p)_{US} + \left(\frac{z_p - z_{US}}{z_{DS} - z_{US}}\right)\left(B(x_p, y_p)_{DS} - B(x_p, y_p)_{US}\right) \end{aligned} \tag{3.34}$$

7. Repeat steps 1-5 for the u and v velocity components.

3.2.3 Method for Locating the Particle in the Triangular Finite Element Mesh

In the cross-sectional planes of the finite element mesh, to find the specific triangular element that contains the particle at the end of a time step, the subroutine LOCATE2D starts with the triangular element that contained the particle at the end of the previous time step and then determines whether the particle is still within that element or has traversed to an adjacent element.

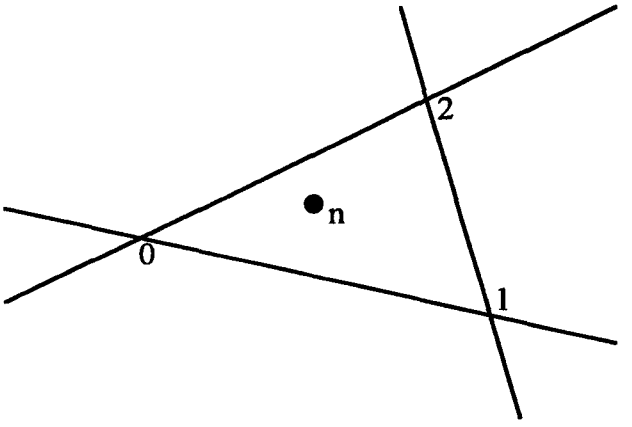

***Figure 3.7:** Triangular element occupied by the particle*

Consider the triangular element in **Figure 3.7**, which represents the previously occupied position of the particle. Once the updated particle coordinates are obtained from the RK integration scheme, they can be expressed in terms of the area coordinates (Zienkiewicz, 1977) of the previous element,

$$\begin{Bmatrix} x_n \\ y_n \end{Bmatrix} = \begin{Bmatrix} x_0 \\ y_0 \end{Bmatrix} a_0 + \begin{Bmatrix} x_1 \\ y_1 \end{Bmatrix} a_1 + \begin{Bmatrix} x_2 \\ y_2 \end{Bmatrix} a_2 \tag{3.35}$$

In this formulation, it is necessary that

$$a_0 + a_1 + a_2 = 1 \tag{3.36}$$

Therefore, the complete set of equations can be expressed in matrix form as follows:

$$\begin{bmatrix} x_0 & x_1 & x_2 \\ y_0 & y_1 & y_2 \\ 1 & 1 & 1 \end{bmatrix} \begin{Bmatrix} a_0 \\ a_1 \\ a_2 \end{Bmatrix} = \begin{Bmatrix} x_n \\ y_n \\ 1 \end{Bmatrix} \tag{3.37}$$

The solution for a_0, a_1, and a_2 can be obtained using any suitable matrix method, for example, Cramer's rule (Dahlquist and Bjorck, 1974). The values of these area coordinates are used to determine if the particle occupies the same element, or indicate the most likely new element if it has moved out of the old one. As examples, consider three special cases shown in **Figure 3.8**:

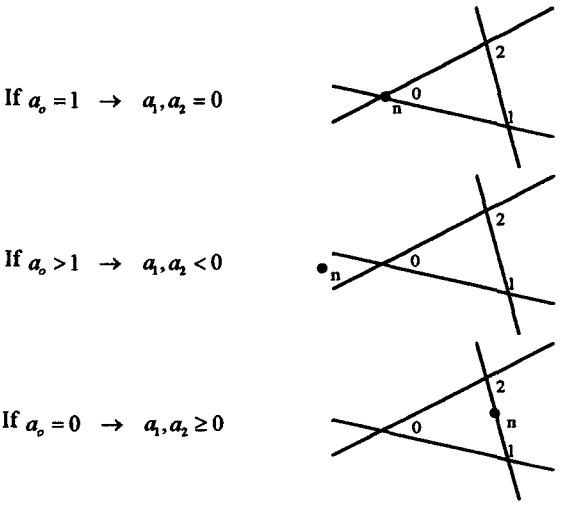

Figure 3.8: *Special cases to illustrate the rules used to locate the particle*

For locating the particle, the general rules that apply to triangular elements are the following (Ren et al., 1995):

1. If $0 \leq a_i, a_j, a_k \leq 1$, then the particle occupies the current element.
2. If $a_i < 0$ and $a_j, a_k \geq 0$, then the particle has traversed to an element that is adjacent to the side j-k, opposite node i.
3. If $a_j, a_k < 0$, then the particle has traversed to one of the elements associated with node i, opposite side j-k.

Based on these rules, the subroutine LOCATE2D solves for the area coordinates, and returns the value of a variable denoted as ILOC, ranging from 1 to 7 and corresponding to each of the possibilities depicted in **Figure 3.9.**

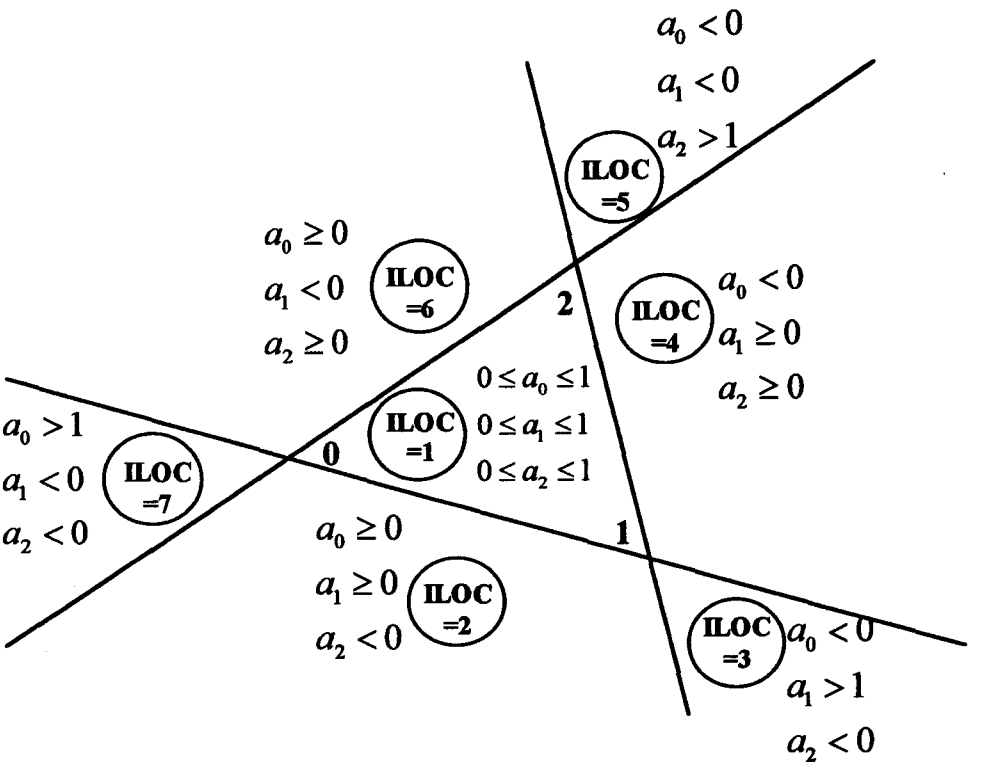

***Figure 3.9**: Particle location possibilities evaluated in subroutine LOCATE2D*

The element that is occupied by the particle is found by calling the subroutine LOCATE2D, using the value of ILOC to determine the search direction, and updating the trial element until ILOC=1 is returned. For the structured finite element meshes used in this work, there are four types of elements that must be considered when executing the particle-locating algorithm, as illustrated in **Figure 3.10**.

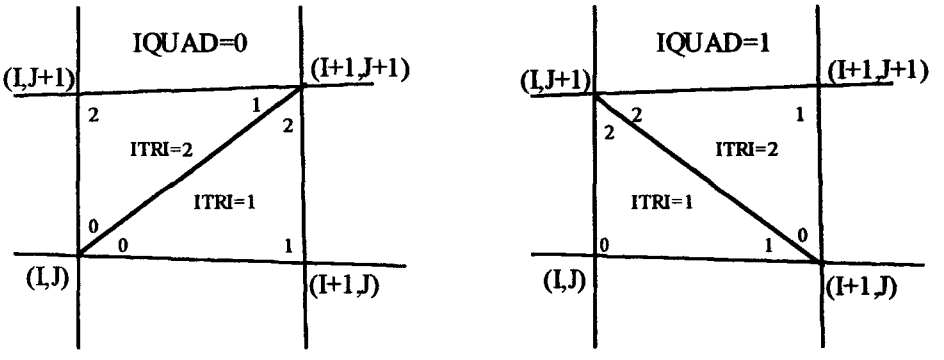

***Figure 3.10**: Possible configurations of the triangular elements in the structured mesh*

Table 3.1: *Possibilities that must be considered for the determination of the next search element for a returned value of ILOC*

ILOC	IQUAD	ITRI	I new	J new	ITRI new
2	0	1	I	J-1	2
	0	2	I	J	1
	1	1	I	J-1	2
	1	2	I+1	J	1 or 2
3	0	1	I+1	J-1	1 or 2
	0	2	I+1	J+1	1 or 2
	1	1	I+1	J-1	1 or 2
	1	2	I+1	J+1	1 or 2
4	0	1	I+1	J	1 or 2
	0	2	I	J+1	1
	1	1	I	J	2
	1	2	I	J+1	1
5	0	1	I+1	J+1	1 or 2
	0	2	I-1	J+1	1 or 2
	1	1	I-1	J+1	1 or 2
	1	2	I-1	J+1	1
6	0	1	I	J	2
	0	2	I-1	J	1 or 2
	1	1	I-1	J	1 or 2
	1	2	I	J	1
7	0	1	I-1	J-1	1 or 2
	0	2	I-1	J-1	1 or 2
	1	1	I-1	J-1	1 or 2
	1	2	I+1	J-1	1 or 2

The value of ILOC has to be applied differently for each of the four types of triangular elements depicted schematically in **Figure 3.10**: a summary of the possibilities is provided in **Table 3.1**.

An example of how the new values of I, J, and ITRI are determined is shown in Fig. 3.11 for IQUAD(I,J)=0, and ITRI=1. It can be observed that for ILOC=3, 4, 5, and 7, the ITRI in the new quadrilateral cannot be obtained with certainty. For such cases, the algorithm simply toggles the ITRI value between 1 and 2 whenever it traverses to a new element. If the proposed new element still does not return a value of ILOC=1, then an additional locator step is carried out.

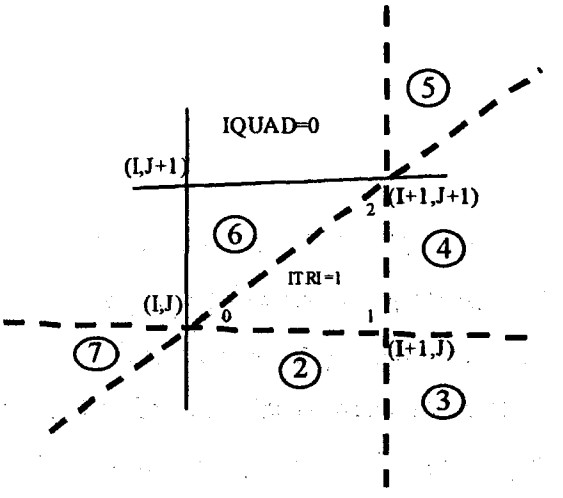

Figure 3.11: *Example used to illustrate updating of the element for IQUAD=0, ITRI=1*

The possibilities summarized in **Table 3.1** were incorporated into the computer program using statements akin to the following pseudo-code:

```
IF (ILOC=2) THEN
    I = I + IQUAD(I,J)*(ITRI-1)
    J = J + (ITRI-2)
IF (ILOC=3) THEN
    I = I + 1
    J = J + (2*ITRI-3)
IF (ILOC=4) THEN
    I = I + (1-IQUAD(I,J))*(2-ITRI)
    J = J + (ITRI-1)
IF (ILOC=5) THEN
    I = I - 1 + 2*(1-IQUAD(I,J))*(2-ITRI)
    J = J + 1
IF (ILOC=6) THEN
    I = I - (1-IQUAD(I,J))*(ITRI-1) - (IQUAD(I,J))*(2-ITRI)
    J=J
IF (ILOC=7) THEN
    I = I - 1 + 2*(IQUAD(I,J))*(ITRI-1)
    J = J - 1
```

3.2.4 Method for Checking When Particle Reaches a Domain Boundary

While computing the particle trajectories, the overall particle-tracking program may encounter the following three possible scenarios:

- The specified maximum number of time steps is reached before the particle reaches a domain boundary
- The particle reaches a domain boundary corresponding to one of the duct walls, before the number of time steps exceeds the specified maximum value
- The particle reaches the outflow boundary at the end of the separation chamber, before the number of time steps exceeds the specified maximum value

For the first case, the computer program stops execution without the need for any special treatment. For the second case, in which the particle reaches a domain boundary, it is necessary in subroutine FIND_3DVELOCITY to recognize this scenario before any interpolations are attempted, in order to prevent the code from trying to interpolate for dependent variables on fictitious elements, that are not a part of the finite element mesh.

Consider the example in **Figure 3.12**, which illustrates a case where the particle reaches the separator chamber wall at $x = a$ (corresponding to the grid line $I = L1$).

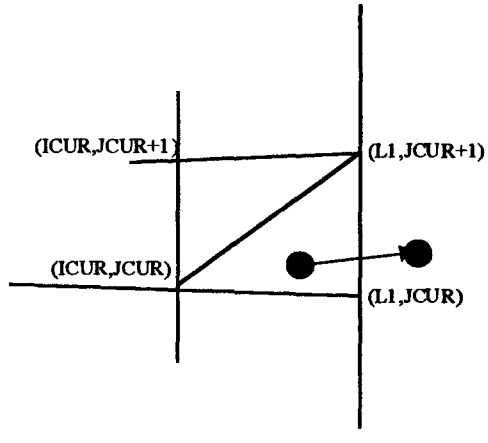

***Figure 3.12:** Example of particle exiting domain at x=a (I=L1)*

At time t, the particle is within the calculation domain, but during the following time step, which advances the time to $t + \Delta t$, it has moved to a point outside the domain boundary. Since interpolation of the dependent variables is based on the particle position

at the beginning of the time step, the code recognizes a boundary violation only after the particle has exited the calculation domain. In such cases, the algorithm is set-up to back-calculate the particle position in all three coordinate directions using the final instantaneous velocity, in order to bring it back to the location where it crossed the wall boundary.

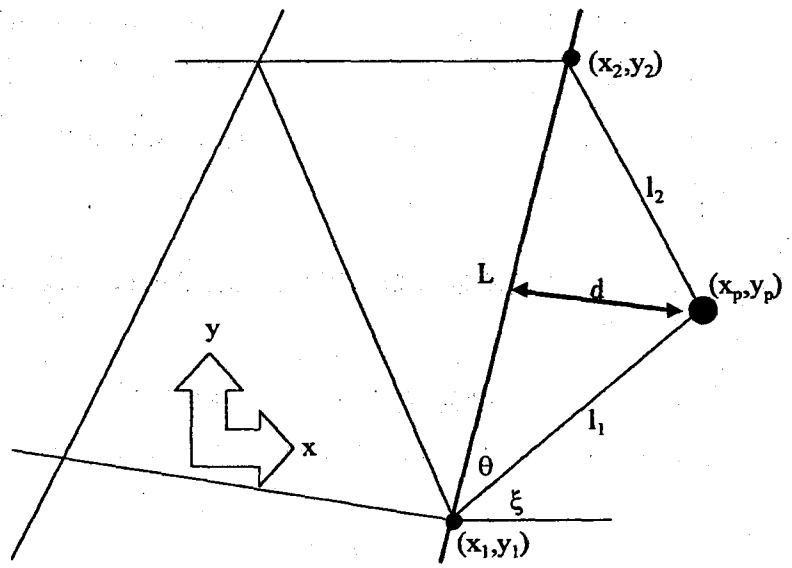

***Figure 3.13:** Back-calculation of final particle position at sidewall boundary*

Consider the particle in **Figure 3.13**, as it approaches the domain boundary, which is given an arbitrary orientation. The first step in the back-calculation procedure involves determining the two boundary nodes between which the particle crossed the domain boundary. This can be conveniently achieved by using the indices (ICUR,JCUR) that represent the latest occupied element. The code is set up so that a boundary violation is identified when ICUR changes to 0 or L1, or when JCUR changes to 0 or M1.

Next, the distance, *d*, between the latest particle position (outside the domain boundary) and the nearest point on the domain boundary is computed using the cosine law (please see notation given in **Figure 3.13**):

$$l_2^2 = L^2 + l_1^2 - 2Ll_1\cos(\theta) \tag{3.38}$$

The distance, *d*, is then given by:

$$d = -l_1 \sin(\theta)$$
$$d = -l_1 \sin\left[\arccos\left(\frac{l_1^2 + L^2 - l_2^2}{2Ll_1}\right)\right] \tag{3.39}$$

The negative sign has been deliberately inserted in the equations in order to emphasize that the particle has exited the domain and it needs to be moved backwards to a location on the domain boundary. The velocity of the particle, in a direction normal to the boundary is also needed for back-calculating the particle position. First, the orientation of the boundary edge is expressed as an angle relative to the x-coordinate direction:

$$\xi = a\tan\left(\frac{y_2 - y_1}{x_2 - x_1}\right) \tag{3.40}$$

Then, the velocity normal to the boundary is calculated using:

$$V_\perp = u_p \cos(\pi/2 - \xi) + v_p \cos(\xi) \tag{3.41}$$

Finally, the time step required to move the particle backwards is obtained by dividing the normal distance by the normal velocity:

$$\Delta t_{final} = d / V_\perp \tag{3.42}$$

The boundary treatment for the case where the particle exits the calculation domain at the outflow boundary of the separation chamber is carried out in a similar fashion. For ducts of constant cross-section, such as the separation chamber considered in this work, the outflow boundary is oriented normal to the *z*-coordinate direction. Therefore, the previous calculation procedure can be simplified by using the final *z* position and *w* velocity of the particle to calculate the final time step required for the back calculation.

Chapter 4

Test Problems

The numerical solution methods presented in Chapter 3 are validated in this chapter by applying them to four different test problems and checking their solutions against analytical and/or numerical solutions available in the published literature.

4.1 Fully Developed Flow in a Rectangular Duct

4.1.1 Problem Statement

The problem considered here involves steady, laminar, fully developed flow of a constant-property Newtonian fluid in a straight duct of uniform rectangular cross-section, akin to that shown schematically in **Figure 2.1**, but *without* the imposed *EM* fields.

In the fully developed regime, the velocity component in the axial, or z, direction, w, is governed by the following equation (Shah and London, 1978):

$$-\frac{dp}{dz}+\frac{\partial}{\partial x}\left(\eta\frac{\partial w}{\partial x}\right)+\frac{\partial}{\partial y}\left(\eta\frac{\partial w}{\partial y}\right)=0 \tag{4.1}$$

Noting that the properties of the fluid are assumed to be constant in this test problem, Equation (4.1) can be rewritten as follows:

$$\frac{\partial^2 w}{\partial x^2}+\frac{\partial^2 w}{\partial y^2}=\left(\frac{dp}{dz}\right)/\eta \triangleq c_w \tag{4.2}$$

In this equation, p is the reduced pressure, as defined earlier in Equation (2.1). With respect to the schematic illustration of the rectangular duct and the Cartesian coordinate system shown in **Figure 2.1**, the boundary conditions on w are the following:

$$w=0 \text{ at } x=0,\ x=2a,\ y=0, \text{ and } y=2b \tag{4.3}$$

The exact solution to this problem is the following (Lundgren et al., 1964; Shah and London, 1978):

$$w=-\frac{16c_w a^2}{\pi^3}\sum_{n=1,3,\ldots}^{\infty}\frac{1}{n^3}(-1)^{(n-1)/2}\left[1-\frac{\cosh(n\pi(y-b)/2a)}{\cosh(n\pi b/2a)}\right]\cos\left(\frac{n\pi(x-a)}{2a}\right) \tag{4.4}$$

The average value of w over the cross-section of the duct is given by:

$$w_{av} = -\frac{c_w a^2}{3}\left[1 - \frac{192}{\pi^5}\left(\frac{a}{b}\right)\sum_{n=1,3,\ldots}^{\infty}\frac{1}{n^5}\tanh\left(\frac{n\pi b}{2a}\right)\right] \tag{4.5}$$

The hydraulic diameter, Reynolds number, and the Fanning Friction for this problem are defined as follows (Shah and London, 1978):

$$D_h = \frac{4ab}{(a+b)}\ ;\ \mathrm{Re} = \frac{\rho \mathrm{w}_{av} D_h}{\eta}\ ;\ f = \frac{\tau_{w,av}}{0.5\rho w_{av}^2} \tag{4.6}$$

where $\tau_{w,av}$ is the average wall shear stress. The product of f and Re is given by the following equation (Shah and London, 1978):

$$f\,\mathrm{Re} = -\frac{8c_w a^2}{w_{av}[1+(a/b)]^2} \tag{4.7}$$

For any given aspect ratio, $AR = b/a$, the exact values of $f\,\mathrm{Re}$ can be computed using Eqs. (4.6) and (4.7). Shah and London (1978) have proposed the following equation for $f\,\mathrm{Re}$ that approximates its exact values with an accuracy of 0.05% or better, for all values of AR:

$$f\,\mathrm{Re} = 24\left(1 - 1.3553AR + 1.9467AR^2 - 1.7012AR^3 + 0.9564AR^4 - 0.2537AR^5\right) \tag{4.8}$$

The control-volume finite element method (CVFEM) presented in **Section 2.1** was used to solve this test problem. The validity of this CVFEM, and its computer implementation, was established by comparing the results with those obtained from the aforementioned exact and approximate solutions provided by Lundgren et al. (1964) and Shah and London (1978).

4.1.2 Results for w_{max}/w_{av} and $f\,\mathrm{Re}$

The CVFEM results were obtained using line-by-line structured grids of *L1*x*M1* nodes. A power-law distribution of the grid lines was used to generate grids that packed more nodes in the vicinity of the walls than in the central regions of the duct. In the lower-left quadrant of the duct cross-section ($0 \le x \le a$ and $0 \le y \le b$), this power-law grid was generated as follows:

$$X(I) = a[(I-1)/\{0.5(L1-1)\}]^{XPOW}\ ;\ \mathrm{Y}(J) = b[(J-1)/\{0.5(M1-1)\}]^{YPOW} \tag{4.9}$$

Only odd values of $L1$ and $M1$ were used, in order to ensure that there would be grid lines along the centerlines of the duct cross-section ($x = a$ and $y = b$). The grid lines in the remaining three quadrants of the duct cross-section were obtained by suitably reflecting those in the lower-left quadrant.

Values of w_{max}/w_{av} and $f\,\mathrm{Re}$ for seven different values of AR, obtained using the CVFEM presented in **Section 2.1**, the corresponding exact solutions (Equations (4.4) and (4.5)) of Lundgren et al. (1964), and the approximate solution (Equation (4.8)) of Shah and London (1978) are presented in **Table 4.1** and **Figure 4.1**. The CVFEM results in this table and figure were obtained using $L1 = 61$, $M1 = 61$, $XPOW = 1.1$, and $YPOW = 1.1$.

Table 4.1: *w_{max}/w_{avg} and $f\,\mathrm{Re}$ values for fully developed flow in a rectangular duct - comparison of CVFEM results with those of Lundgren et al. (1964) and Shah and London (1978)*

Aspect Ratio AR	w_{max}/w_{avg} Lundgren et al. (1964)	w_{max}/w_{avg} CVFEM	$f\mathrm{Re}$ Shah and London (1978)	$f\mathrm{Re}$ CVFEM
1.000	2.0962	2.0991	14.2296	14.2332
0.750	2.0774	2.0804	14.4782	14.4822
0.500	1.9918	1.9953	15.5573	15.5560
0.400	1.9236	1.9275	16.3767	16.3775
0.250	1.7737	1.7789	18.2340	18.2468
0.125	1.6283	1.6363	20.5898	20.6105
0.100	1.6009	1.6101	21.1759	21.2002

The data presented in Table 4.1 show that, for all values of the aspect ratio, AR, the CVFEM results differ from those of Lundgren et al (1964) and Shah and London (1978) by less than ±0.6%. These differences are hardly perceptible in the graphical presentation of the results in **Figure 4.1**

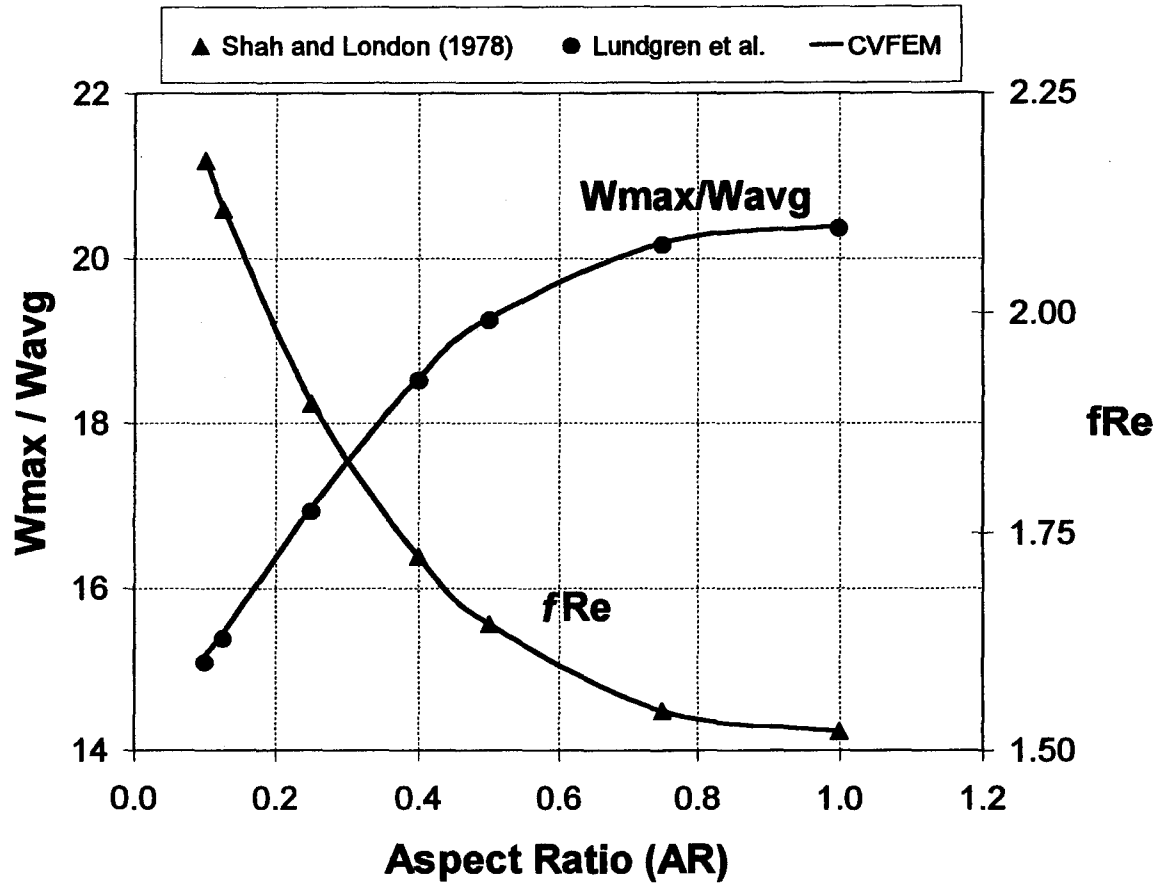

Figure 4.1: *Variation of w_{max}/w_{avg} and fRe and with aspect ratio, AR, for fully developed flow in a rectangular duct - comparison of CVFEM results with published data (Lundgren et al., 1964; Shah and London, 1978)*

4.1.3 Grid Independence Checks

All numerical solution methods must satisfy the following consistency requirement: as the computational grid is refined, the numerical solution must asymptotically approach the exact solution. Furthermore, the differences between numerical solutions obtained on successively finer grids should become progressively smaller, and, eventually, essentially negligible, to within the limit imposed by machine round-off characteristics. The CVFEM simulations were run on successively finer grids, and the solutions were examined to ensure that they met the aforementioned requirements. Five different power-law grids, similar to that represented by Equation (4.9), were used in these tests: *L1xM1* = 21x21, 41x41, 61x61, 81x81, and 101x101, with *XPOW* = *YPOW* = 1.2, 1.2, 1.1, 1.1, and 1.05, respectively. The results are presented in **Figure 4.2**.

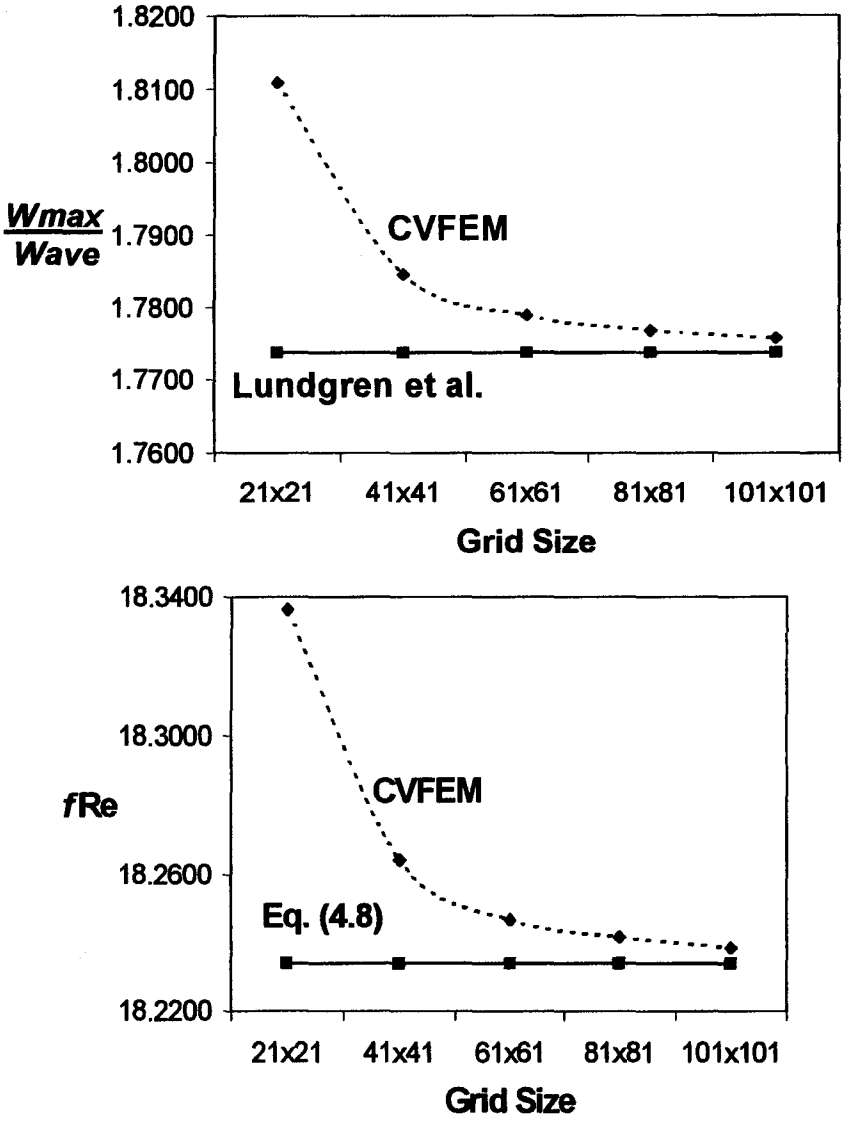

Figure 4.2: *Variation of the CVFEM results with grid refinement*

The results presented in **Figure 4.2** show that the CVFEM results do satisfy the consistency and grid-independence requirements.

4.2 Particle Settling in a Stationary Fluid Subjected to Gravity and Electromagnetic Forces

4.2.1 Problem Statement

In this test problem, a smooth, rigid, electrically non-conducting, spherical particle is allowed to settle in an electrically conducting fluid. The fluid is Newtonian, its properties are assumed to be constant, and it is stationary far from the particle ($U_f = 0$). It is also assumed here that the virtual mass and Basset forces are negligible. Under these conditions, the particle momentum equation, Equation (2.40), reduces to the following form:

$$m_p \frac{d\vec{U}_p}{dt} = \vec{F}_{DRAG} + \vec{F}_{BUOYANCY} + \vec{F}_{EM,p} \tag{4.10}$$

In this equation, the force terms are given by the following equations:

$$\begin{aligned} \vec{F}_{DRAG} &= 3\pi D_p \eta \left(\vec{U}_f - \vec{U}_p\right) \\ \vec{F}_{BUOYANCY} &= \left(\frac{\pi D_p^3}{6}\right)(\rho_p - \rho_f)\vec{g} \\ \vec{F}_{EM,p} &= -\frac{3}{4}\left(\frac{\pi D_p^3}{6}\right)\vec{F}_{EM,UnitVol} \end{aligned} \tag{4.11}$$

With respect to the finite element mesh and Cartesian coordinate system depicted in **Figure 3.4**, the following were imposed: $\vec{g} = g\vec{k}$, $\vec{E} = -E\vec{i}$, $\vec{B} = B_o\vec{j}$, where $\vec{i}$, $\vec{j}$, and $\vec{k}$ are unit vectors in the x, y, and z directions, respectively. In addition, the particle Reynolds number is assumed to be less than or equal to one (Stokes regime): $\mathrm{Re}_p \le 1$. Then, noting that $\vec{U}_f = 0$, and with $\vec{U}_p = U_p\vec{k}$, the particle momentum in the z direction is governed by the following equation:

$$m_p \frac{dU_p}{dt} = -3\pi D_p \eta U_p + \left(\frac{\pi D_p^3}{6}\right)(\rho_p - \rho_f)g + \frac{3}{4}\left(\frac{\pi D_p^3}{6}\right)\sigma_f E B_o \tag{4.12}$$

The terminal velocity of the particle can be obtained from Equation (4.12) by setting the acceleration term to zero: $dU_p/dt = 0$. Using this approach, the following expressions are obtained for the terminal velocity of the particle under the following three

combinations of the gravity and *EM* force: only gravity and zero *EM* force; only *EM* force and zero gravity; and both gravity and *EM* force:

Only Gravity and Zero EM Force: $$(U_p)_{Terminal} = (\rho_p - \rho_f) g \frac{D_p^2}{18\eta} \tag{4.13}$$

Only EM Force and Zero Gravity: $$(U_p)_{Terminal} = \frac{3}{4} \sigma_f E B_o \frac{D_p^2}{18\eta} \tag{4.14}$$

Both Gravity and EM Force: $$(U_p)_{Terminal} = \left[(\rho_p - \rho_f) g + \frac{3}{4} \sigma_f E B_o \right] \frac{D_p^2}{18\eta} \tag{4.15}$$

The transient solution for the particle velocity and its complete trajectory can be obtained by integrating Equation (4.10) with respect to time. The analytical results are the following:

$$U_p = \frac{c_2}{c_1} \left[\exp(c_1 t) - 1 \right] \tag{4.16}$$

$$x_p = \frac{c_2}{c_1} \left\{ \frac{1}{c_1} \left[\exp(c_1 t) - 1 \right] - t \right\} \tag{4.17}$$

In these equations, the constants c_1 and c2 are given by:

$$\begin{aligned} c_1 &= -\frac{18\eta}{\rho_f D_p^2} \\ c_2 &= \frac{18\eta}{\rho_f D_p^2} U_f + \frac{3\sigma E B_o}{4\rho_p} + \left(1 - \frac{\rho_f}{\rho_p} \right) g \end{aligned} \tag{4.18}$$

Numerical solutions to this problem were obtained using the particle-tracking algorithm described in **Section 3.2**, with a finite element mesh akin to that depicted in **Figure 3.4** and a uniform distribution of the grid lines in the *x*, *y*, and *z* directions (with *LI* = 21, *MI* = 21, and *NI* = 21). The following physical properties and problem parameters, which apply to the electromagnetic filtration of molten aluminum, were used:

Density of fluid, $\rho_f = 2{,}374$ kg/m^3

Dynamic viscosity of fluid, $\eta = 2.998 \times 10^{-3}$ kg/m-s

Conductivity of fluid, $\sigma_f = 2.95 \times 10^6$ mho/m

Mass density of particle, $\rho_p = 3{,}990$ kg/m^3 (4.19)

Particle diameter, $D_p = 2.5 \times 10^{-5}$ m

Electric field strength, E = 1.0 V/m

Magnetic flux density, $B_o = 0.050$ T

4.2.2 Particle Terminal Velocity

Analytical and numerical solutions corresponding to the three combinations of conditions depicted in Equations (4.13) to (4.15) are given in **Table 4.2**.

Table 4.2: *Comparison of numerical and analytical solutions for the terminal velocity of a particle settling in a stationary fluid*

Conditions	Analytical Solution	Numerical Solution
Only gravity, no EM force	0.1836 mm/s	0.1836 mm/s
Only EM force, no gravity	1.2812 mm/s	1.2812 mm/s
Both gravity and EM force	1.4648 mm/s	1.4648 mm/s

The results in **Table 4.2** show that for each of the three cases considered, the numerical results match the analytical results exactly. These results also demonstrate that, for the physical properties and problem parameters given in Equation (4.19), the electromagnetic field produces an order of magnitude increase in the terminal velocity of the particle over that obtained with gravity alone.

This problem was also run with the finite element mesh at several different orientations with respect to the Cartesian coordinate system ($\vec{i}, \vec{j}, \vec{k}$ unit vectors). In all cases, the numerical and analytical results for the particle terminal velocity matched exactly, as in **Table 4.2**.

4.2.3 Particle Velocity Distribution and Particle Trajectory

For the properties and problem parameters given in Equation (4.19), and for the initial conditions x_p=0 and U_p=0, the particle-tracking algorithm was used to compute the variation of particle velocity with time, as well as the corresponding particle trajectory. The finite element mesh was the same as that described in the previous subsection. The numerical results and the corresponding analytical solutions (obtained using Equations (4.16) to (4.18)) are plotted in **Figure 4.3**. The time step in the computer simulation was set equal to one-tenth the particle velocity relaxation time:

$$\Delta t = \frac{\tau_V}{10} = \left(\frac{\rho_p D_p^2}{18\eta} \right) / 10 \tag{4.20}$$

Smaller time steps were also tried, and it was established that the numerical solutions become essentially insensitive to time-step refinements below $\Delta t = \tau_v / 10$.

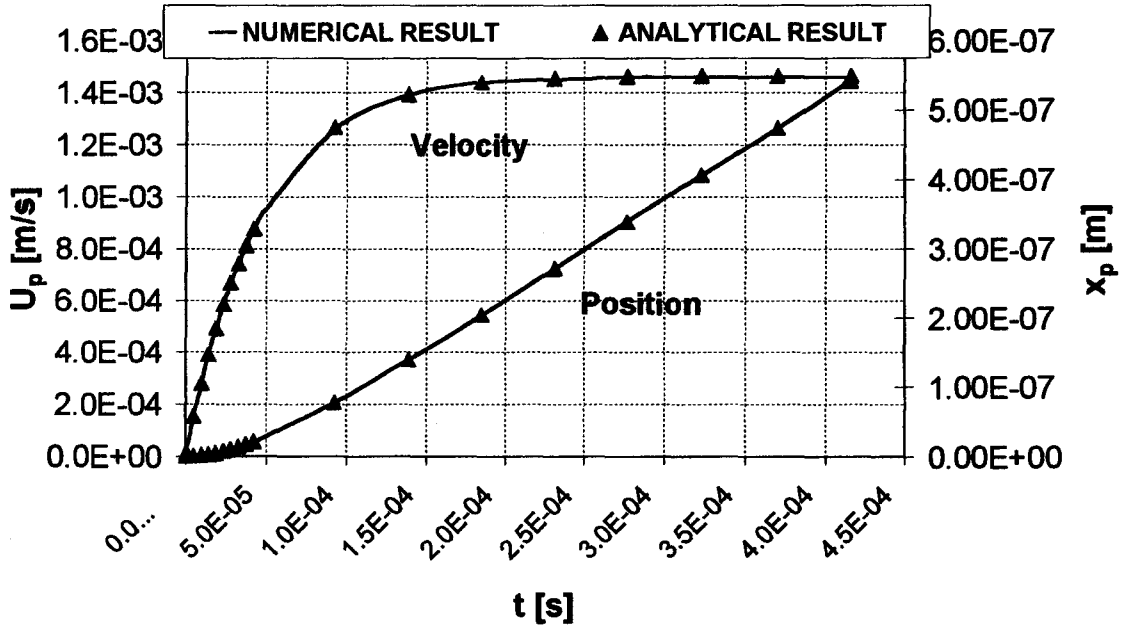

Figure 4.3: *Particle settling in a stationary fluid under the influence of gravity and EM force: Particle velocity distribution and trajectory*

The results plotted in **Figure 4.3** show that the agreement between the numerical and analytical results is uniformly excellent.

4.3 Motion of a Particle in a Couette Flow Layer Adjacent to a Solid, Impermeable, Plane Wall

4.3.1 Problem Statement

This test problem is schematically illustrated in **Figure 4.4**.

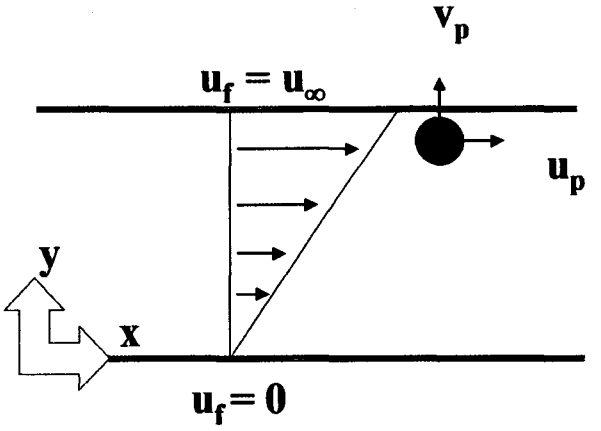

Figure 4.4: *Particle motion in a Couette flow layer adjacent to a solid, impermeable, plane wall.*

The fluid is Newtonian, and its properties are assumed to be constant. The fluid flows steadily past a solid, impermeable, plane wall located at $y = 0$. The fluid velocity in a direction normal to the wall is zero, and its velocity parallel to the wall is invariant with x and varies linearly with y:

$$u_f = (y/H)u_\infty \tag{4.21}$$

The height of the Couette layer is H, and the fluid velocity at $y = H$ is u_∞.

The particles are small, rigid, smooth spheres. In this test problem, it is assumed that the particle trajectories are influenced by the drag and lift forces only. The buoyancy, virtual mass, Basset, and EM forces on the particle are assumed to be nonexistent or negligibly small. The particle Reynolds number is assumed to be less than or equal to one (Stokes regime): $\mathrm{Re}_p \leq 1$. It is also assumed that the equation proposed by Saffman (1965) for the lift force applies in this problem. Under these conditions, the components of the particle momentum equation in the x and y directions can be simplified and expressed as follows:

$$\frac{du_p}{dt} = \frac{1}{\tau_V}\left(u_f - u_p\right)$$
$$\frac{dv_p}{dt} = -\frac{1}{\tau_V}v_p + \frac{3C}{2\pi}\frac{\rho_f}{\rho_p}\frac{1}{D_p}\varsigma^{1/2}\left(u_f - u_p\right)\left(\frac{dU_f}{dy}\right)^{1/2} \tag{4.22}$$

The following nondimensional variables and parameters are introduced at this stage:

$$t^* = t\frac{H}{u_\infty}\ ;\ y^* = \frac{y}{H}\ ;\ u_p^* = \frac{u_p}{u_\infty}\ ;\ u_f^* = \frac{u_f}{u_\infty}\ ;\ \delta_H = \frac{D_p}{H}$$
$$\lambda = \frac{\rho_p}{\rho_f}\ ;\ St = \frac{\rho_p D_p^2 u_\infty}{18\eta H}\ ;\ \Psi = \frac{3C}{2\pi}\frac{1}{\delta\lambda}\frac{1}{\sqrt{\mathrm{Re}}} \tag{4.23}$$

Then, the components of the nondimensional particle momentum can be expressed as follows, *dropping the asterisk (*) superscript associated with the dimensionless variables*:

$$\frac{du_p}{dt} = \frac{1}{St}\left(u_f - u_p\right)$$
$$\frac{dv_p}{dt} = -\frac{1}{St}v_p + \Psi\left(u_f - u_p\right) \tag{4.24}$$

The corresponding nondimensional *initial conditions* for this problem are:

$$\text{At t=0} \qquad y_o = 1,\quad u_o \geq 0,\quad v_0 < 0 \tag{4.25}$$

Naumov (1995) presents the following analytical solution to the equations that govern this problem (it has been established in this work that these expressions do indeed satisfy Equation (4.24):

$$\text{if } \Psi \neq \frac{1}{St^2} \qquad y = \frac{s_1}{r_1}\left[\exp\left(r_1 t\right) - 1\right] + \frac{s_2}{r_2}\left[\exp\left(r_2 t\right) - 1\right] + 1 \tag{4.26}$$

$$if\ \Psi = \frac{1}{St^2} \qquad y = s_1 \frac{St}{4}\left[1 - \exp\left(\frac{-2t}{St}\right)\right] + s_2 t + 1 \tag{4.27}$$

where

$$r_1 = -\frac{1}{St} - \sqrt{\Psi}\ ;\ r_2 = -\frac{1}{St} + \sqrt{\Psi}$$
$$s_1 = \frac{1}{2}\left[v_o - (1-u_o)\sqrt{\Psi}\right]\ ;\ s_2 = \frac{1}{2}\left[v_o + (1-u_o)\sqrt{\Psi}\right] \tag{4.28}$$

Attention is now focused on cases for which $\Psi < 1/St^2$. For these cases, the analytical solution, Equation (4.26), permits the deduction of a criterion which the initial conditions must satisfy for the particle to reach the wall at $y = 0$, despite the action of the lift force which opposes the movement of the particle towards the wall. When the initial conditions violate this criterion, then the lift force is able to prevent the particle from reaching the wall. This criterion on the initial conditions is determined by setting y=0 as $t \to \infty$. The result can be expressed in the following form:

$$v_o \le \Psi u_o St - \frac{1}{St} \tag{4.29}$$

4.3.2 Particle Trajectories

The particle trajectories corresponding to the conditions St=1.0, u_o=1.0, $\delta = 0.05$, and $\Psi = 0.1$ were obtained using the analytical solution (given in Equation (4.26)) and also the particle-tracking algorithm described in **Section 3.2**.

For these conditions, the criterion expressed in Equation (2.29) yields a critical value of v_0= -0.9: for v_o > -0.9, the analytical solution shows that the lift force prevents the particle from reaching the wall; for v_o < -0.9, however, the particle reaches the wall despite the lift force that opposes its movement towards the wall.

Particle trajectories obtained from the analytical and numerical solutions, for v_0 = -1.0, -0.9, and –0.7 are plotted in **Figure 4.5**. The numerical results were obtained with a time step of $\Delta t = \tau_V / 1000$, where $\tau_V = \rho_p D_p^2 / 18\eta$. The problem was run in terms of dimensional variables: the value of the height of the Couette layer, H, was arbitrarily set at 0.01 m, and the values of U_∞, ρ_p, and other properties and variables were adjusted appropriately to achieve the aforementioned values of the nondimensional parameters.

As can be see from the results plotted in **Figure 4.5**, the agreement between the analytical and numerical solutions is excellent.

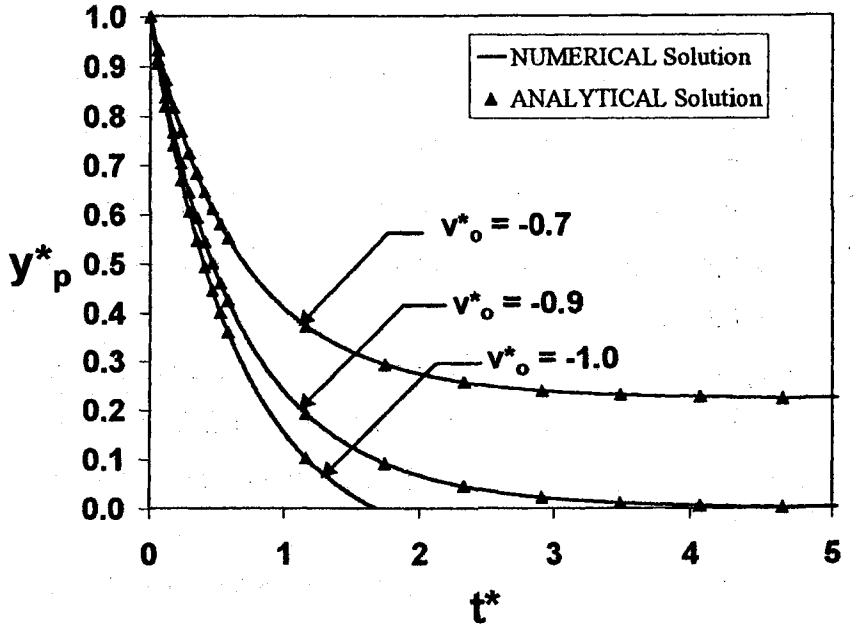

Figure 4.5: Particle trajectories in a Couette flow layer adjacent to a solid, impermeable, plane wall

4.4 Motion of a Particle in a Forced Vortex Flow Field, With and Without the Inclusion of Basset Force

4.4.1 Problem Statement

This test problem is schematically illustrated in **Figure 4.6.** A constant-property Newtonian fluid is assumed. The angular velocity vector that characterizes the forced vortex flow is directed in the positive z direction: $\vec{\omega} = \omega\vec{k}$. The fluid velocity field is entirely constrained to the x-y plane, and is given by $\vec{U}_f = \vec{\omega} \times \vec{r}$. The particle is a small, rigid, smooth, sphere, and it is assumed that the particle Reynolds number is less than or equal to one throughout the calculation domain (Stokes regime).

This test problem was used to validate the formulation and implementation of the Basset force term in the particle-tracking algorithm. This validation was done by

checking the numerical predictions against the analytical solutions to this problem proposed by Druzhinin and Ostrovsky (1994).

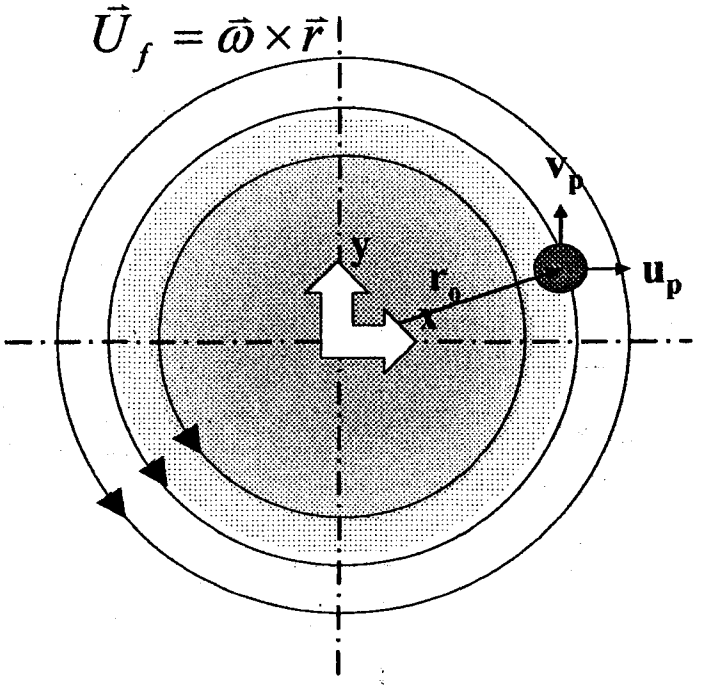

Figure 4.6: *Particle motion in a forced vortex flow*

In the particle momentum equation, the drag, virtual mass, and Basset forces are retained. The buoyancy, Saffman lift, and EM forces are not considered in this test problem. Thus, the particle momentum equation is the following:

$$\frac{d\vec{U}_p}{dt} = \left(\frac{\rho_f}{\rho_p}\right)\left(\frac{D\vec{U}_f}{Dt}\right) + \frac{18\eta}{\rho_p D_p^2}\left(\vec{U}_f - \vec{U}_p\right) + \frac{1}{2}\left(\frac{\rho_f}{\rho_p}\right)\left(\frac{d\vec{U}_f}{dt} - \frac{d\vec{U}_p}{dt}\right) + \frac{9}{\sqrt{\pi}}\frac{\sqrt{\rho_f \eta}}{\rho_p D_p}\int_0^t \frac{\frac{d\vec{U}_f}{dt} - \frac{d\vec{U}_p}{dt}}{\sqrt{t-t'}}\,dt' \tag{4.30}$$

Using previously defined dimensionless variables and parameters, the particle momentum equation can be rewritten in non-dimensional form as follows:

$$\frac{d\vec{U}_p}{dt}=\frac{1}{\lambda}\frac{D\vec{U}_f}{Dt}+\frac{1}{St}\left(\vec{U}_f-\vec{U}_p\right)+$$
$$\frac{1}{2\lambda}\left(\frac{d\vec{U}_f}{dt}-\frac{d\vec{U}_p}{dt}\right)+\frac{9}{\lambda\delta}\frac{1}{\sqrt{\pi\,\mathrm{Re}}}\int_0^t\frac{\frac{d\vec{U}_f}{dt}-\frac{d\vec{U}_p}{dt}}{\sqrt{t-t'}}dt' \tag{4.31}$$

Druzhinin and Ostrovsky integrated Equation (4.31) using a series function for the velocity. Their analytical solution for the two-dimensional vortex problem, with and without the Basset force, is given in the following form:

$$u_p=-\omega y-\frac{D_p^2}{18\eta}\left(\rho_f-\rho_p\right)\omega^2 x+\Delta u_p$$
$$v_p=\omega x-\frac{D_p^2}{18\eta}\left(\rho_f-\rho_p\right)\omega^2 y+\Delta v_p \tag{4.32}$$

where Δu_p and Δv_p are the velocity corrections associated with the Basset force, and are given by:

$$\Delta u_p=\frac{1}{36}\left(\frac{D_p^2\rho_f}{\eta}\right)\left(1-\frac{\rho_p}{\rho_f}\right)\omega^{3/2}r\sin\left(\omega t-\frac{\pi}{4}\right)$$
$$\Delta v_p=-\frac{1}{36}\left(\frac{D_p^2\rho_f}{\eta}\right)\left(1-\frac{\rho_p}{\rho_f}\right)\omega^{3/2}r\cos\left(\omega t-\frac{\pi}{4}\right) \tag{4.33}$$

Transforming Eqs. (4.32) and (4.33) to cylindrical coordinates, Druzhinin and Ostrovsky obtained the following expressions for the radial and tangential velocity components:

$$\left(V_r\right)_p=-\left(\rho_f-\rho_p\right)\frac{D_p^2}{18\eta}\left[1-\left(\frac{D_p^2\rho_f}{8\eta}\omega\right)^{1/2}\right]\omega^2 r$$
$$\left(V_\theta\right)_p=\left[1+\left(\rho_f-\rho_p\right)\frac{D_p^2}{18\eta}\left(\frac{D_p^2\rho_f}{8\eta}\omega^3\right)^{1/2}\right]\omega r \tag{4.34}$$

These expressions demonstrate that the particle migrates across the flow streamlines when its density is different than that of the fluid. This will occur whether or not the Basset force correction, given by the second term in parentheses, is applied. When

$\rho_p > \rho_f$, the particle moves away from the center, and when $\rho_p < \rho_f$, the particle migrates toward the center of the vortex.

4.4.2 Particle Trajectories

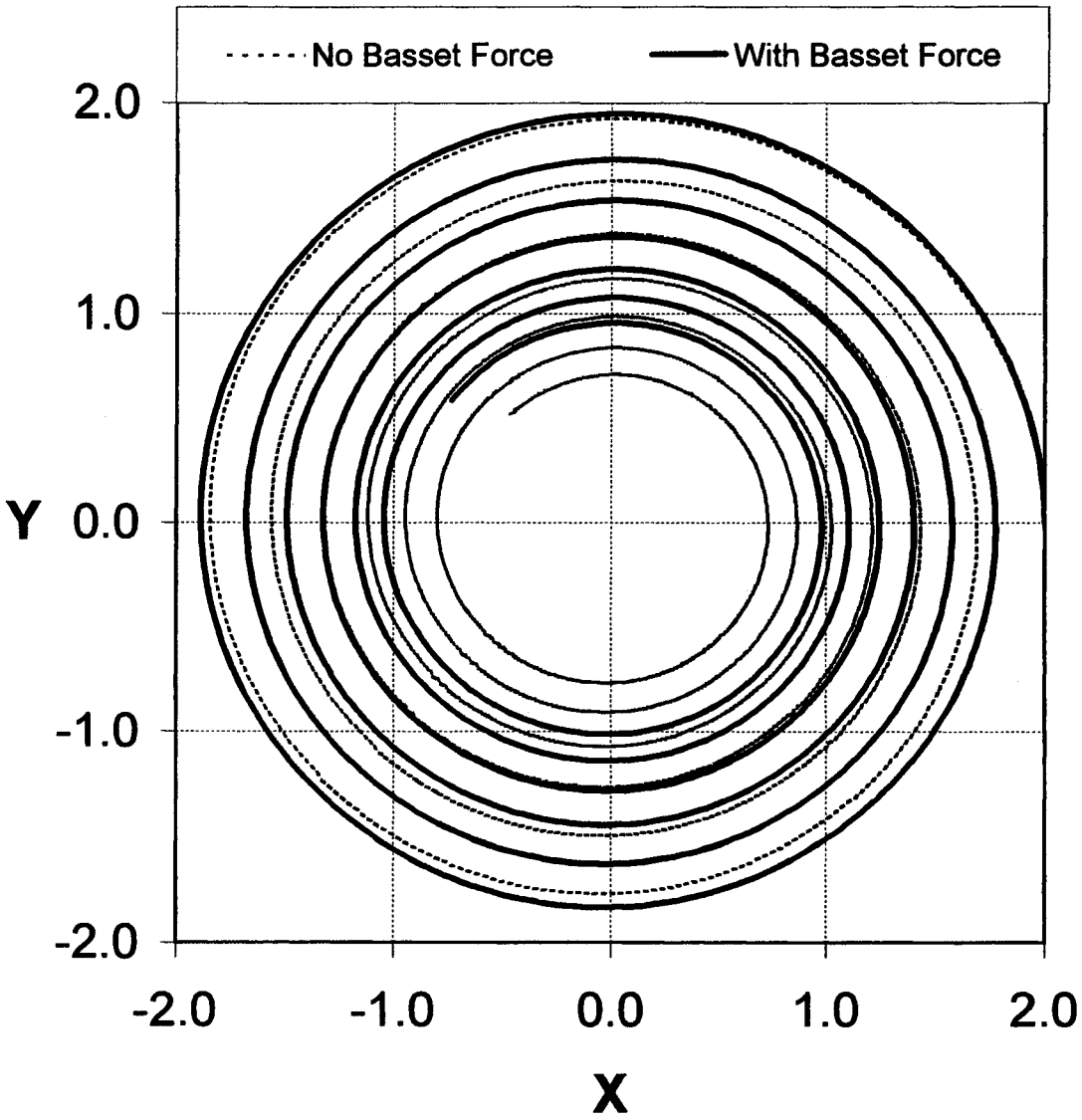

Figure 4.7: Particle trajectory in a forced vortex for λ = 0.5, St = 0.022, and ω =2

This problem was solved with a forced vortex velocity field in a two-dimensional square domain of dimensions 4 x 4 units, as shown in **Figure 4.7.** This calculation domain was discretized using a two-dimensional finite element mesh, similar to the cross-section mesh shown in **Figure 3.4.** A uniform structured line-line-line grid was used,

with LI = 51 and MI = 51. The z direction is irrelevant here, because the flow field is two-dimensional, and the particle starts and remains in the chosen x-y plane. The nondimensional time step used in the simulations was $\Delta t / \tau_v = 0.1$.

The Basset correction reduces the radial drift velocity for all density ratios, and enhances or diminishes the angular velocity for particles that are lighter or heavier than the fluid, respectively. These characteristics were faithfully reproduced by the results obtained using the proposed particle-tracking algorithm and its computer implementation.

Figure 4.7 shows the particle trajectory for the case where the density ratio is ρ_p / ρ_f=0.5, the angular velocity is ω = 2, and the Stokes number is St=0.022. When compared to the particle trajectory produced by the analytical solution, given by Equation (4.32), the results produced by the proposed particle-tracking code differ from the analytical results by less than ±0.04 units.

Chapter 5

Demonstration Problem

5.1 Overview

The scope and possibilities offered by the proposed numerical solution methods vis-à-vis the design of electromagnetic systems for the separation of solid inclusions from molten aluminum are explored in this chapter in the context of a demonstration problem. The demonstration problem is illustrated schematically in **Figure 2.1**. It involves steady, laminar, fully developed flow of molten aluminum in a separation chamber, which is a straight duct of rectangular cross-section. The walls of this duct are assumed to be electrically non-conducting. The molten aluminum is fed to the duct from a large upstream plenum, and it is assumed to enter with a uniform velocity normal to the inlet plane. At that point, the relative velocity between the inclusions and the molten aluminum is assumed to be zero. Within the separation chamber, the inclusions migrate laterally under the action of surface and body forces that they experience. After a sufficiently large distance downstream of the inlet, the fluid flow becomes fully developed, as was discussed in **Section 1.3.3**. Only the fully developed regime is investigated in this demonstration problem.

The longitudinal axis of the separation chamber is oriented along the z direction of the Cartesian coordinate system. Immersed electrodes, upstream and downstream of the chamber, generate an electric field so that the current flows in the positive z direction, parallel to the main fluid flow. The applied magnetic field is generated by a suitable electromagnet, such that the field strength is uniform throughout the separation chamber and is oriented in the x-direction, parallel to the wider side of the duct, as illustrated in **Figure 2.1**. These electric and magnetic fields create a resultant electromagnetic (EM) body force on the electrically conducting molten aluminum.

The fully developed flow of aluminum in this demonstration problem was predicted using the CVFEM described in **Section 3.1**. In order to predict the inclusion

trajectories in the molten aluminum within the separation chamber, it is necessary to solve the particle momentum equation, which was discussed in detail in **Section 2.5**. The particle-tracking algorithm presented in **Section 3.2** was used to solve the particle momentum equation and obtain inclusion trajectories.

In this chapter, first, representative calculations will be used to assess the orders of magnitude of the forces experienced by the inclusions, and characterize the relative importance these forces in the determination of the particle trajectories. Next, the results of a parametric study will be presented for the demonstration problem. Finally, a method for quantifying the effectiveness of the electromagnetic separation system will be proposed.

In this demonstration problem, the density, dynamic viscosity, and electrical conductivity of the molten aluminum, and the mass density of the solid inclusions (particles), were kept fixed throughout at the following values: ρ_f = 2,374 kg/m^3; η = 2.998 x 10^{-3} kg/m-s; σ_f = 2.95 x 10^6 mho/m; and ρ_p = 3,990 kg/m^3. The electric field strength was also maintained fixed at the following value: E = 1.0 V/m. The length of the longer side of the duct cross-section was fixed at $2a$ = 0.02 m; thus, a = 0.01 m. For the other relevant nondimensional and dimensional parameters of this problem, the ranges of values given in **Table 5.1** were investigated.

Table 5.1: *Values of some of the nondimensional and dimensional parameters that characterize the demonstration problem*

Parameter	Range
Duct Aspect Ratio, *AR*	1, 0.5, 0.2
Reynolds Number, Re_{D_h}	1, 10, 100, 1000
Magnetic Field Strength, B_o	0T, 0.001T, 0.01T, 0.1T
Particle Diameter, D_p	5μm, 15μm, 30μm, 90μm

These values of the dimensional and nondimensional parameters are representative of some prototype electromagnetic systems for the separation of inclusions from molten aluminum (Patel and El-Kaddah, 1997). Another point to be noted here is

that in the presentation of the results in subsequent sections of this chapter, reference will be made to some of the nondimensional parameters that were introduced and discussed in Chapter 2. In particular, reference will be made to the Hartman number, M, defined as follows:

$$M = \sqrt{N \cdot \mathrm{Re}} = B_0 D_H \sqrt{\frac{\sigma}{\eta}}$$

All computer simulations of the demonstration problem were done with power-law type of finite element meshes in the duct cross-section (designed in accordance with Equation (4.9) and related discussions) and a uniform grid in the z direction. The cross-sectional grid was characterized by $LI = MI = 61$, and $XPOW = YPOW = 1.25$. The number of nodes and size of the axial grid can be arbitrary, because the flows considered here were all fully developed (thus, w is invariant in the z direction); in this work, 21 uniformly spaced cross-sectional plane were used to discretize the length of the separation chamber (fixed at 1 m in this work). In each run, the particle trajectory was computed with a uniform time step of $\Delta t = \tau_v / 10$.

5.2 Forces Experienced by the Particle Along its Trajectory

The magnitudes of the drag, buoyancy, virtual mass, Basset, lift, and EM forces experienced by the particle over the course of its trajectory force were investigated for one particular combination of parameters: AR = 1.0, Re = 100, B_o = 0.01T, and D_p = 90μm.

First, the values of each of the nondimensional groups, $\left(\frac{\cdot\cdot}{\cdot\cdot}\right)$, that appear in the expressions for the dimensionless forces in Equation (2.66) were calculated using exact values of the properties and dimensions used in this demonstration problem. The corresponding orders of magnitude are summarized in **Table 5.2**.

Table 5.2: Orders of magnitude of the dimensionless groups in the non-dimensional particle momentum equation for AR = 1.0; Re = 100, B_o = 0.01T, and D_p = 90μm

Dimensionless Group	Order of Magnitude
$\left(\frac{1}{St}\right)$	10^3
$\left(1-\frac{1}{\lambda}\right)$	1
$\left(\frac{1}{2\lambda}\right)$	1
$\left(\frac{9}{\pi^{1/2}\lambda\delta\,\mathrm{Re}^{1/2}}\right)$	10
$\left(\frac{3C}{2\pi\,\mathrm{Re}^{1/2}\,\lambda\delta}\right)$	10
$\left(\frac{3N}{4\lambda}\right)$	10^{-1}

Then, the time varying magnitudes of the actual *y*-direction and *z*-direction components of the aforementioned forces were obtained from the corresponding particle trajectory calculations. The results are plotted in **Figures 5.1(a)** and **5.1(b).** These plots reveal several interesting characteristics for the electromagnetic filtration problem. Along the y-direction, the particle trajectory is influenced by a large value of the relative velocity, caused by the drag force balancing against the combined buoyancy and *EM* forces. Consequently, the lift force along the negative *z*-direction becomes significant, and the unsteady Basset and virtual mass forces are large initially. Once the particle relative acceleration starts to drop from its high initial value, the virtual mass force also drops off significantly. However, the Basset force continues to remain relatively high as a result of its "history" effect.

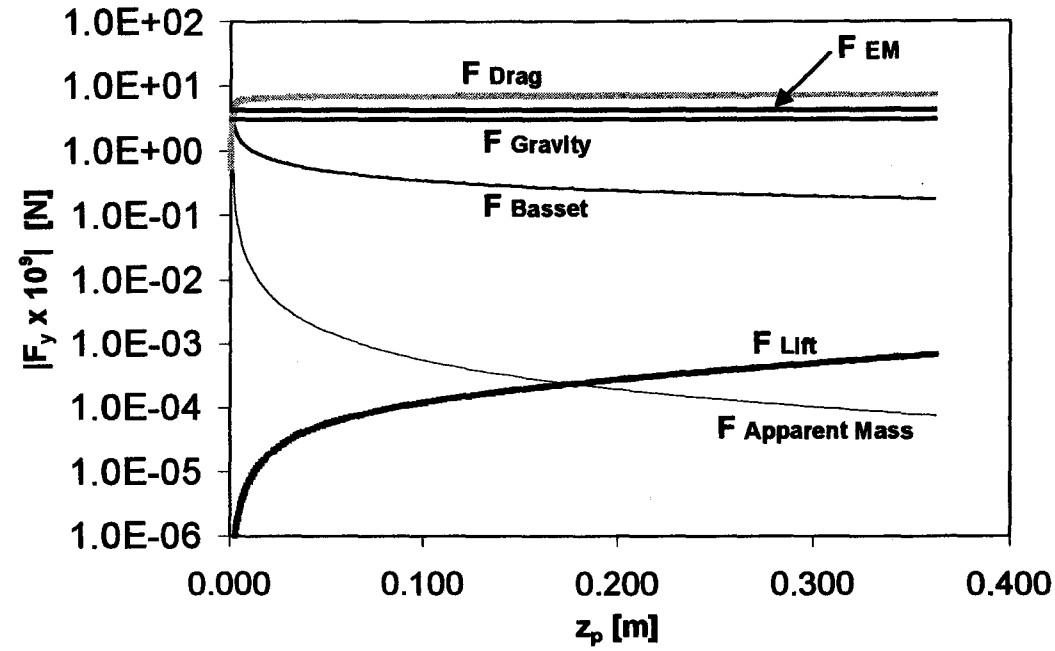

(a)

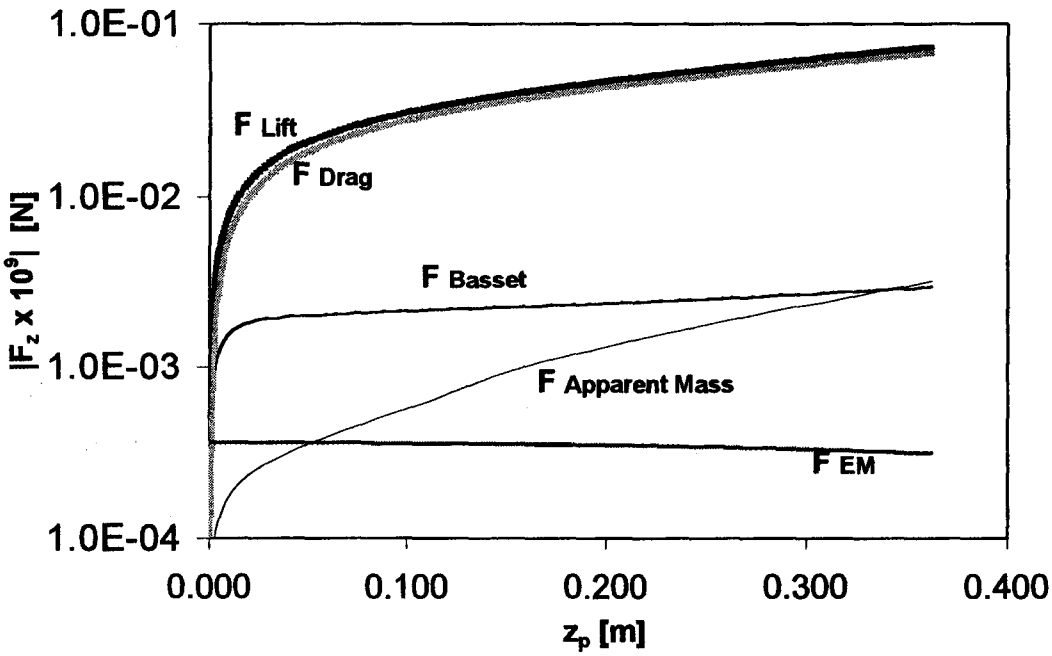

(b)

Figure 5.1: *Time-varying forces experienced by the particle for AR = 1, Re = 10, B_x = 0.01 T, and D_p = 90μm: (a) along the y direction; (b) along the z direction*

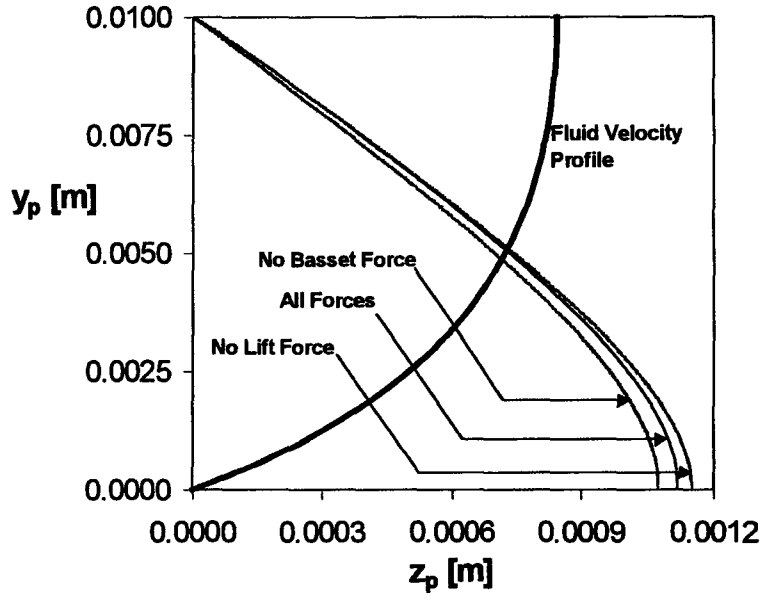

(a)

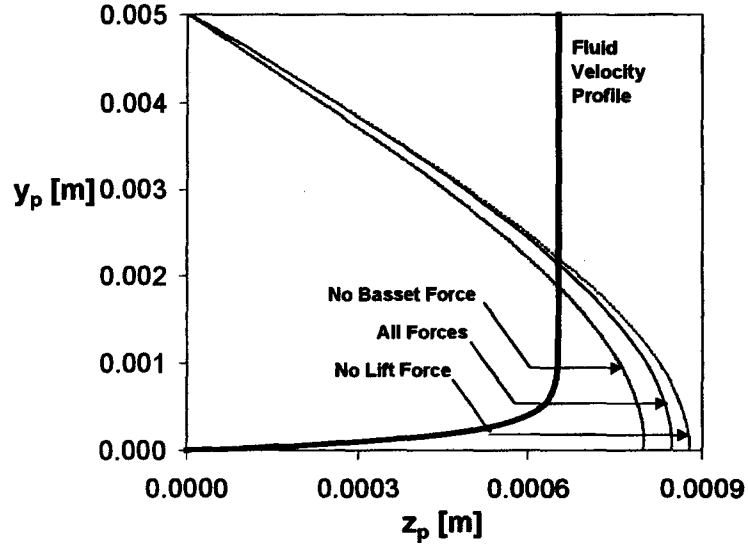

(b)

Figure 5.2: *Particle trajectory calculations with and without Basset and lift forces for the cases where Re = 10, B_x = 0.01 T, D_p =90μm: (a) AR = 1; (b) AR = 0.5.*

Along the y-direction, the lift force is negligible as a result of the small relative velocity in the z direction, and its upward trend is a result of the increased w-velocity gradient, dw/dy, as the particle migrates toward the wall. The Basset and virtual mass forces exhibit an opposite trend in the z direction than was observed in the y direction.

This is due to the fact that the particle is given the same initial w-velocity as that of the fluid, but begins to slow down as it traverses toward the wall.

The particle trajectory calculation is shown in Fig. 5.2a, along with the cases where the lift and Basset forces are individually turned off. Based on the orders of magnitude observed in Fig. 5.1, it can be concluded that the discrepancy caused by turning off the Basset force is a result of inadequate modeling of the particle momentum along the y-direction. Similarly, the discrepancy associated with removing the lift force is due to the inadequate modelling of the particle momentum along the z-direction. The results in Fig. 5.2b illustrate the same findings for a low aspect ratio duct case, where the velocity profile is flatter due to a higher magnetic interaction parameter.

5.3 Parametric Study of Particle Trajectories

This section provides a summary of particle trajectory calculations for the full range of parameters defined in **Section 5.1**. A total of 192 cases were considered, and the results are presented in **Figures 5.3** to **5.14**. The presentation of these results is grouped into twelve sets of plots, each set corresponding to a particular combination of AR and D_p. Each set is comprised of four graphs, one for each Reynolds number. Each graph then has four trajectory calculations (plotted in terms of non-dimensional quantities, y/a and z/a), each corresponding to a different value of the Hartman number, M. The trajectory calculations were carried out with the initial particle position at the center of the duct, until 2,000,000 time steps based on $\Delta t = \tau_\nu / 10$ were reached, or until the particle moved a distance of 50a (=1.0m) in the z-direction.

Two main observations can be made concerning the trajectories shown in **Figures 5.3** to **5.14**:

1. For fixed AR, D_p, and M, the length required for separation approximately scales with Re.
2. For fixed AR, D_p, and Re, the length required for separation approximately scales with $1/M$.

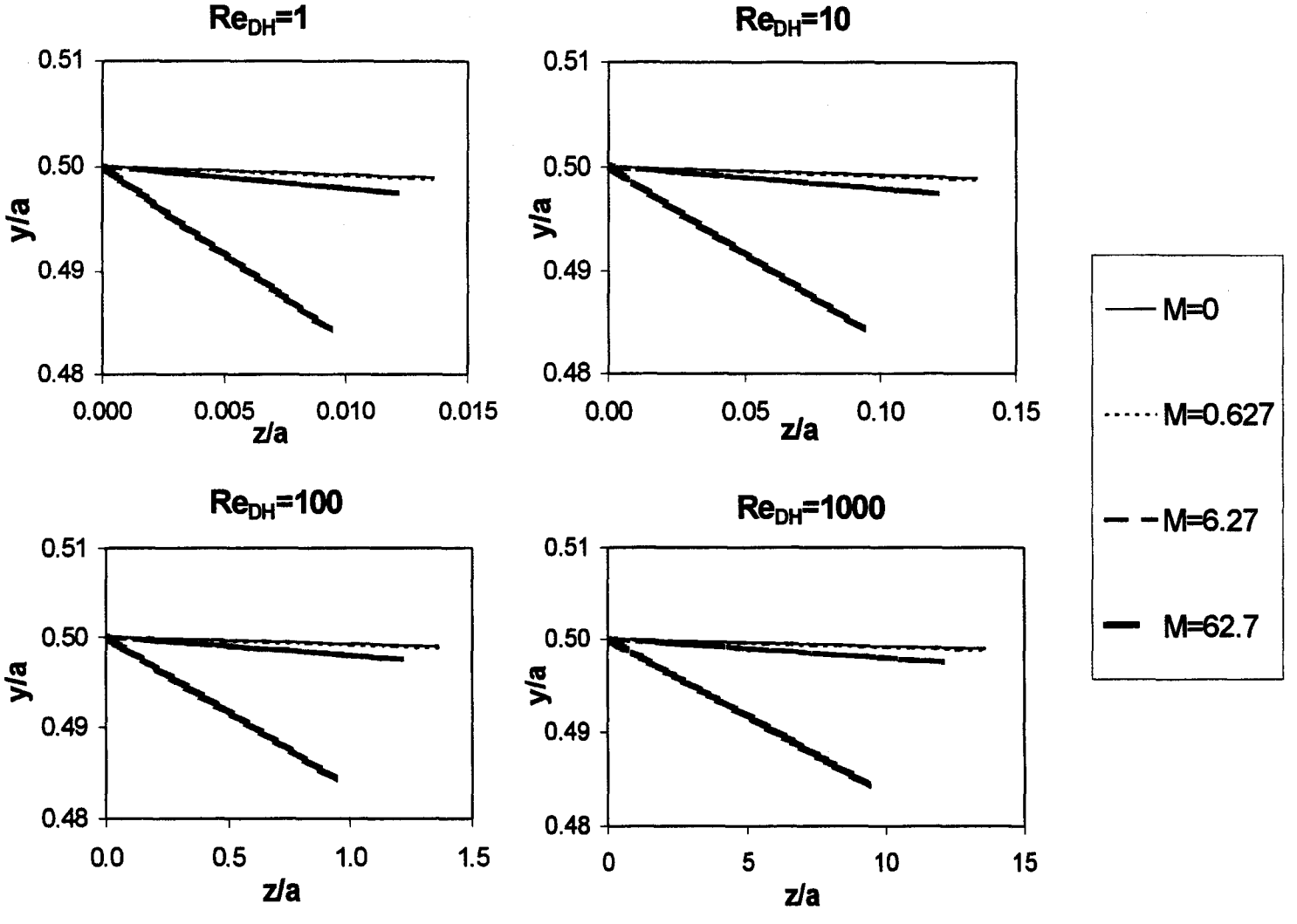

Figure 5.3: Particle trajectory calculations for $AR = 1$ and $D_p = 5$ μm

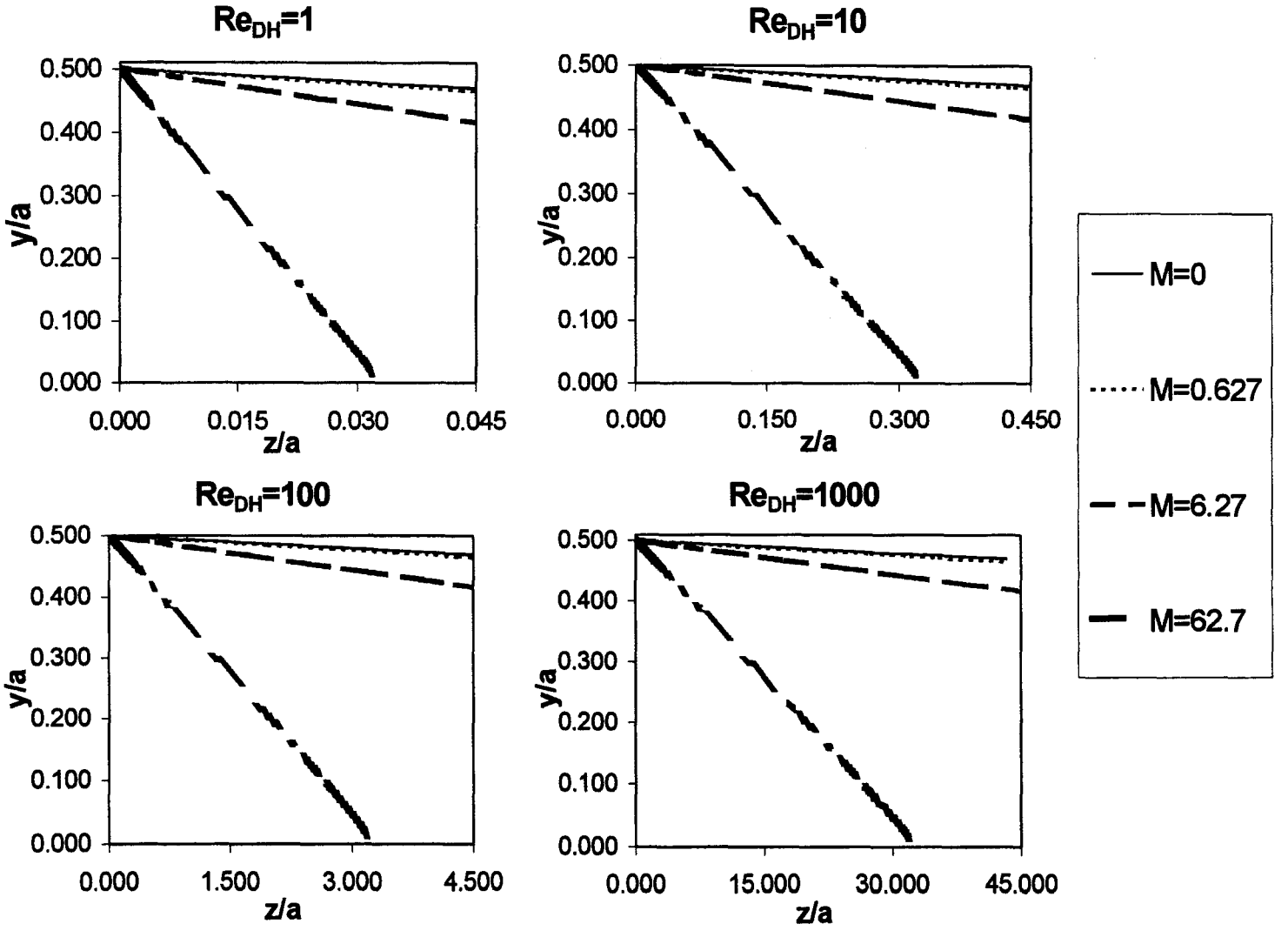

Figure 5.4: Particle trajectory calculations for $AR = 1$ and $D_p = 15$ μm

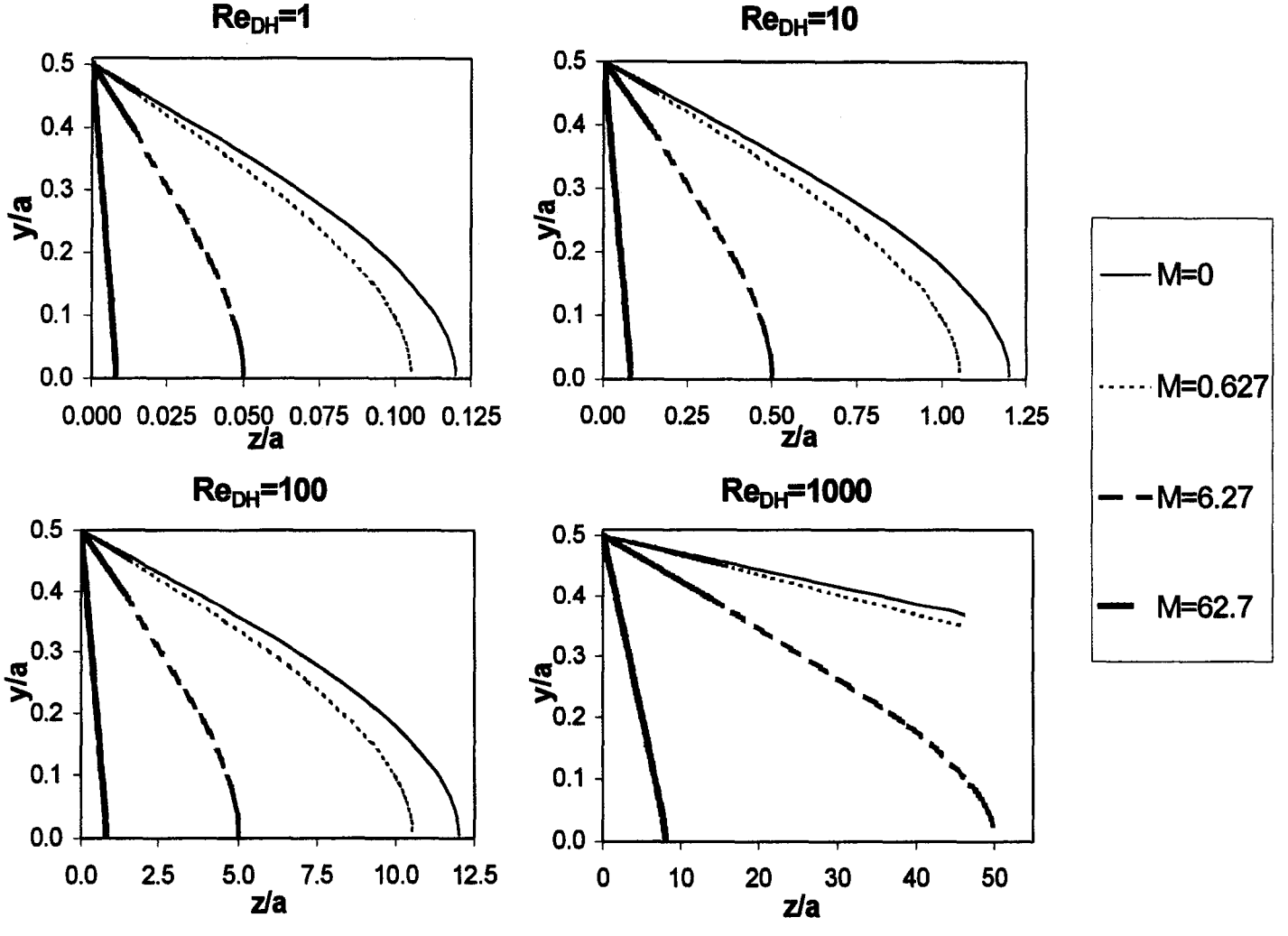

Figure 5.5: Particle trajectory calculations for $AR = 1$ and $D_p = 30$ μm

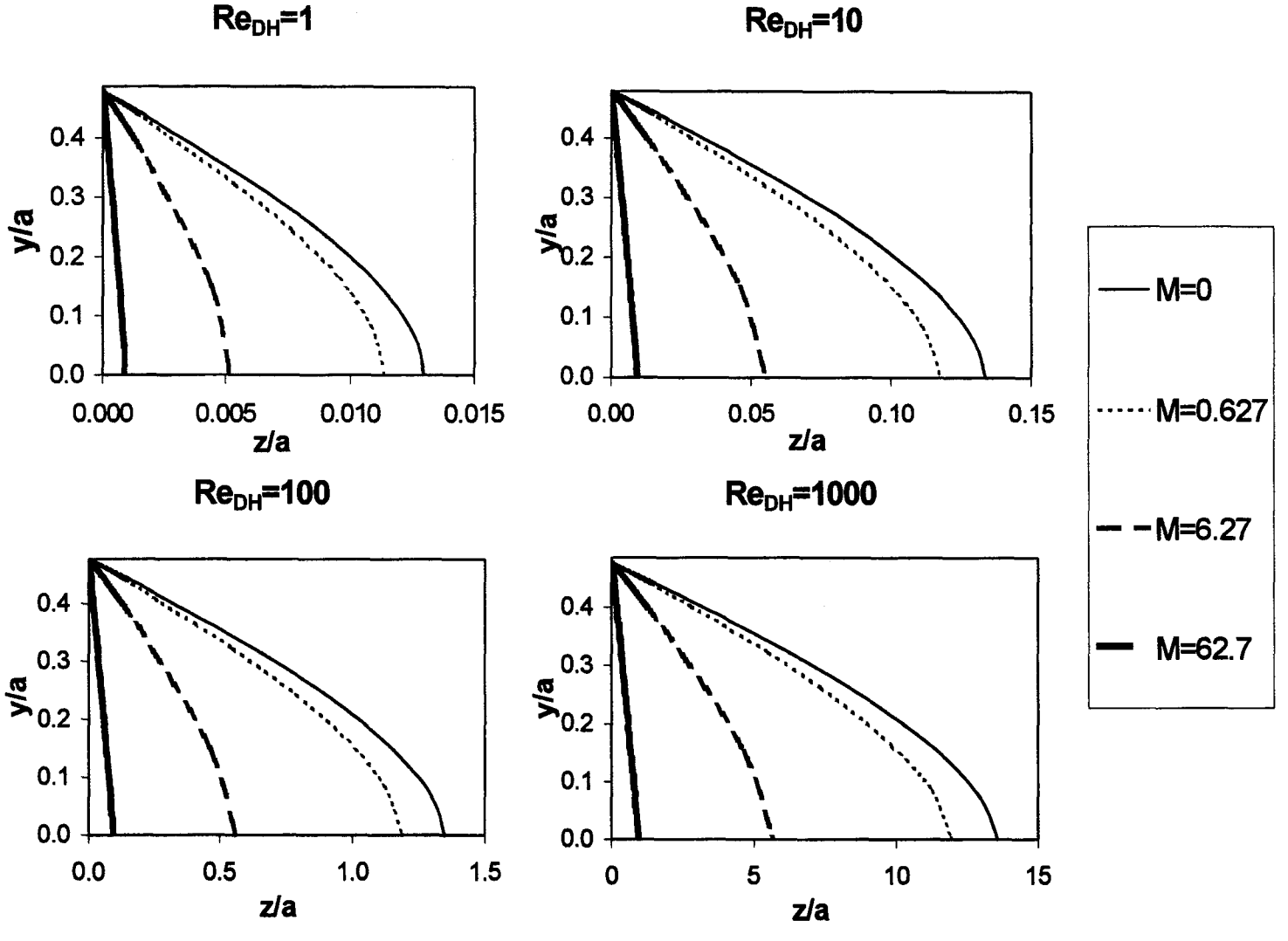

Figure 5.6: Particle trajectory calculations for $AR = 1$ and $D_p = 90$ μm

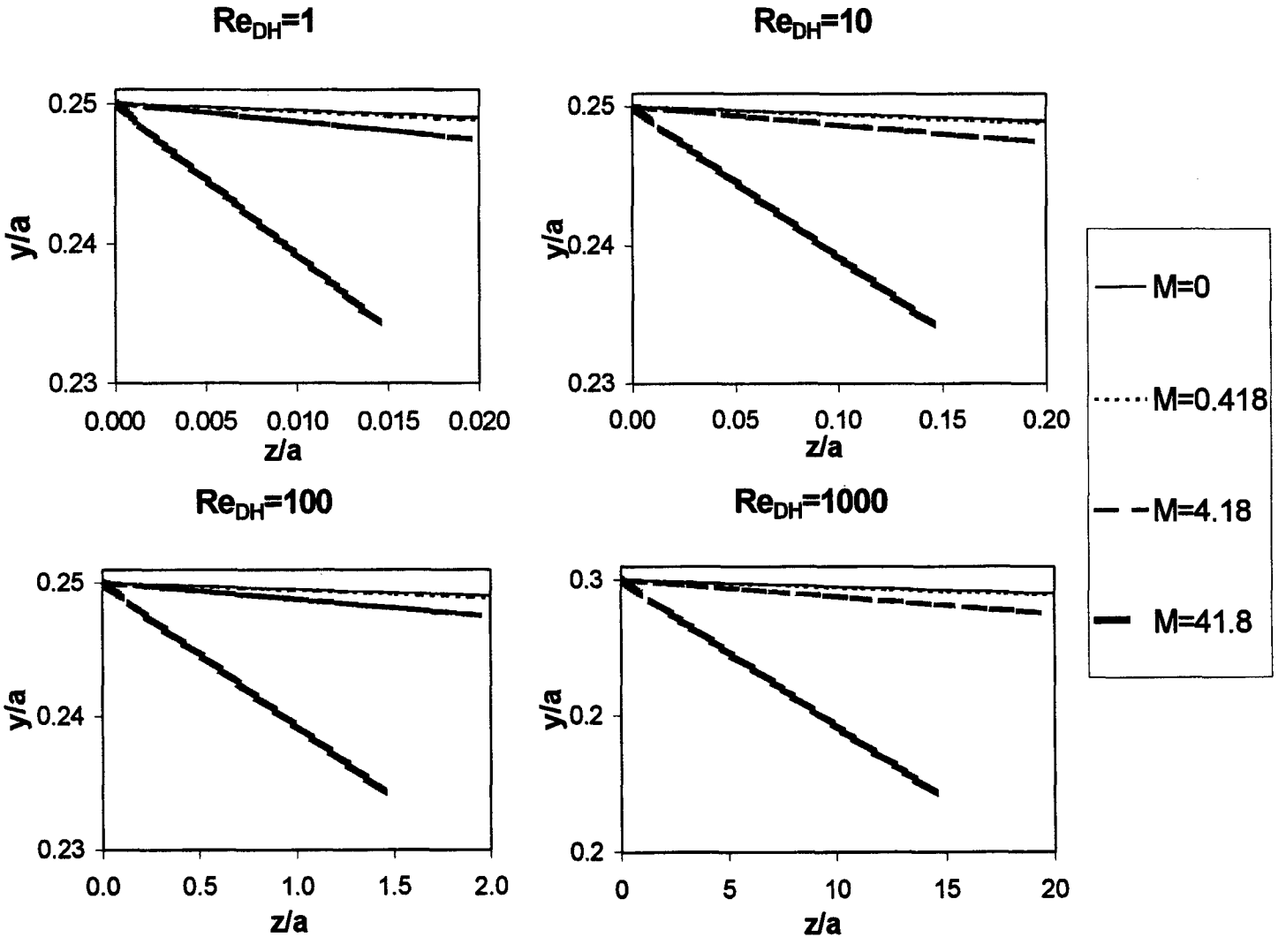

Figure 5.7: Particle trajectory calculations for $AR = 0.5$ and $D_p = 5$ μm

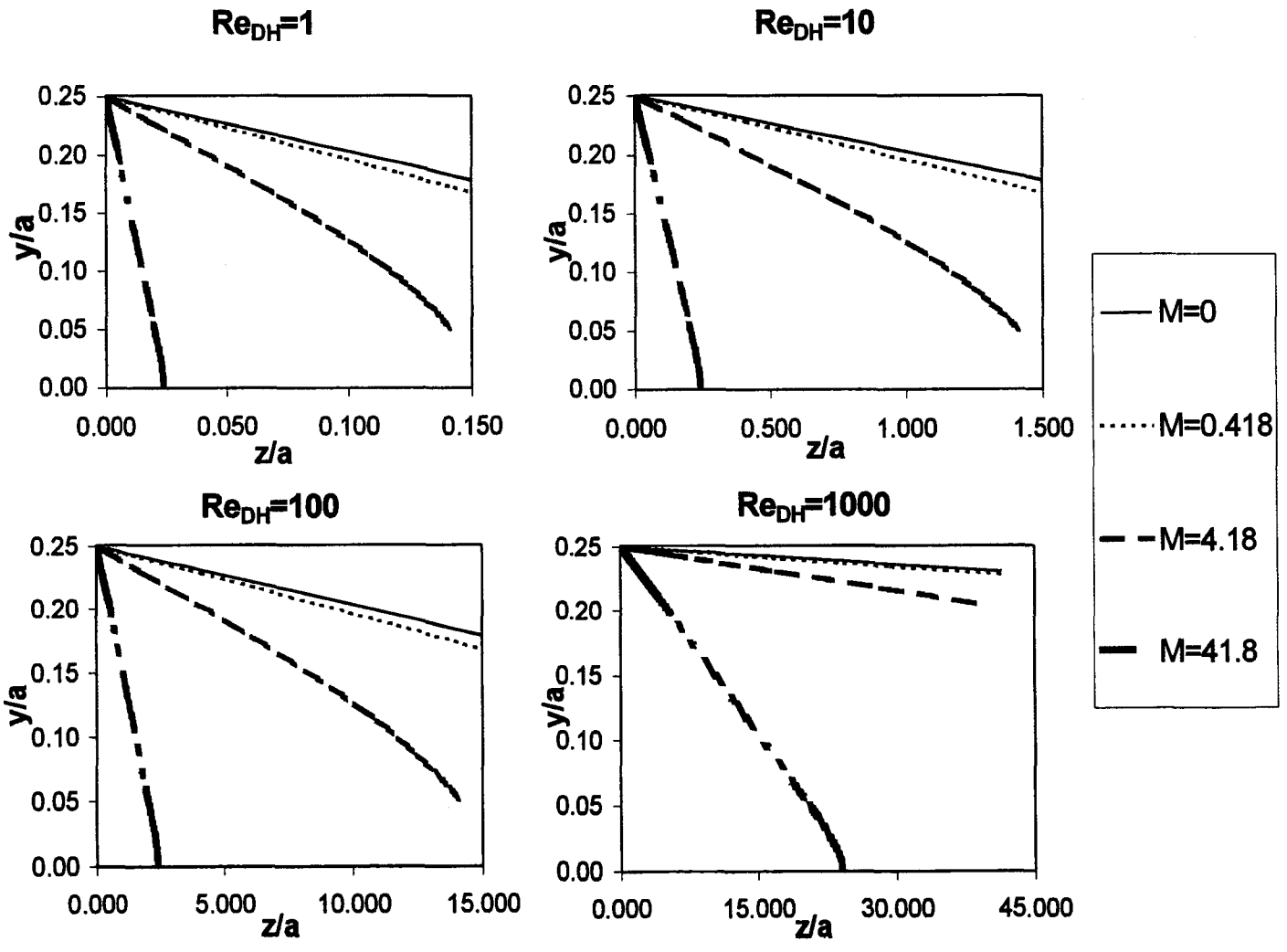

Figure 5.8: Particle trajectory calculations for $AR = 0.5$ and $D_p = 15$ μm

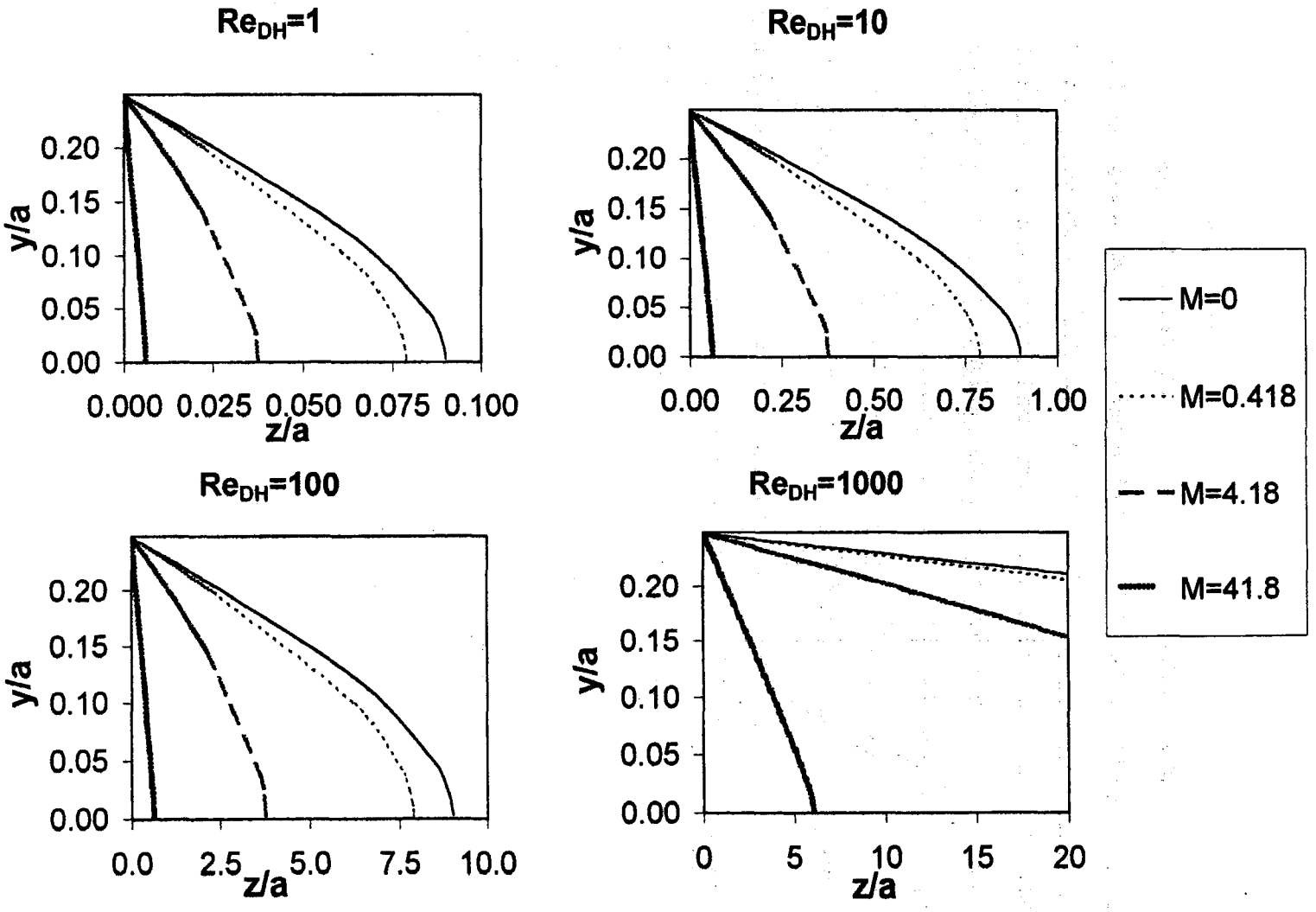

Figure 5.9: Particle trajectory calculations for $AR = 0.5$ and $D_p = 30$ μm

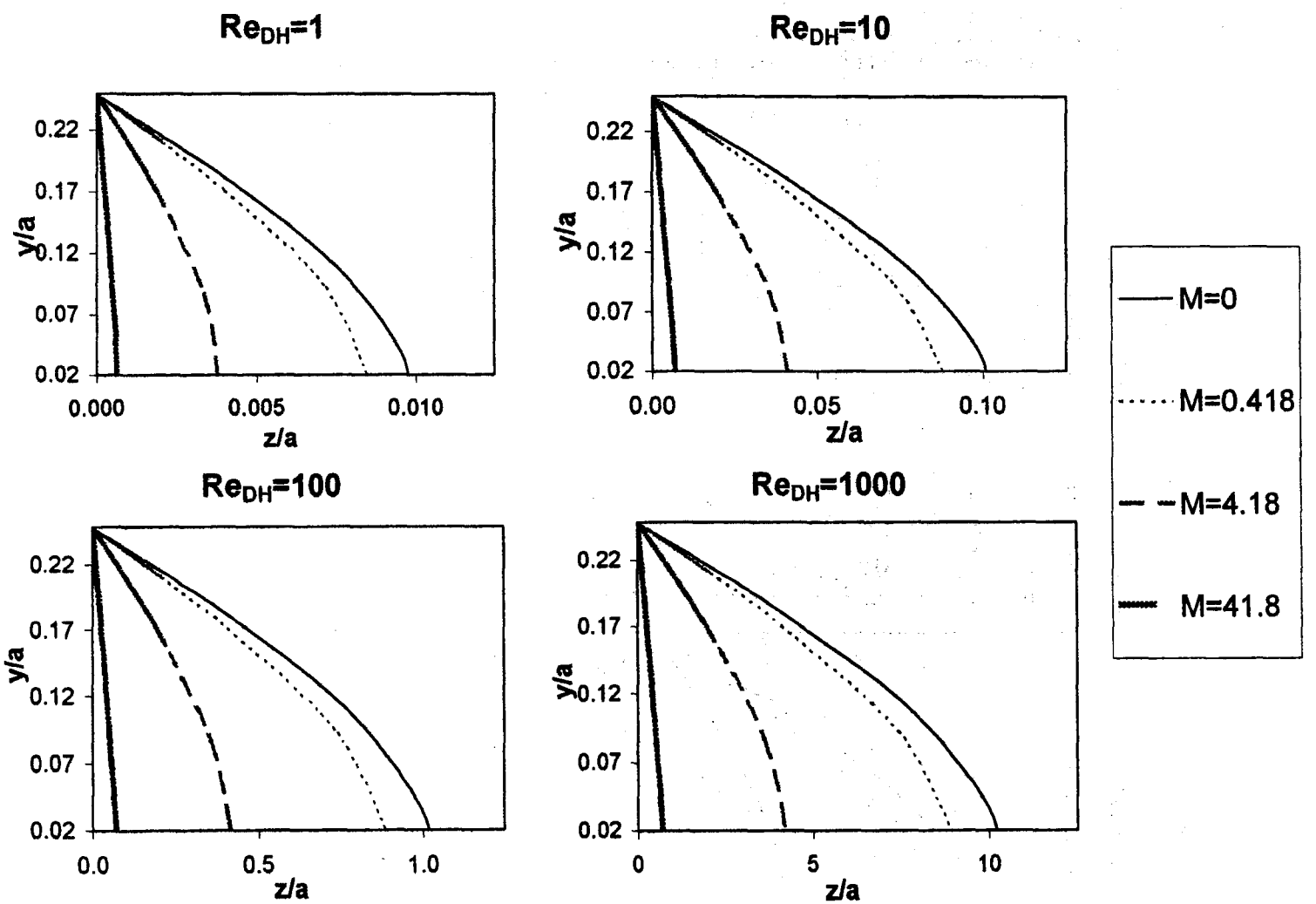

Figure 5.10: Particle trajectory calculations for $AR = 0.5$ and $D_p = 90$ μm

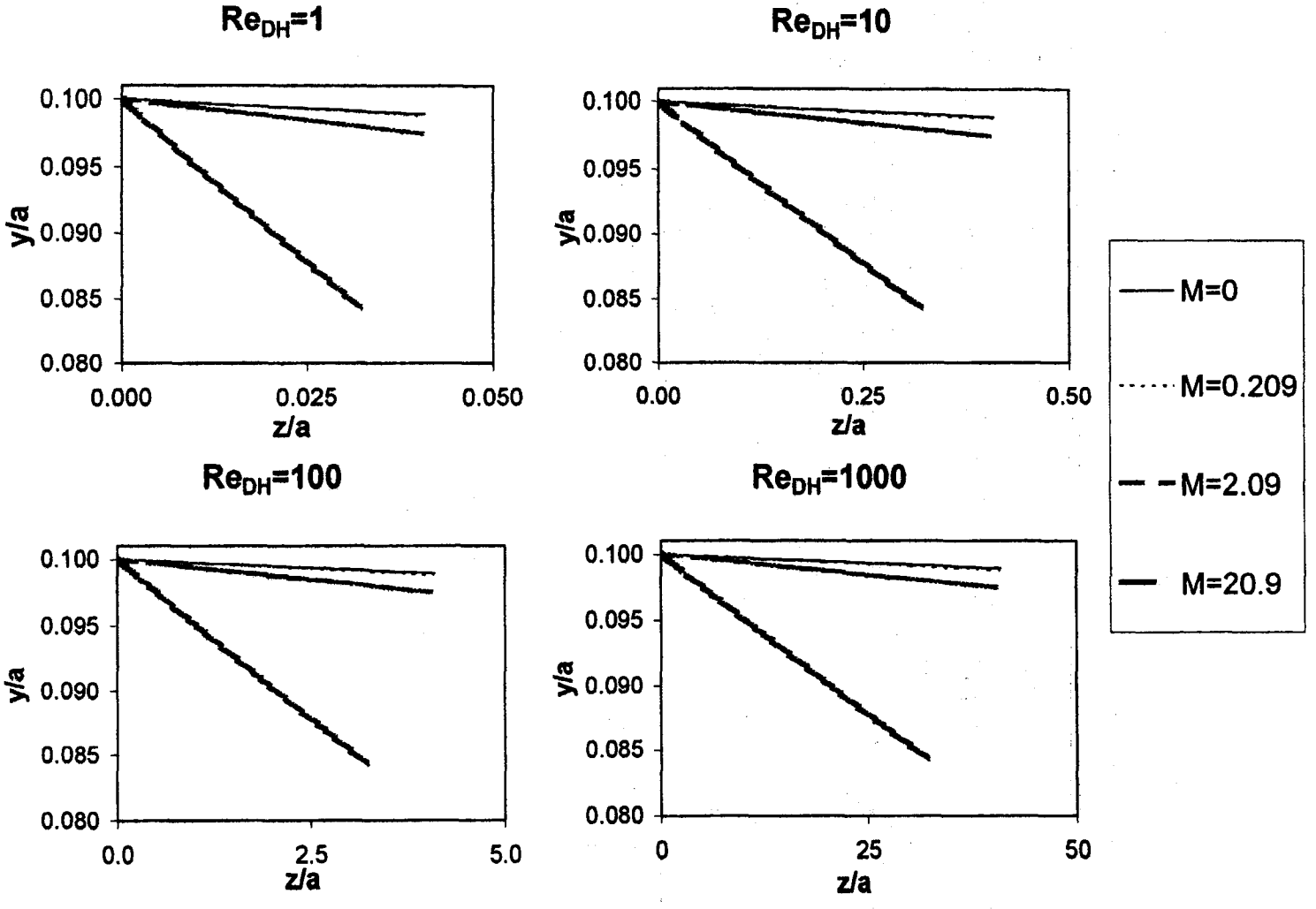

Figure 5.11: Particle trajectory calculations for $AR = 0.2$ and $D_p = 5$ μm

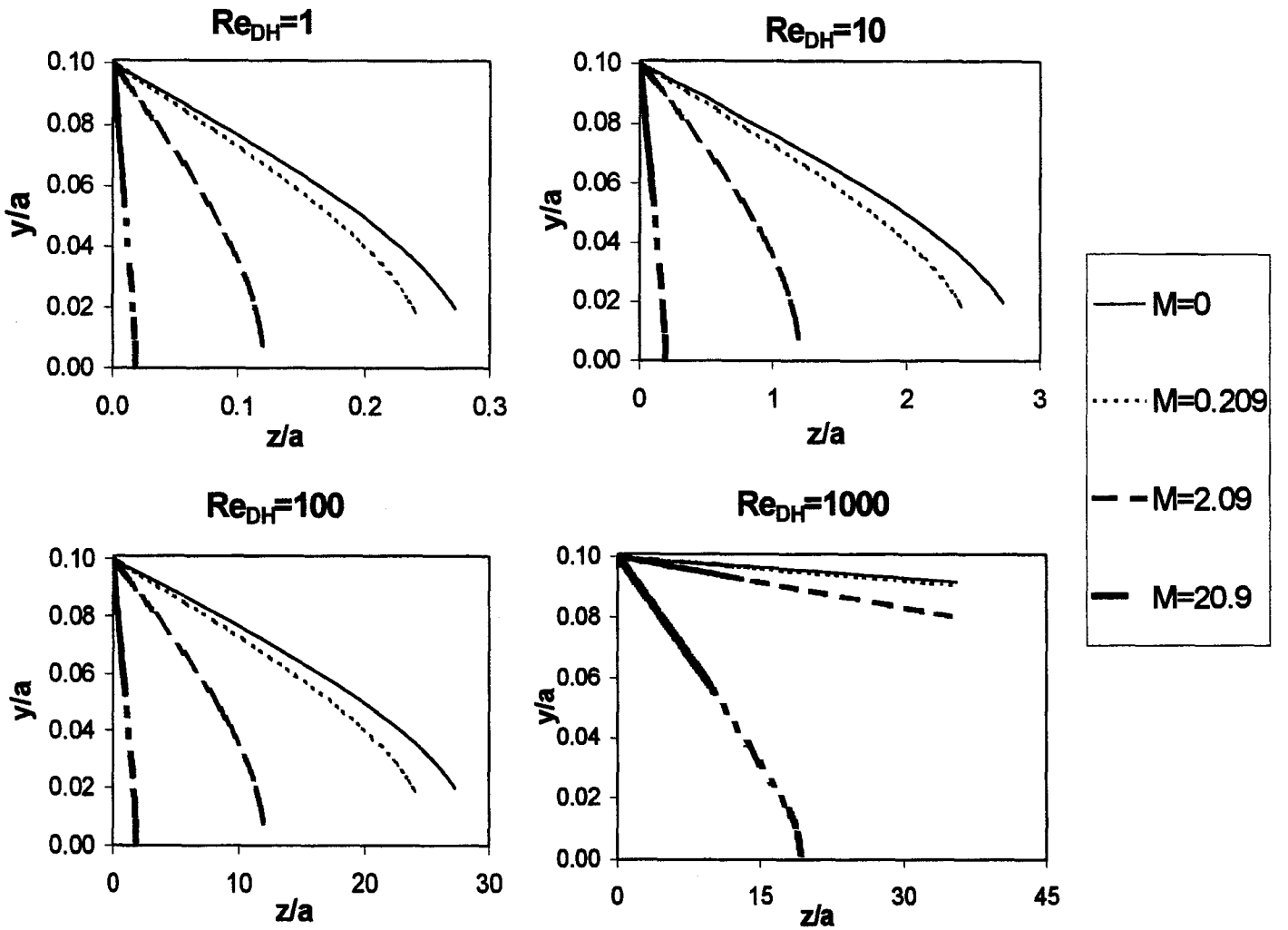

Figure 5.12: Particle trajectory calculations for $AR = 0.2$ and $D_p = 15$ μm

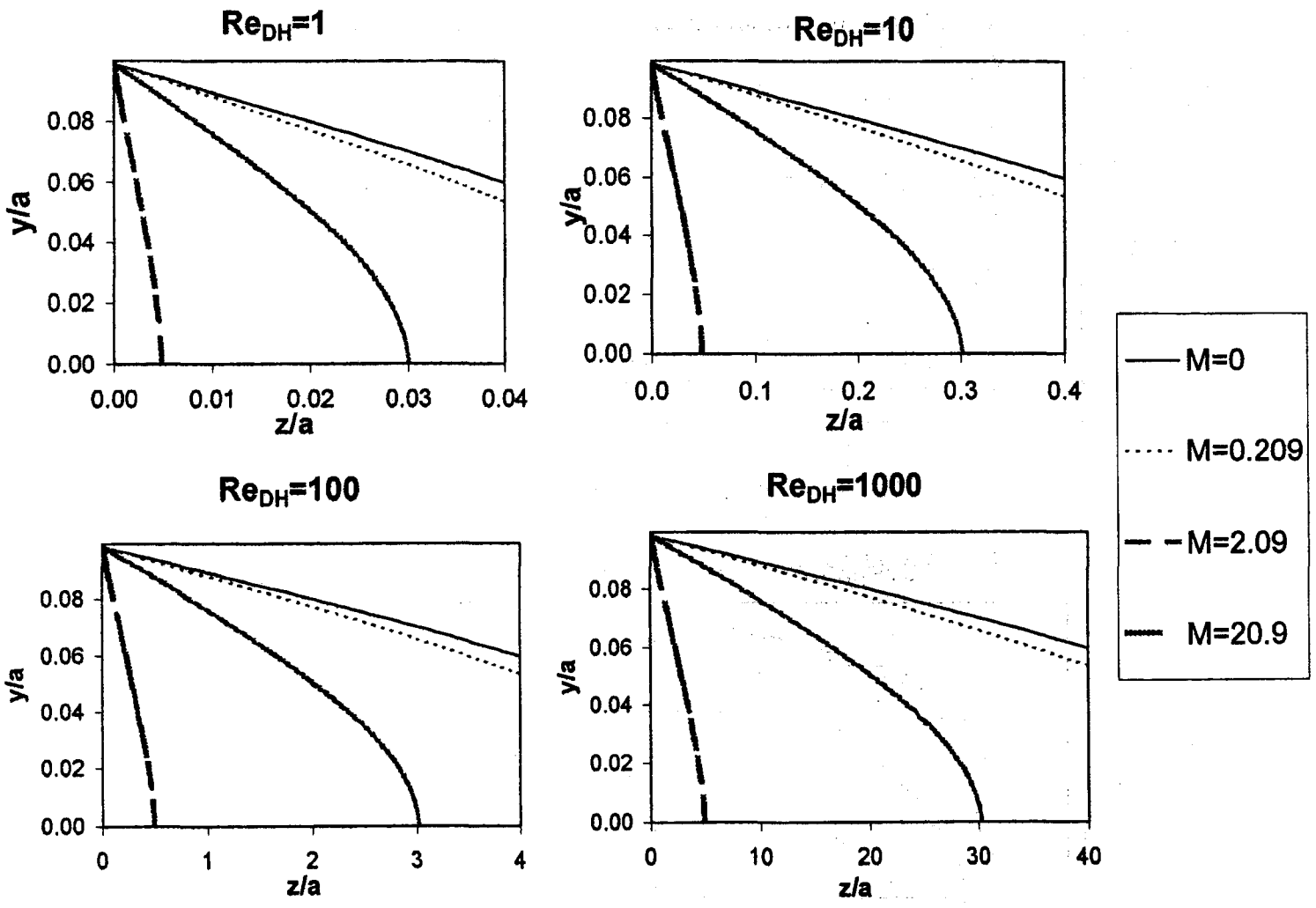

Figure 5.13: Particle trajectory calculations for $AR = 0.2$ and $D_p = 30$ μm

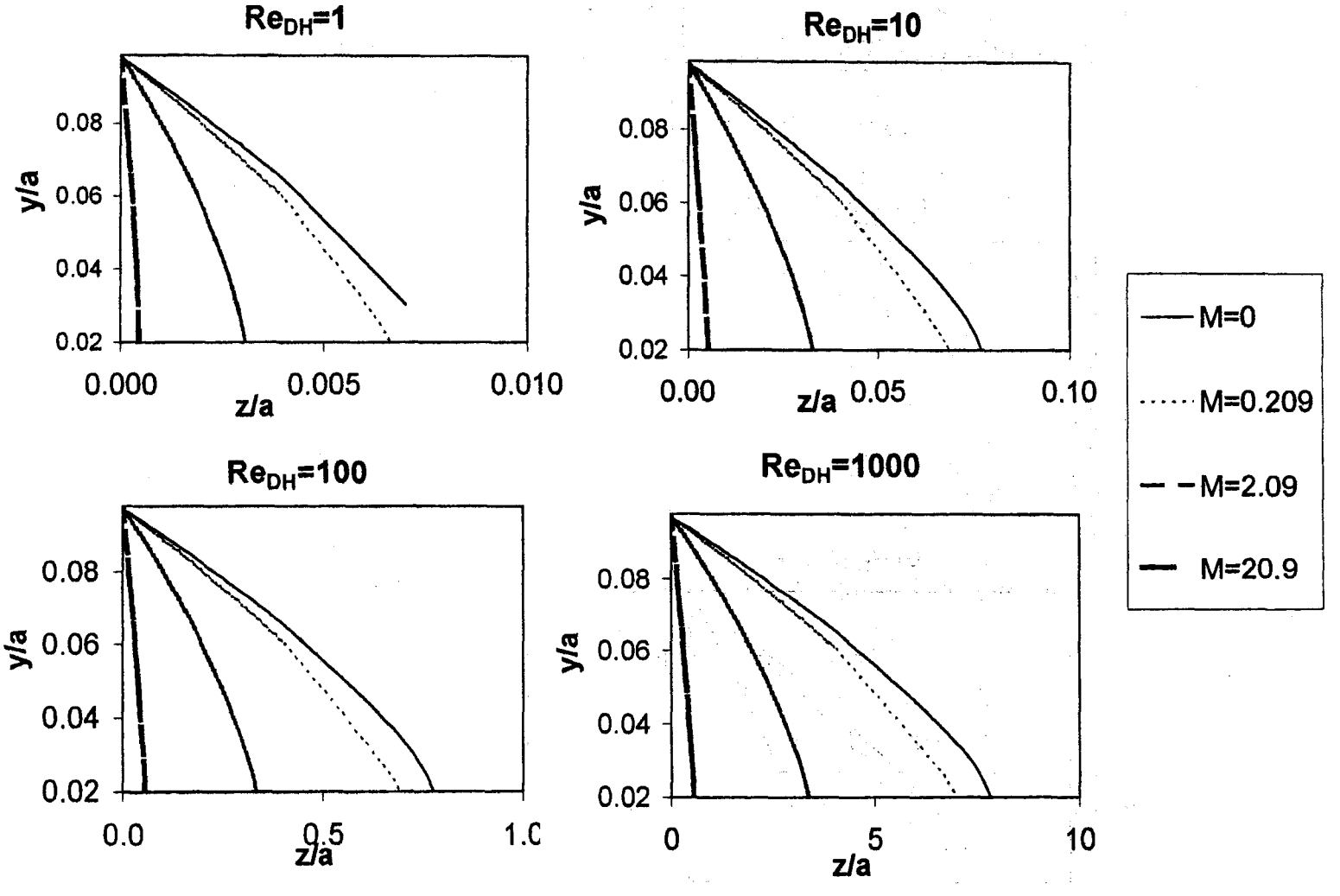

Figure 5.14: Particle trajectory calculations for $AR = 0.2$ and $D_p = 90$ μm

5.4 Evaluation of the Effectiveness of an Electromagnetic Separation System

In this section, a method to evaluate the effectiveness of an electromagnetic separation system is proposed. The aim here is also to demonstrate the usefulness of the proposed numerical solution methods in assessing the relative merits of specific EM separator designs.

5.4.1 Problem Statement

The particular EM separation system being evaluated here is illustrated in Fig. 5.15.

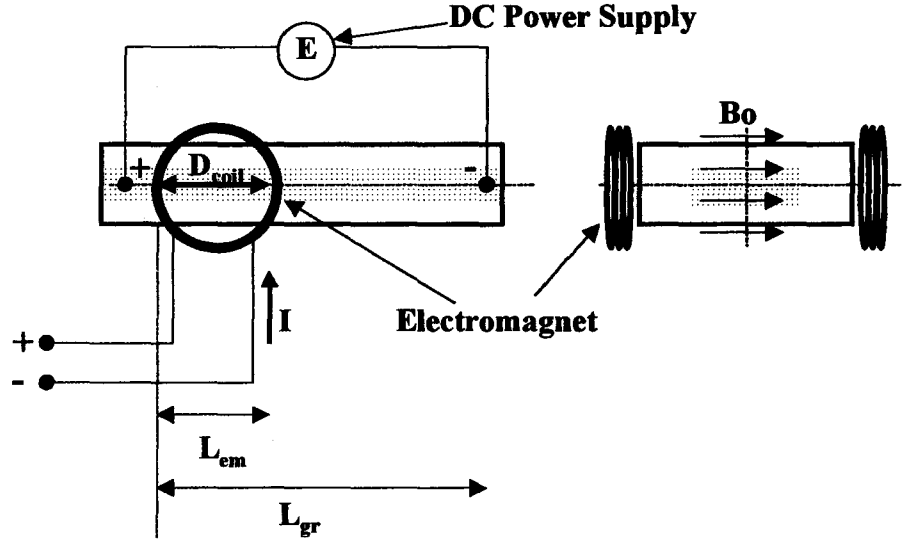

Figure 5.15: Schematic illustration of electromagnetic separation system

In the evaluation of an electromagnetic separation system, the following performance measures are useful:

- Smallest size of particle that can be separated at the desired fluid flow rates
- Power consumption required for separation
- Mass of aluminum processed per unit of power consumption

The total power required for separation of the particles from the molten aluminum is the sum of the powers expended to pump the molten aluminum, create the desired electric field, and generate the desired magnetic flux density.

5.4.2 Pumping Power

In the fully developed regime of a horizontal separation chamber, the pumping power input is needed to overcome the wall shear stress and the braking effect of the applied EM fields on the molten aluminum. It can be calculated using the computed pressure gradient in the *z* direction, the minimum length of the separation chamber that is necessary to separate the particles from the molten aluminum, the area of the flow passage cross-section, and the average fluid velocity. In this analysis, for a given value of the particle effective diameter, D_p, the minimum length of the separation chamber was assumed to be the *z*-direction distance from the inlet plane that is required to separate a particle (make it reach one of the duct walls) entering the duct at the center of the inlet plane. It was also assumed here that the velocities of the molten aluminum and the particles are essentially the same at the inlet plane. In the context of these assumptions and conditions, the ***minimum*** pumping power requirements are given by the following equations:

$$\text{Only gravity, no } EM \text{ force: } P_{pumping} = \left(-\frac{dp}{dz}\right) L_{gr} A_{cs} w_{av} \tag{5.1}$$

$$\text{Gravity and } EM \text{ force: } P_{pumping} = \left(-\frac{dp}{dz}\right) L_{em} A_{cs} w_{av} \tag{5.2}$$

5.4.3 Power Required to Generate the Electric Field

The ***minimum*** power input required for generating the uniform electric field via immersed electrodes is given by:

$$P_E = IV = (jA_{cs})(E_z L_{em}) = \sigma E_z^2 A_{cs} (L)_{em} \tag{5.3}$$

Here, it is assumed that the ohmic electrical power losses in the supply wires are negligible, compared to the other power inputs.

5.4.4 Power Required to Generate the Magnetic Flux Density

The *minimum* power input required to generate the desired uniform magnetic flux density using an electromagnet is given by.

$$P_B = I^2 R = \left(\frac{D_{coil} B_o}{N_{turns}\mu}\right)^2 \mathbf{R} l_{wire} = \left(\frac{\pi \mathbf{R}}{N_{turns}\mu^2}\right) L_{em}^3 B_o^2 \multimap \tag{5.4}$$

where, N_{turns} is the number of turns in the solenoid, $\mathbf{R}$ is the resistance of the wire per unit length. The electromagnet is assumed to produce a uniform magnetic flux density within the molten aluminum over the whole required distance for particle separation (distance from inlet plane needed for the particle to strike one of the walls). Hence, as the separation length increases, so will the size of solenoid coils. The approximate orders of magnitude for these parameters are shown below:

$$\begin{aligned} &L_{em} \approx D_{coil} \\ &\mathbf{R} \approx O[10^{-2}] \\ &N_{turns} \approx O[10^{2}] \\ &\mu \approx O[10^{-6}] \\ &\Gamma = \left(\frac{\pi \mathbf{R}}{N_{turns}\mu^2}\right) \approx O[10^{8}] \end{aligned} \tag{5.5}$$

5.5.5 Total Minimum Power Input

Hence, the *total minimum power input* required for combined gravity and *EM* assisted separation is the following:

$$(P_{Total})_{EM} = (-dp/dz) w_{av} L_{em} A_{cs} + \sigma E_z^2 L_{em} A_{cs} + \Gamma L_{em}^3 B_o^2 \tag{5.6}$$

When gravity alone is used for filtration, the power required is:

$$(P_{Total})_{gr} = (-dp/dz) w_{av} L_{gr} A_{cs} \tag{5.7}$$

5.5.6 Effectiveness of EM Separation System

The EM system effectiveness will be defined as the ratio of minimum power input required to separate the inclusions using only gravity to that which is needed when the separation is EM-assisted:

$$\varepsilon \triangleq \left(\frac{L_{gr}}{L_{em}}\right)\left[\frac{(-dp/dz)w_{av}}{(-dp/dz)w_{av}+\sigma E_z^2+\frac{\Gamma}{A_{CS}}L_{em}^2B_o^2}\right] \tag{5.8}$$

where $\varepsilon = 1$ represents the situation where the EM field is turned off.

Equation (5.8) can be used to gain insight into how the overall power consumption can be reduced using an EM separation system. When gravity alone is used for separation, the value of L_{gr} can become significant. An effectiveness that is greater than one is achieved when:

$$\frac{L_{gr}}{L_{em}} > \frac{(-dp/dz)w_{av}+\sigma E_z^2+\Gamma L_{em}^2B_o^2/A_{CS}}{(-dp/dz)w_{av}} \tag{5.9}$$

Fig. 5.16(a) and 5.16(b) show the EM separation effectiveness as a function of magnetic interaction parameter and Reynolds number, for particles that are 5μm and 90μm, respectively. In general, the results of this study suggest that EM separation can be made very effective as long as the selected interaction parameter is high enough to ensure inclusion separation for the desired duct Reynolds number. When the Reynolds number exceeds a certain threshold (which depends on the particle size, duct aspect ratio, and interaction parameter), the separation distance and the cost of the electromagnet could become excessively large. An example of this phenomenon can be seen in Fig. 5.16(a) for Reynolds numbers of 100 and 1000. The results further suggest that if N is increased beyond the maximum value used in this study, then effective EM separation can take place at a higher Re as well.

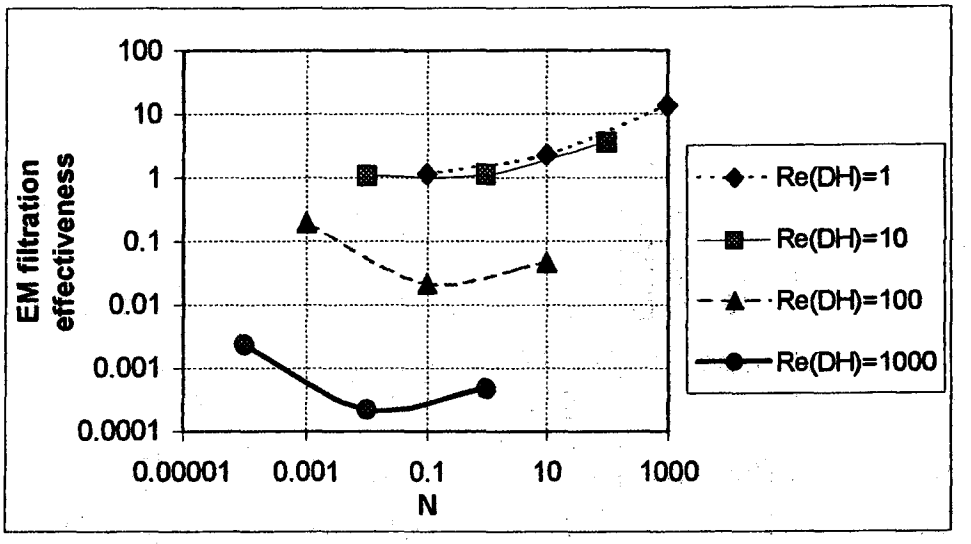

(a)

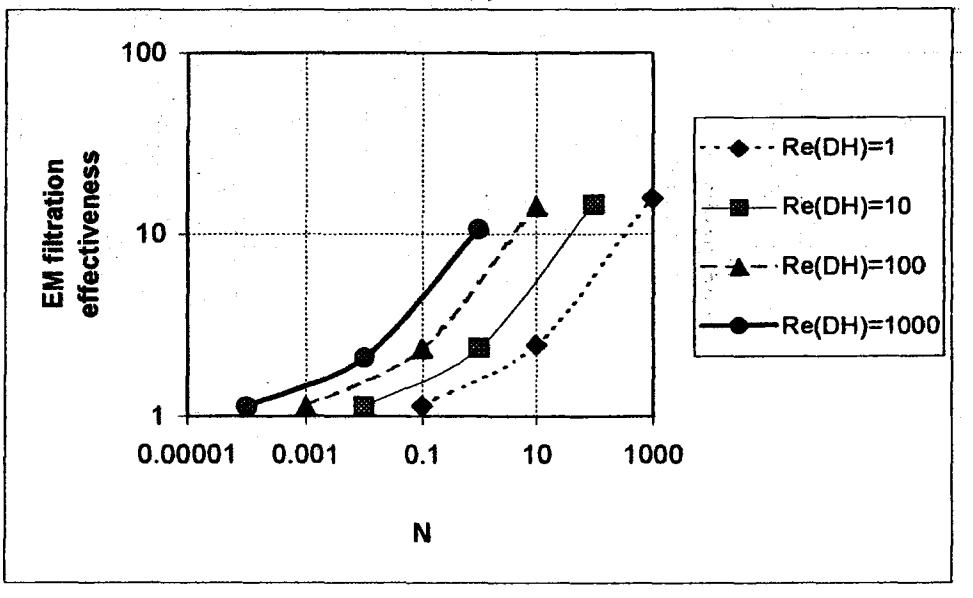

(b)

Figure 5.16: Effectiveness of the EM separation vs. interaction parameter and Reynolds Number at $AR = 1$: (a) $D_p = 5\mu m$, and (b) $D_p = 90\ \mu m$

Chapter 6

Conclusion

A brief review of the thesis and its *main contributions* are presented first in this chapter. After that, several suggestions for extensions of this work are discussed

6.1 Review of the Thesis and its Main Contributions

In Chapter 1, the aims and motivation of the thesis were stated, and a brief overview was given of the techniques that are used for the removal of impurities and inclusions from molten metals. A review of the pertinent published literature was also presented. This included electromagnetic filtration principles, control-volume finite-element methods, fully developed and three-dimensional parabolic flows in straight ducts subjected to electromagnetic fields, motion of a particle in a fluid continuum, particle tracking algorithms, and computer simulations of electromagnetic separation.

In Chapter 2, the mathematical models required for the analysis of electromagnetic separation processes were presented. The physical problem of interest was described first along with a summary of assumptions regarding the fluid flow, particle trajectory, and electromagnetic aspects. Next, specialized versions of the Navier-Stokes equations for modeling three-dimensional parabolic flows in ducts were presented and discussed, assuming that the electromagnetic fields are decoupled from the fluid motion. *Then, an order of magnitude analysis was carried out on the nondimensional magnetohydrodynamic equations, which confirmed that the induced electric field was negligible in the problems of interest. It was analytically shown that in the fully developed flow regime, the z-momentum equation is sufficient to fully describe this class of magnetohydrodynamic flows, and this problem can be viewed as a particular case of a general, steady, two-dimensional diffusion-type problem.*

Next, the governing particle momentum equation was presented in Lagrangian form, and each of the forces experienced by the particle was discussed concisely. These forces included the Stokes drag, buoyancy, virtual or apparent mass, Basset, Saffman lift,

and electromagnetic forces. *The particle momentum equation was cast in a nondimensional form, and an order of magnitude analysis was performed using typical values of the relevant physical quantities. This analysis showed that it is important to retain all of the aforementioned forces in computer simulations of EM separation systems akin to those considered here.* Lastly, the assumption of one-way coupling in the momentum transfer between fluid and particle was shown to be adequate for typical mass concentrations of inclusions found in molten aluminum.

Chapter 3 described the numerical methods that were formulated and used to solve the mathematical models presented in Chapter 2. A concise description of a control-volume finite-element method (CVFEM) for the solution of steady diffusion-type problems was presented. *This CVFEM was then supplemented with a proposed iterative scheme to determine the value of the axial pressure gradient that yields a desired value of Reynolds number.* A particle-tracking algorithm based on the fourth-order Runge-Kutta scheme was also proposed. *The design of this algorithm required the adaptation of a particle-locating algorithm proposed by Ren et al. (1995), in order to efficiently locate the particle in structured computational meshes composed of two-dimensional triangular and three-dimensional triangular prismatic finite elements. A method was also proposed for computing the time and position of the particle when it reaches a wall.*

In Chapter 4, several test problems were solved using the proposed numerical methods, and the results were compared with those found in the published literature. The test problems involved calculations of fully developed fluid flow in straight ducts of rectangular cross-section, computer predictions of particle settling in a stationary fluid, particle trajectory calculations inside a Couette layer to validate the implementation of the Saffman lift, and particle trajectory calculations inside a forced vortex flow to validate the implementation of the Basset force or "history" term.

In Chapter 5, the proposed mathematical models and numerical solution methods were applied to a simple electromagnetic separation system. This exercise was undertaken to highlight the scope and explore the possibilities offered by the proposed methods, vis-à-vis their use in the design and optimization of EM separation systems for molten aluminum. *The influences of the various forces on the trajectory of non-conducting particles inside molten metals subjected to electromagnetic forces were*

characterized and discussed, and the importance of including the Basset and Saffman lift forces in the particle momentum equation was further illustrated.

Another original contribution of this thesis was a proposal for quantifying the effectiveness of an EM separation system, via a suitably defined effectiveness parameter. This effectiveness parameter was used to illustrate how an EM-assisted separation system can reduce the overall power consumption compared to a system that relies purely on gravity assisted sedimentation of the inclusions.

6.1 Recommendations for Extensions of This Work

The main contributions of this thesis were the formulation, testing, and application of methods for numerical investigations of EM separation systems applicable to the filtration of molten metals. The scope of this study was limited to the EM separation of solid inclusions in steady, laminar, fully developed flows of molten aluminum in straight ducts of uniform rectangular cross-section.

The first extension to this work could include the study of developing flows of the molten metals subjected to uniform EM fields, and the prediction of particle dynamics therein. A literature review of numerical methods for the prediction of three-dimensional parabolic flows in ducts has been provided in this thesis, and it could serve a starting point for this suggested extension.

Another, relatively simple, extension of this work would be to analyze other duct cross-sections and compute trajectories of particle with finite electrical conductivity. Such a study could provide useful insights into approaches for designing EM systems with optimized shapes of the separation chamber.

The problem of interest should be extended to include non-uniform and time-periodic electric and magnetic fields, and duct walls of finite electrical conductivity. This would be particular interest when considering the commercial implementation of EM separation processes, since the electric field can be induced inside the melt using a single alternating magnetic field, without the need for immersed electrodes (El-Kaddah, 1995). The mathematical model would need to be extended to include the complete set of magnetohydrodynamic governing equations, and a numerical method for the prediction of the electric and magnetic fields would have to be formulated and implemented.

Finally, the author would like to recommend that the theoretical aspects of this work be complemented with systematic experimental work, in order to confirm the predicted trajectories of single particles in the melt, and to develop a prototype EM separation system that could be scaled up for commercial applications.

References

Anderson, J.D. (1995), *Computational Fluid Dynamics*, McGraw-Hill, New York.

Andres, U. (1976), *Magnetohydrodynamic & Magnetohydrostatic Methods of Mineral Separation*, John Wiley & Sons.

Antille, J., Krahenbuhl, Y., Von Kaenel, R., and Weber, J.C. (1992), "Fluid Flow Control: A Must for the Aluminum Industry", *Light Metals*, pp. 1247-1256.

Asmolov, E.S. (1993), "Particle Motion in a Laminar Boundary Layer on a Transverse Velocity Relaxation Length", *Izvestiya Rossiiskoi Akademii Nauk, Mekhanika Zhidkosti i Gaza*, No. 1 pp. 86-93.

Baker, A.J. (1974), "Finite-Element Solution Theory for Three-Dimensional Boundary Layer Flows", *Comp. Meth. Appl. Mech. and Eng.*, Vol. 4, pp. 367-386.

Baker, A.J. (1983), "Finite Element Computational Fluid Dynamics", Hemisphere Publishing Co. / McGraw-Hill, New York.

Baliga, B.R. (1978), "A Control-Volume-Based Finite Element Method for Convective Heat and Mass Transfer", Ph.D. Thesis, University of Minnesota, Minneapolis.

Baliga, B.R. (1997), ""Control-Volume Finite Element Methods for Fluid Flow and Heat Transfer", in Minkowycz, W.J. and Sparrow, E.M. (eds.), *Advances in Numerical Heat Transfer*, Vol. 1, Chapter 3, pp. 97-135, Taylor and Francis, Washington, D.C.

Baliga, B.R. and Patankar, S.V. (1980), "A New Finite-Element Formulation for Convection-Diffusion Problems", *Numer. Heat Transfer*, Vol. 3, pp 393-409.

Baliga, B.R. and Patankar, S.V. (1983), "A Control-Volume Finite Element for Two-Dimensional Fluid Flow and Heat Transfer", *Numerical Heat Transfer*, Vol. 6, pp. 245-261.

Baliga, B.R. and Patankar, S.V. (1988), "Elliptic Systems: Finite Element Method II", in *Handbook of Numerical Heat Transfer* (Eds. Minkowycz, W.J., Sparrow, E.M., Schneider, G.E., and Pletcher, R.H.), John Wiley & Sons, New York, Chapter 11, pp. 421-461.

Baliga, B.R. and Saabas, H.J. (1992), "Control-Volume Finite element Methods for Incompressible Fluid Flow", Proc. III Portuguese Conference on Computational Mechanics, Keynote Lecture on Fluid Dynamics, C2.1-C2.20, Coimbra, Portugal.

Basset, A.B. (1888), *Treatise on Hydrodynamics*, Vol. 2, Chapter 22, pp 285-297, Deighton Bell, London.

Batchelor, G.K. (1967), *An Introduction to Fluid Dynamics*, Cambridge University Press, Cambridge, U.K.

Bird, R.B., Stewart, W.E., and Lightfoot (1960), E.N., *Transport Phenomena*, John Wiley & Sons, New York.

Boussinesq, J. (1903), *Theorie Analyhtique de la Chaleur*, Vol. 2, p. 224, L'Ecole Polytechnique, Paris.

Branover, H. (1978), *Magnetohydrodynamic Flow in Ducts*, John Wiley & Sons, 1978.

Briley, W.R. (1974), "Numerical Method for Predicting Three-Dimensional Steady Viscous Flow in Ducts", *J. Comp. Physics*, Vol. 14, pp. 8-28.

Burden, R.L. and Faires, J.D. (1997), *Numerical Analysis*, 6th Edition, Brooks/Cole, Pacific Grove, California.

Caretto, L.S., Curr, R.M., and Spalding, D.B. (1972), "Two Numerical Methods for Three-Dimensional Boundary Layers", *Comp. Meth. Appl. Mech. Eng.*, Vol. 1, pp. 39-57.

Carlson, G.A. and Hornbeck, R.W. (1973), "A Numerical Solution of Laminar Entrance Flow in a Square Duct", *J. Applied Mechanics*, Vol. 40, pp. 25-30.

Cherukat, P., McLaughlin, J.B., and Graham, A.L. (1994), "The Inertial Lift on a Rigid Sphere Translating in a Linear Shear Flow Field", *Int. J. of Multiphase Flow*, Vol. 20, No. 2, pp 339-353.

Cherukat, P., McLaughlin, J.B., and Dandy, D.S. (1999), "A Computational Study of the Inertial Lift on a Sphere in a Linear Shear Flow Field", *Int. J. of Multiphase Flow*, Vol. 25, pp 15-33.

Cherukat, P. and McLaughlin, J.B. (1990), "Wall-Induced Lift on a Sphere", *Int. J. of Multiphase Flow*, Vol. 26, No. 5, pp 899-907.

Conti, C. et. al. (1989), "*Process for Separating the Inclusions Contained in a Bath of Molten Metal by Filtration*", U.S. Patent 4837385.

Cowling, T.G. (1957), *Magnetohydrodynamics*, John Wiley & Sons, New York.

Cramer, K.R. and Pai, S.I. (1973), *Magnetofluid Dynamics for Engineers and Applied Physicists*, Scripta publishing company, McGraw-Hill.

Crowe, C., Sommerfeld, M., and Tsuji, Y. (1998), *Multiphase Flows with Droplets and Particles*, CRC Press.

Curr, R.M., Sharma, D., and Tatchell, D.G. (1972), "Numerical Predictions of Some Three-Dimensional Boundary Layers in Ducts", *Comp. Meth. Appl. Mech. Eng.*, Vol. 1, pp. 143-158.

Currie, I.G. (1974), *Fundamentals Mechanics of Fluids*, McGraw-Hill, New York.

Dalquist, G.G. and Bjorck, A. (1974), *Numerical Methods*, Prentice-Hall, Englewood Cliffs, New Jersey, U.S.A.

Dandy, D.S. and Dwyer, H.A. (1990), "A Sphere in Shear Flow at Finite Reynolds Number: Effect of Shear on Particle Lift Drag and Heat Transfer", *J. Fluid Mech.*, Vol. 216, pp. 381-410.

Davidson, J.H., Kulacki, F.A., and Dunn, P.F. (1987), "Convective Heat Transfer With Electric and Magnetic Fields", in *Handbook of Single-Phase Convective Heat Transfer*, Kakac, S., Shah, R.K., and Aung, W. (Eds.), John Wiley & Sons, New York.

Del Giudice, S., Strada, M., and Comini, G. (1981), "Three-Dimensional Laminar Flow in Ducts", *Numerical Heat Transfer*, Vol. 4, pp. 215-228.

Druzhinin, O.A., and Ostrovsky, L.A. (1994), "The Influence of Basset Force on Particle Dynamics in Two-dimensional Flows", Physica D, Vol. 76, pp. 34-43.

Eckert, E.R.G. and Drake, R.M. (1972), *Analysis of Heat and Mass Transfer*, McGraw-Hill, New York.

Eckert, C.E., Miller, R.E., Apalian, D., and Mutharasan, R. (1984), "Molten Aluminum Filtration: Fundamentals and Models", pp. 1281-1304, *Light Metals.*

El-Kaddah, N., Szekely, J., and Carlsson, G. (1984), "Fluid Flow and Mass Transfer in an Inductively Stirred Four-Ton Melt of Molten Steel: A Comparison of Measurements and Prediction", *IEEE Metallurgical Transactions B*, Vol. 15B, pp. 663-640, December.

El-Kaddah, N., Szekely, J., Taberlet, E., and Fautrelle, Y. (1986), "Turbulent Recirculating Flow in Induction Furnaces: A Comparison of Measurements with Predictions over a Range of Operating Conditions", *IEEE Metallurgical Transactions B*, Vol. 17B, pp. 687-693, December.

El-Kaddah, N. (1988), "A Comprehensive Mathematical Model of Electromagnetic Separation of Inclusion in Molten Metals", *IEEE transactions on Industrial Applications*, pp. 1162-1167.

El-Kaddah, N. (1990), "Apparatus and Method for Improved Filtration of Inclusions from Molten Metals", U.S. Patent 4909836.

El-Kaddah, N., Patel, A.D., and Natarajan, T.T. (1995), "The Electromagnetic Filtration of Molten Aluminum Using an Induced-Current Separator", Journal of Materials, pp. 46-49.

El-Kaddah, N. (1996), "Electromagnetic Filtration - An Emerging Technology for the Production of Ultra Clean Metal", *Emerging Separation Technologies for Metals II*, Ed. Bautista, R.G., The Minerals, Metals and Materials Society, pp. 203-213.

Engh, T.A. (1992), *Principles of Metal Refining*, New York, NY:Oxford University Press.

Fan, L.S. and Zhu, C. (1998), *Principles of Gas-Solid Flows*, Cambridge University Press, Cambridge, U.K.

Ferziger, J.H. and Peric, M. (1999), *Computational Methods for Fluid Dynamics*, 2nd Revised Edition, Springer Verlag, Berlin.

Fleming, D.P. and Sparrow, E.M. (1969), "Flow in the Hydrodynamic Entrance Region of Ducts of Arbitrary Cross-Section", *ASME J. Heat Transfer*, Vol. 91, pp. 345-354.

Frisvold, F., Engh, T.A., Johansen, S.T., and Pedersen, T. (1992), "Removal of Inclusions - A Survey and Comparison of Principles", pp. 1125-1132, *Light Metals*.

Gates, R. (1900), "Diamagnetic Separation", US Patent 653344.

Gauckler, L.J., Waeber, M.M., Conti, C., and Jacob-Duliere, M. (1985), "Ceramic Foam for Molten Metal Filtration", *Journal of Metals*, pp. 47-50, September.

Gillon, P. (1995), "Materials Processing with High Direct-Current Magnetic Fields", JOM, May.

Goldstein, R.J. and Kreid, D.K. (1967), "Measurements of Laminar Flow Development in a Square Duct Using a Laser-Doppler Flowmeter", *J. Applied Mechanics*, Trans. ASME, Vol. 34, pp. 813-818.

Gresho, P.M. and Sani, R.L. (1998), *Incompressible Flow and the Finite Element Method*, John Wiley & Sons, New York.

Hartnett, J.P., Irvine, T.F., Cho, Y.I., and Greene, G.A. (1961-2001), *Advances in Heat Transfer*, Vols. 1 – 34, Academic Press, New York.

Hassan, Y.A., Rice, J.G., and Kim, J.H. (1983), "A Stable Mass-Flow-Weighted Two-Dimensional Skew Upwind Scheme", *Numer. Heat Transfer*, Vol. 14, pp. 395-408.

Hobson, D.O., Alexeff, I., and Sikka V.K. (1988), "Method and Apparatus for Removal of Gaseous Liquid and Particulate Contaminants from Molten Metals", U.S. Patent 4786230.

Hookey, N.A. (1989), "A CVFEM for Two-Dimensional Viscous Compressible Fluid Flow", Ph.D. Thesis, Department of Mechanical Engineering, McGill University, Montreal, Quebec.

Hoole, S.R., and Hoole, P.R. (1995), *A Modern Short Course in Engineering Electromagnetics,* Oxford University Press, Oxford, U.K.

Incropera, F.P. and DeWitt, D.P. (1990), *Fundamentals of Heat and Mass Transfer,* 3rd Edition, John Wiley & Sons, New York.

Johnson, R.W., *The Handbook of Fluid Dynamics,* CRC Press, Boca Raton, Florida.

Kalikhman, L.E. (1967), *Elements of Magnetogasdynamics,* Saunders, Philadelphia.

Kreith, F. and Bohn, M.S. (2001), *Principles of Heat Transfer,* 6th Edition, Brooks.Cole, Pacific Grove, California.

Leenov, D. and Kolin, A. (1954), "Theory of Electromagnetophoresis. I. Magnetohydrodynamic Forces Experienced by Spherical and Symmetrically Oriented Cylindrical Particles", *Journal of Chemical Physics,* Vol. 22, No. 4, pp. 683-688, April.

Lundgren, T.S., Sparrow, E.M., Starr, J.B. (1964), "Pressure Drop Due to the Entrance Region in Ducts of Arbitrary Cross-Section", J. Basic Eng., Trans. ASME, Series D, Vol. I6, pp. 620-626.

Marty, P. and Alemany, A. (1982), "Theoretical and Experimental Aspects of Electromagnetic Separation", *Metallurgical Aspects of Magnetohydrodynamics,* ed. H.K. Moffatt & M.R.E. Proctor, London: Light Metals Society, pp. 245-259.

Marty, P., Alemany, A., Ricou, R., and Vives, C. (1982), "pressure and Velocity Distribution Around an Obstacle Immersed in Liquid Metal Subjected to Electromagnetic Forces", Third Beer-Sheva International Seminar on Magnetohydrodynamic Flows and Turbulence (Beer-Sheva, Israel: Ben-Gurion University of the Negev), pp. 245-259.

Masson, C., Saabas, H.J., and Baliga, B.R. (1994), "Co-Located Equal-Order Control-Volume Finite Element Method for Two-Dimensional Axisymmetric Incompressible Fluid Flow", *Int. J. Num. Methods in Fluids,* Vol. 18, pp. 1-26.

Maxey, M.R. and Riley, J.J. (1983), "Equation of Motion for a Small Rigid Sphere in a Non-uniform Flow", *Phys. Fluids,* Vol. 26, No. 4, pp. 883-889.

McLaughlin, J.B. (1991), "Inertial Migration of a Small Sphere in Linear Shear Flows", *J. of Fluid Mech.,* vol. 224, pp. 261-274.

Minkowycz, W.J. and Sparrow, E.M. (1997), *Advances in Numerical Heat Transfer,* Vol. 1, Taylor & Francis, Washington, D.C.

Moore, A.D. (1972), "Electrostatics", *Scientific American*, Vol. 47, pp. 47-58.

Moran, M.J. and Shapiro, H.N. (2000), *Fundamentals of Engineering Thermodynamics*, 4th Edition, John Wiley & Sons, New York.

Murariu, V., Rezlescu, N., Rotariu, O., and Badescu, V. (1997), "The Influence of Suspension Concentration on the Filtration Efficiency on an Axial HGMF Cell With Bounded Flow Field", *Int. J. of Applied Electromagnetics and Mechanics 8*, pp 297-305, IOS Press.

Naumov, V.A. (1995), "Influence of Saffman's Lift Force on the Motion of a Particle in Couette Layer", *J. of Engineering Physics and Thermophysics*, Vol. 68, No. 5, pp. 683-686.

Naumov, V.A. (1997), "Motion of a Solid Particle in a Rotating Fluid", *Theoretical Foundations of Chemical Engineering*, Vol. 31, No. 6, pp. 515-519.

Odar, F. and Hamilton, W.S. (1964), "Forces on a Sphere Accelerating in a Viscous Fluid", *J. Fluid Mech.*, Vol. 18, pp. 302-314.

Odar, F. (1966), "Verification of the Proposed Equation for Calculation of the Forces on a Sphere Accelerating in a Viscous Fluid", *J. Fluid Mech.*, Vol. 25, pp. 591-592.

Oseen, C.W. (1927), *Hydrodynamik*, p.132, Leipzig.

Panofsky, W. and Phillips, M. (1956), *Classical Electricity and Magnetism*, Addison-Wesley, Reading, Massachusetts.

Patankar, S.V. and Karki, K.C. (1999), "Calculation of Particle Trajectories in Complex Meshes", *Numerical Heat Transfer*, Part B, 35:431-437.

Patankar, S.V. (1980), *Numerical Heat Transfer and Fluid Flow*, Hemisphere Publishing Corp.

Patankar, S.V. and Spalding, D.B. (1972), "A Calculation Procedure for Heat, Mass and Momentum Transfer in Three-Dimensional Parabolic Flows", *Int. J. Heat and Mass Transfer*, Vol. 15, pp. 1787-1806.

Patel, A.D. and El-Kaddah, N. (1997), "Kinetics of Inclusion Removal From Molten Aluminum Under an Applied Alternating Magnetic Field", *Light Metals* 1997, Ed. Huglen, R., The Minerals, Metals & Materials Society, pp. 1013-1018.

Pham, T.T. (1983), "A Control-Volume Finite-Element Method for Three-Dimensional Parabolic Flow and Heat Transfer in Ducts, With Application to Laminar Thermal-Hydraulics in Rod-Bundle Geometries", *M.Eng. Thesis*, Department of Mechanical Engineering, McGill University, Montreal, Canada.

Prakash, C. (1986), "An Improved Control-Volume Finite-Element Method for Heat and Mass Transfer, and for Fluid Flow Using Equal-Order Velocity-Pressure Interpolation", *Numer. Heat Transfer*, Vol. 9, pp. 253-276.

Prakash, C. and Patankar, S.V. (1985), "A Control Volume Based Finite Element Method for Solving the Navier-Stokes Equations Using Equal-Order Velocity-Pressure Interpolation", *Numver. Heat Transfer*, Vol. 8, pp. 259-280.

Prakash, C. and Patankar, S.V. (1985), "A Control-Volume-Based Finite Element Method for Solving the Navier-Stokes Equations Using Equal-Order Velocity-Pressure Interpolation", *Numerical Heat Transfer*, Vol. 8, pp. 259-280.

Pratap, V.S. and Spalding, D.B. (1976), "Fluid Flow and Heat Transfer in Three-Dimensional Duct Flows", *Int. J. Heat and Mass Transfer*, Vol. 19, pp. 1183-1188.

Proudman, I. and Pearson, J.R.A. (1957), "Expansions at Small Reynolds Numbers for the Flow Past a Sphere and a Circular Cylinder", *J. Fluid Mech.*, Vol. 2, pp. 237-262.

Raithby, G.D. and Schneider, G.E. (1988), "Elliptic Systems: Finite-Difference Method II", in *Handbook of Numerical Heat Transfer* (Eds. Minkowycz, W.J., Sparrow, E.M., Schneider, G.E., and Pletcher, R.H.), John Wiley & Sons, New York, Chapter 7, pp. 241-291.

Reddy, J.N. (1993), *An Introduction to the Finite Element Method*, 2nd Edition, McGraw-Hill, New York.

Reeks, M.W., and McKee, S. (1984), "The Dispersive Effects of Basset History Forces on Particle Motion in a Turbulent Flow", Phys. Fluids, No. 27, Vol. 7, pp. 1573ff.

Ren, J., Zeng, G., and Liu, S. (1995), "Interactive Particle Tracing Algorithm for Unstructured Grids", Lecture Notes in Computer Science, v.1024, p.59.

Rhie, C.M. and Chow, W.L. (1983), "Numerical Study of the Turbulent Flow Past an Airfoil With Trailing Edge Separation", *AIAA Journal*, Vol. 21, pp. 1525-1532.

Rice, J.G. and Schnipke, R.J. (1986), "An Equal-Order Velocity-Pressure Formulation that Does Not Exhibit Spurious Pressure Modes", *Comp. Meth. Appl. Mech. and Eng.*, Vol. 58, pp. 135-149.

Roache, P.J. (1982), *Computational Fluid Dynamics*, Hermosa Publishers, Albuquerque, New Mexico.

Roberts, D.W. and Forester, C.K. (1979), "Parabolic Procedure for Flows in Ducts of Arbitrary Cross-Sections", *AIAA Journal*, Vol. 17, pp. 33-40.

Rohsenow, W.M. and Hartnett, J.P. (1973), *Handbook of Heat Transfer*, McGraw-Hill, New York.

Romig, M.F. (1964), "The Influence of Electric and Magnet Fields on Heat Transfer to Electrically Conducting Fluids", in *Advances in Heat Transfer*, Hartnett, J.P. et al. (Eds.), Academic Press, Vol. 1, pp. 267 – 354.

Romig, M.F. (1973), "Electric and Magnetic Fields", in *Handbook of Heat Transfer*, Rohsenow, W.M. and Hartnett, J.P. (Eds.), McGraw-Hill, New York, Chapter 11, pp. 1 – 27.

Rubinow, S.I. and Keller, J.B. (1961), "The Transverse Force on a Spinning Sphere Moving in a Viscous Fluid", *J. Fluid Mech.*, Vol. 11, pp. 447-459.

Saabas, H.J. (1991), "A Control-Volume Finite Element Method for Three-Dimensional, Incompressible, Viscous Fluid Flow", Ph.D. Thesis, Dpartment of Mechanical Engineering, McGill University, Montreal, Canada.

Saabas, H.J. and Baliga, B.R. (1994), "A Co-Located Equal-Order Control-Volume Finite Element Method for Multidimensional, Incompressible Fluid Flow – Part I: Formulation", *Numerical Heat Transfer*, Vol. 26, pp. 381-407.

Saffman, P.G. (1965), "The Lift on a Small Sphere in a Slow Shear Flow", *J. Fluid Mech*, vol. 22, part 2, pp 385-400.

Schlichting, H. (1968), *Boundary-Layer Theory*, McGraw-Hill, New York.

Schneider, G.E. and Raw, M.J. (1986), "A Skewed Positive Influence Coefficient Upwind Procedure for Control-Volume-Based Finite Element Convection-Diffusion Computation", Numerical Heat Transfer, Vol. 9, pp. 1-26.

Segerlind, L.J. (1976), *Applied Finite Element Analysis*, John Wiley & Sons, New York.

Shah, R.K. and London, A.L. (1978), *Laminar Flow Forced Convection in Ducts*, in Advances in Heat Transfer (Hartnett, J.P. et al., Eds.), Supplement 1, Academic Press, New York.

Shivkumar, S., Wang, L., and Apelian, D. (1991), "Molten Metal Processing of Cast Aluminum Alloys", *Journal of Metals*, pp. 26-32.

Shyy, W. (1994), "Elements of Pressure-Based Computational Algorithms for Complex Fluid Flow and Heat Transfer", *Advances in Heat Transfer*, Vol. 24, pp. 191-275.

Sparrow, E.M., Lin, S.H., and Lundgren, T.S. (1964), "Flow Development in the Hydrodynamic Entrance Region of Tubes and Ducts", *Physics of Fluid*, Vol. 7, pp. 338-347.

Sparrow, E.M., Hixon, C.W., and Shavit, G. (1967), "Experiments on Laminar Flow Development in Rectangular Ducts", J. Basic Engineering, Trans. ASME, Vol. 89, pp. 116-124.

Stroble, C. (1942), "Flissigkeit Durch Elektrischen Strom.", Reichspatent 729487.

Tritton, D.J. (1988), *Physical Fluid Dynamics*, 2nd Edition, Oxford University Press, Oxford, U.K.

Van Doormaal, J.P. and Raithby, G.D. (1984), "Enhancements of the SIMPLE Method for Predicting Incompressible Fluid Flows", Numerical Heat Transfer, Vol. 7, pp. 1-19.

Venditti, D.A. (1998), "An h-Adaptive Control-Volume Finite Element Method for Steady, Two-Dimensional Fluid Flow and Heat Transfer", *M.Eng. Thesis*, Department of Mechanical Engineering, McGill University, Montreal, Canada.

Venditti, D.A. and Baliga, B.R. (1998), "An h-Adaptive Strategy for CVFEM Simulations of Visocus Incompressible Flow", *Proc. 6th Annual Conference of the CFD Society of Canada (CFD '98)*, Quebec City, Quebec, pp. VIII-65 – VIII-70.

Verte, A. (1961), "Process of Treating a Liquid Metal", Authors Certificate no. 141592, Class 31c, 13. Byull. Izobret. No 19.

Vives, C., A. and Ricou, R. (1982), "Liquid-Solid Separation in a Molten Metal by a Stationary Electromagnetic Field", Third Beer-Sheva International Seminar on Magnetohydrodynamic Flows and Turbulence (Beer-Sheva, Israel: Ben-Gurion University of the Negev), pp. 245-259.

White, F.M. (1991), *Viscous Fluid Flow*, 2nd Edition, McGraw-Hill, New York.

Zienkiewicz, O.C. (1977), *The Finite Element Method*, 3rd Edition, McGraw-Hill, New York.